Award Number:  W81XWH-12-1-0074


TITLE:   Dissecting and Targeting Latent Metastasis


PRINCIPAL INVESTIGATOR:   Joan Massagué, PhD


CONTRACTING ORGANIZATION:

Sloan Kettering Institute for Cancer Research
New York, NY 10065

REPORT DATE:    September 2014


TYPE OF REPORT:  Annual


PREPARED FOR:  U.S. Army Medical Research and Materiel Command
                          Fort Detrick, Maryland  21702-5012

# REPORT DOCUMENTATION PAGE

*Form Approved*
*OMB No. 0704-0188*

| 1. REPORT DATE | 2. REPORT TYPE | 3. DATES COVERED |
|---|---|---|
| September 2014 | Annual | 1 Sep 2013 – 31 Aug 2014 |

**4. TITLE AND SUBTITLE**

Dissecting and Targeting Latent Metastasis

**5a. CONTRACT NUMBER**

**5b. GRANT NUMBER**
W81XWH-12-1-0074

**5c. PROGRAM ELEMENT NUMBER**

**6. AUTHOR(S)**

Joan Massagué

E-Mail: j-massague@ski.mskcc.org

**5d. PROJECT NUMBER**

**5e. TASK NUMBER**

**5f. WORK UNIT NUMBER**

**7. PERFORMING ORGANIZATION NAME(S) AND ADDRESS(ES)**

Sloan Kettering Institute for
Cancer Research
1275 York Avenue
New York, NY 10065

**8. PERFORMING ORGANIZATION REPORT NUMBER**

**9. SPONSORING / MONITORING AGENCY NAME(S) AND ADDRESS(ES)**

U.S. Army Medical Research and Materiel Command
Fort Detrick, Maryland 21702-5012

**10. SPONSOR/MONITOR'S ACRONYM(S)**

**11. SPONSOR/MONITOR'S REPORT NUMBER(S)**

**12. DISTRIBUTION / AVAILABILITY STATEMENT**

Approved for Public Release; Distribution Unlimited

**13. SUPPLEMENTARY NOTES**

**14. ABSTRACT**

Metastasis is physically and psychologically devastating, frequently incurable, and the cause of 90% of deaths from breast cancer. Invasive breast tumors release cancer cells from the outset, and thousands of these cells infiltrate distant organs before the primary tumor is diagnosed and removed. Microscopic cancer colonies that remain in a patient's organs after the removal of a breast tumor constitute latent metastasis of breast cancer (LMBC). These cells retain the potential to form overt metastasis for years. Targeting LMBC with new drugs offers an untapped opportunity to prevent metastasis. This research project aims at identifying the cell types, organ sites, tissue niches, metastasis genes, and signaling functions that support the survival and fitness of LMBC cells. In year 02 we made progress in isolating latent metastatic cells from breast cancer and lung cancer. We implemented transcriptional analysis of selected cancer cell populations in highly heterogeneous tumor microenvironments. We identified L1CAM as a mediator of vascular cooption by disseminated metastasis-initiating cells in different organs, and as a potential therapeutic target against metastasis. We identified connexin 43 (Cx43) and protocadherin 7 (PCDH7) as components of gap junctions that mediate survival and colony initiation in breast cancer cells that infiltrate the brain. We showed that gap junction modulators can be safely used as inhibitors of brain metastasis of breast cancer.

**15. SUBJECT TERMS**
Breast cancer; latent metastasis; disseminated cancer cells; circulating cancer cells; tumor initiating cells; metastatic niche; vascular cooption; L1CAM; SOX genes; WNT pathway; astrocytes; gap junctions

| 16. SECURITY CLASSIFICATION OF: | | | 17. LIMITATION OF ABSTRACT | 18. NUMBER OF PAGES | 19a. NAME OF RESPONSIBLE PERSON USAMRMC |
|---|---|---|---|---|---|
| **a. REPORT** | **b. ABSTRACT** | **c. THIS PAGE** | UU | 85 | **19b. TELEPHONE NUMBER** *(include area code)* |
| U | U | U | | | |

**Standard Form 298 (Rev. 8-98)**
Prescribed by ANSI Std. Z39.18

**CONGRESSIONALLY DIRECTED MEDICAL RESEARCH PROGRAM**

**Award DOD W81XWH-12-1-0074**

**Principal Investigator: Joan Massagué, PhD**

**ANNUAL REPORT**
**9/1/13 – 8/31/14**

**Table of Contents**

## INTRODUCTION

Metastasis is physically and psychologically devastating, frequently incurable, and the cause of 90% of deaths from breast cancer (*1, 2*). Thousands of tumor cells may infiltrate the organs of a breast cancer patient before the primary tumor is diagnosed and removed. While the vast majority of these cells die, a residual population adopts a low-proliferation state that protects these cells from death (*3, 4*). This population constitutes latent metastasis of breast cancer (LMBC), and it likely requires powerful mechanisms to survive long-term in the newly invaded microenvironments. This stress is compounded by the impact of therapy that the patient will receive after diagnosis.

In spite of the obvious scientific interest and medical importance of this problem, almost nothing is known about the molecular mechanisms that support the survival and fitness of disseminated cancer cells prior to the initiation of metastatic outgrowth in host tissues. Progress in this field has been hampered by a lack of model systems of latent metastasis. Yet, an understanding of these mechanisms would allow the development of novel therapeutic approaches to target disseminated breast cancer cells in order to prevent metastasis. The overall goal of this project is to identify the genes and pathways in cancer cells and in their host tissues that support latent metastasis in general and LMBC in particular.

## KEYWORDS

Breast cancer; latent metastasis; disseminated cancer cells; circulating cancer cells; tumor initiating cells; metastatic niche; vascular cooption; L1CAM; SOX genes; WNT pathway; astrocytes; gap junctions.

## OVERALL PROJECT SUMMARY

### Progress under Task 1: To develop experimental models of latent metastasis.

**Previous progress:** In Year 01 of this project we had obtained indolent derivatives of cell lines from HER2-positive breast cancer (HCC1954 cell line), triple-negative breast cancer (MDA231) and, for the purpose of comparative analysis of another type of cancer, lung adenocarcinoma (H2087 cell line). Briefly, the tumor cells were labeled with GFP-luciferase to track them and with an antibiotic resistance gene (hygromycin/blasticidin) to isolate them from the mouse tissues. The labeled cells were injected into the left cardiac ventricle of athymic mice, which are deficient in T and B cells. Inoculation allowed the distribution of cancer cells throughout the body, as verified by imaging of the mice by bioluminescent imaging (BLI) after inoculation. Mice were monitored for two months. A few mice developed overt metastases during this period. These lesions were harvested and placed in culture for the isolation of aggressive metastatic cell line derivatives. Most mice however did not develop detectable metastasis over this two-month period, or developed a low level of BLI signals that remained stable and did not progress. We then harvested tissues of interest (brain, lung, liver, bone marrow, and kidney) to obtain tumor cells that were able to survive as micro-metastasis without forming overt metastasis. The isolated latent metastatic cells were expanded in culture, demonstrating that these cells have the capacity to actively proliferate under favorable conditions. From the HER2-positive breast cancer cell line HCC1954 we isolated latency-competent derivatives that can populate the brain, bone marrow

and lungs (HCC1954-LMBC1 cells). A more aggressive derivative (HCC1954-BrM) was also obtained. Latent bone metastasis derivatives were isolated from triple-negative breast cancer cell lines (MDA231-SCP6, and MDA231-Bo-LMBC1), along with more aggressive derivatives. From the H2087 lung adenocarcinoma cell line we isolated latent lung and kidney metastatic cell derivatives (H2087-LMLC1), along with aggressively lung and bone metastatic derivatives.

Focusing on HCC1954-LMBC1 and H2087-LMLC1 as our initial models for study, we confirmed that on reinjection into mice these cells retain the capacity to infiltrate various organs and to engage in a low-cycling state that can last for months, with stochastic, low frequency generation of lethal macrometastatic lesions. These results indicate that the metastatic cell lines have the two key properties that we sought: (i) to be able to adopt a latent state after infiltrating target tissues, and (ii) to retain metastasis-initiating capabilities that can give rise to lethal lesions in vital organs. The above-described latent metastatic cells lines are being used to illuminate the molecular basis for the latent metastasis state.

**Progress Item 1.1.** We developed similar models for other tumor types (lung adenocarcinoma, renal cell carcinoma) in order to identify commonalities and differences with the LMBC models. These studies will be complemented by assays in colorectal cancer organoids, which are patient-derived cancer cells grown in stem-cell conditions on matrigel (*5*). Organoids can be generated efficiently from single cancer cells and exhibit hierarchical differentiation, containing both stem cells and their differentiated progeny. They are currently the most representative *in vitro* cancer surrogates, displaying tumor heterogeneity and extracellular matrix interactions, and are amenable to genetic manipulation *in vitro* (*6*). In collaboration with the laboratory of Eduard Batlle (IRB Barcelona), we have obtained organoid cultures derived from the primary tumors of three patients with metastatic colorectal cancer. We labeled the organoid-forming CRC cells with a mCherry-luciferase vector and inoculated these cells into athymic mice. We have found that these cells are competent to form metastases in the lung and liver of mice, mirroring the metastasis organ profile of CRC in humans. Thus the biology of metastasis in this organoid xenograft model mimics the biology of metastatic colon cancer in patients, in whom brain metastases typically remain latent early in the course of the disease, with overt macrometastases appearing much later than liver and lung tumor outgrowths.

**Progress Item 1.2.** We are developing similar models from transgenic mouse mammary tumors (MMTV-ErbB2) in immunocompetent syngeneic hosts in order to incorporate the role of immunity in LMBC.

## Progress under Task 2: Identify genes and pathways specifically activated in LMBC.

**Progress Item 2.1.** We conducted genome-wide transcriptomic profiling of the HCC1954-LMBC and H2087-LMLC lines by RNA-Seq under normal and stress conditions to identify stroma-independent gene expression signatures. Analysis of the data provides evidence for a new paradigm in the biology of latent metastasis. LMLCs down regulate expression of several genes in response to stress (**Figure 1A-B**). Gene ontology analysis indicates majority of these down regulated genes encode for cell surface proteins. As a consequence, the biological processes negatively impacted are the cell surface receptor linked signal transduction; processes regulating cell proliferation and death (**Figure 1C**). Various members of the SOX family transcription factors, which are master regulators of progenitor cell stages (*7*), are highly enriched in the

H2087-LMLC lines suggesting the disseminated tumor cells are stem cell like (**Figure 1D**). HCC1954-LMBC lines are enriched for CD44^{high}/CD24^{low} surface marker expression, denoting a stem/progenitor phenotype (**Figure 1E**)(**8**). These exciting findings form the basis for further tasks currently ongoing.

## Progress under Task 4: Establish the functional relevance of LMBC genes and pathways.

**Progress Item 4.1.** We recently completed and published (**Valiente et al Cell 2014**) our finding that that circulating cancer cells that enter the brain parenchyma use the adhesion molecule L1CAM to stretch out along existing brain capillaries, forming intimate contact with pre-existing blood vessels in a process termed <u>vascular cooption</u> (*9-12*). Brain metastases occur in 20-40% of advanced stage cancers and represent the most prevalent intracranial malignancy in adults (*13, 14*). Lung and breast cancers are the most common sources. Despite treatment advances at other metastatic sites, current clinical management of brain metastases affords limited disease control and most patients succumb to tumor progression less than twelve months after diagnosis (*13, 15*). The mechanisms underlying this disease process must therefore be understood so that they may be parlayed into rational therapeutic strategies.

The brain's unique microenvironment poses a formidable barrier to metastatic cancer cells. Recent progress has begun to unravel the complex cellular and molecular interactions responsible for the initiation of brain metastases. Circulating cancer cells that mechanically lodge in brain capillaries must first traverse the reinforced vessel walls that constitute the blood-brain barrier (BBB). We previously identified genes and functions that mediate cancer cell extravasation through the BBB in experimental models and predict brain metastasis in the clinic (*16*). Once inside the brain parenchyma, metastatic cells remain associated with the microvasculature (*10-12*). Expression of the cell adhesion molecule L1CAM in the cancer cells mediates their tight adhesion to the abluminal capillary basal lamina as a requirement for the initiation of metastatic outgrowth (**Figure 2A, 2B**). L1CAM is a large, multi-domain protein that normally functions as a neuronal adhesion molecule, mediating axon pathfinding in the developing brain (*17, 18*). RNAi-mediated depletion of L1CAM in metastasis-initiating cells not only disrupts vascular cooption, but also inhibits the ability of injected cancer cells to form viable metastases in mice, and prolongs the survival of such mice (**Figure 2C-I**).

Strikingly, aberrant L1CAM expression has been demonstrated at the leading edge of primary tumors, and is associated with invasion, metastasis and poor prognosis in many human cancers including lung, breast and colon carcinomas (*19-24*). This suggested that the selective advantage gained from L1CAM-expression might not be restricted to the brain. Indeed, we recently found in our models that L1CAM is required for breast cancer metastasis to lung, bone and liver (**Figure 3A-C**) as well as for outgrowth of orthotopically implanted tumors in mice (**Figure 3C**). RNAi-mediated depletion of L1CAM also inhibits the formation of metastases in syngeneic allografts in immunocompetent mice. These results suggest that **L1CAM-engagement in vascular cooption is a general mechanism for the survival and outgrowth of disseminated cancer cells in different organ sites**.

To investigate the role of L1CAM in metastatic dissemination of endogenous tumors in immunocompetent subjects we recently obtained L1CAM[flox/flox] mice from the Schachner/Schaefer laboratories (University of Mainz). We are planning to breed these mice

with mice bearing Cre conditional Kras$^{G12D}$ and p53$^{-/-}$ alleles (*25*) and erbB2 alleles (*26*). Tumors will be induced by endotracheally administering lentiviral-Cre into mice, allowing dissection of the role of L1CAM in tumor initiation and metastasis in these syngeneic mouse models.

**Progress Item 4.2.** Circulating cancer cells that infiltrate the brain die from exposure to reactive astrocytes. Paradoxically, aggressive metastatic lesions are rich in astrocytes. We recently found that breast cancer and lung cancer cells that evade the anti-metastatic action of astrocytes use gap junction components to turn astrocytes in their favor. Brain metastatic cells express astrocytic protocadherin 7 (PCDH7) and the gap junction component connexin 43 (Cx43). PCDH7 interacts with Cx43 hemi-channels to assemble carcinoma-astrocyte gap junctions **(Figure 4)**. Carcinoma PCDH7 and Cx43 mediate brain metastasis in mouse models and are clinically associated with brain relapse in human breast and lung tumors. PCDH7 or Cx43 depleted brain metastatic cells can still traverse the blood-brain barrier and co-opt cerebral capillaries, but fail to form overt metastatic lesions **(Figure 5)**. Based on these insights, we introduce a therapeutic strategy against brain metastases based on existing modulators of gap junction function. Treatment of mice with negative modulators of Cx43 gap junctions suppresses the progression of established metastases, suggesting a therapeutic approach for a lethal complication of cancer with few treatment options. This work is currently submitted for publication (**Chen et al submitted for publication**).

**Progress Item 4.3.** We performed TRAP and RNA-Seq based transcriptomic analysis of cell lines in culture, in order to identify stroma-independent gene expression signatures disseminated in mouse brain tissue. We have collected TRAP data from L1CAM +/- brain metastatic cells grown on plastic or grown within brain parenchyma tissue. We are currently bioinformatically analyzing these data. Although the analysis still is at an early stage, we have already identified an L1CAM-driven Cell Adhesion Program and a L1CAM-dependent hyper activation of Notch signaling downstream of L1CAM-engagement during vascular co-option.

**Progress Item 4.4.** We are testing the role of additional genes and pathways on the ability of LMBC cells to survive in host tissues after inoculation in mice. As SOX family members are enriched in the H2087 LMLC lines, we have generated RNAi constructs targeting these transcription factors. We are testing the gene knock down effect on LMLC survival in oncospheres and in vivo. Bioinformatic analysis of our transcriptomic data from H2087 cells using signaling pathway classifiers indicates that LMLC lines have an attenuated WNT signaling activity **(Figure 6)**. This finding is provocative because WNT signaling in disseminated lung adenocarcinoma cells is critical for metastatic outgrowth (*27*). In parallel we found that these cells overexpress WNT ligand inhibitors, which are likely responsible for this attenuated response. We are generating RNAi constructs targeting these genes to test the hypothesis that latent metastatic cells secrete WNT ligand inhibitors to proactively enforce a slow cycling program that protects these cells from recognition by the innate immune system.

### Progress under Task 5: Establish the clinical relevance of LMBC genes and pathways

**Progress Item 5.1.** We interrogated annotated human metastasis tissue samples by immunohistochemistry to determine the activity of genes and pathway of interest in frozen tissues and paraffin sections of lung cancer metastasis to brain. The results (*12*) demonstrate that L1CAM is aberrantly expressed in brain metastatic tissue in patients **(Figure 7A-B)**.

**Progress under Task 6***: Mechanism of action of LMBC genes and pathways.**

**Progress Item 6.1.** We generated a doxycycline-inducible shL1CAM-expressing construct to allow reversible inhibition of L1CAM in mice after the formation of overt macrometastases in order to establish whether L1CAM is required for maintenance of DTCs/metastasis initiating capacity in metastases derived from H2030-BrM lung adenocarcinoma cells **(Figure 8A)**. We are currently conducting these functional assays. We have expanded significantly our knowledge on vascular co-option during this year, and we can conclude that this mechanism underlies the ability of DTC to proliferate. This statement applies to both aggressive and indolent cell lines. We have characterized in both types of cancer metastasis models a critical regulator, the cell adhesion molecule L1CAM. The ability of L1CAM to regulate the process of co-option applies to metastasis in different organ sites.

**Progress Item 6.2.** We achieved **pre-clinical therapeutic results** by targeting gap junction function with tonabersat and meclofenamate, two structurally distinct drugs that perturb gap junction activity (**Chen et al submitted for publication**). In our experiments, both drugs as single agents were effective against brain colonization by highly aggressive breast cancer cells. Carboplatin has shown only modest improvements in overall survival in patients with breast cancer (*28*), as it does in our models. However, in combination with tonabersat or meclofenamate, carboplatin acutely suppressed the outgrowth of established metastatic colonies **(Figure 8B-C)**. Tonabersat and meclofenamate are orally bioavailable and well tolerated systemically in humans at the doses tested. The results suggest a novel therapeutic avenue for the treatment of brain metastasis, and therefore warrant additional preclinical and clinical investigation.

## KEY RESEARCH ACCOMPLISHMENTS

- Isolation of latent metastatic cells from breast cancer and lung cancer.
- Implementation of translating ribosome affinity purification (TRAP) for transcriptional analysis of selected cancer cell populations in highly heterogeneous tumor microenvironments.
- Identification of L1CAM in breast cancer cells as a mediator of vascular cooption by aggressive as well as latent metastasis-initiating cells in different organs.
- Identification of L1CAM as a potential therapeutic target against metastasis in different organs.
- Identification of Cx43 and PCDH7 as components of gap junctions that mediate survival and colony initiation in breast cancer cells that infiltrate the brain.
- Identification of gap junction modulators as inhibitors of brain metastasis of breast cancer.

## CONCLUSION

The overall goals of this project are to biologically dissect, molecularly deconstruct, and conceptually understand LMBC, in order to target its viability for the prevention of metastasis. Our progress towards this goal is right on schedule. We have accomplished the tasks that were scheduled for the period of this Progress Report. We have encountered new and unexpected findings. There have been no major unforeseen problems in the development of this work.

## CHANGES IN PERSONNEL

- Ashley M. Laughney is a postdoctoral fellow who replaced Swarnali Acharyya.
- Danilo G. Macalinao is a graduate student who replaced Qiong Wang.
- Lan He is a research technician who replaced Lai-Fong Chow-Tsang
- Weiping Shu is occupying the Senior Research Technician position originally listed on the proposal.
- Qing Chen a postdoctoral scholar will remain the same.

## PUBLICATIONS, ABSTRACTS AND PRESENTATIONS

a. **Publications**

1. Lay Press: Nothing to report

2. Peer-Reviewed Scientific Journals:

- Valiente, M., Obenauf, A.C., Jin, X., Chen, Q., Zhang, X.H.F., Lee, D.J., Chaft, J.E., Kris, M.G., Huse, J.T., Brogi, E. and Massagué, J. Serpins promote cancer cell survival and vascular cooption in brain metastasis. **Cell** 156, 1002-1016 (2014) PMC3988473

  This paper attracted widespread attention as illustrated by the following editorial commentaries on the significance of our findings: Pezzela, F. and Harris, A.L. **New Engl. J. Med.** 370, 2146-7, 2014; Erler, J.T. **Nature** 508, 46-47, 2014; Ye, W. **EMBO J.** 33, 786-787, 2014; Hutchinson, L, **Nat. Rev. Clin. Oncol.** 11, 241, 2014; Zaromytidou, A. **Nature Cell Biol.**, 16, 307 (2014); Ferrarelli, L.K. **Sci. Signal. 7**, ec72, 2014; **Cancer Disc.** DOI: 10.1158/2159-8290.CD-RW2014-057.

- Chen, Q., Boire, A., Valiente, M., Jiin, X., Pawta, R., Xu, K., and Massagué, J. Assembly and Targeting of Cancer Cell-Astrocyte Gap Junctions in Brain Metastasis. *Submitted for publication*

3. Invited Articles:

- Oskarsson, T., Batlle, E. and Massagué, J. Metastatic stem cells. **Cell Stem Cell** 14, 306-321 (2014). PMC 3998185

4. Abstracts: Nothing to report

**Presentations made during the last year.**

b.1. International:

- ISREC Symposium on *Metastatic Colonization*, Crans Montana, Valais, Switzerland

- AACR Annual Meeting Major Symposium on *Cancer Cell Niche*, San Diego, CA

- EMBO Conference on *Cellular Signalling and Cancer Therapy*, Cavtat-Dubrovnik, Croatia

- The Mendel Lecture, Masaryk University, Brno Czech Republic

b.2. National:

- *Deconstructing CNS metastasis,* Neurology Grand Rounds, Albert Einstein College of Medicine, NY

## INVENTIONS, PATENTS AND LICENSES

- Massagué, J., and Valiente, M. Inhibiting Cancer Metastasis. International Patent Application PCT/US14/56379. Filed September 18, 2014. This application claims priority to United States Provisional Application No. 61/879514 filed September 18, 2013.
- Massagué, J, Boire, A., and Chen, Q., Methods For Treating Brain Metastasis. United States Provisional Patent Application No. 62/052,966 Filed September 19, 2014.

## REPORTABLE OUTCOMES

- Identification of L1CAM as a therapeutic target to eliminate disseminated cancer cells.
- Identification of the gap junction modulators tonabersat and meclofenamate as inhibitors of brain metastasis.

## OTHER ACHIEVEMENTS

2013 American Italian Cancer Foundation Prize, to Joan Massagué

## REFERENCES

1. C. DeSantis, J. Ma, L. Bryan, A. Jemal, Breast cancer statistics, 2013. *CA: a cancer journal for clinicians* **64**, 52-62 (2014).
2. National Comprehensive Cancer Network (NCCN) NCCN Clinical Practice Guidelines in Oncology: Breast Cancer, Version 3.2014., (2014).
3. A. F. Chambers, A. C. Groom, I. C. MacDonald, Dissemination and growth of cancer cells in metastatic sites. *Nature reviews. Cancer* **2**, 563-572 (2002).
4. T. Oskarsson, E. Batlle, J. Massague, Metastatic stem cells: sources, niches, and vital pathways. *Cell stem cell* **14**, 306-321 (2014).
5. T. Sato, H. Clevers, Growing self-organizing mini-guts from a single intestinal stem cell: mechanism and applications. *Science* **340**, 1190-1194 (2013).
6. G. Schwank, B. K. Koo, V. Sasselli, J. F. Dekkers, I. Heo, T. Demircan, N. Sasaki, S. Boymans, E. Cuppen, C. K. van der Ent, E. E. Nieuwenhuis, J. M. Beekman, H. Clevers, Functional repair of CFTR by CRISPR/Cas9 in intestinal stem cell organoids of cystic fibrosis patients. *Cell stem cell* **13**, 653-658 (2013).
7. A. Sarkar, K. Hochedlinger, The sox family of transcription factors: versatile regulators of stem and progenitor cell fate. *Cell stem cell* **12**, 15-30 (2013).
8. M. Al-Hajj, M. S. Wicha, A. Benito-Hernandez, S. J. Morrison, M. F. Clarke, Prospective identification of tumorigenic breast cancer cells. *Proceedings of the National Academy of Sciences of the United States of America* **100**, 3983-3988 (2003).
9. J. Holash, P. C. Maisonpierre, D. Compton, P. Boland, C. R. Alexander, D. Zagzag, G. D. Yancopoulos, S. J. Wiegand, Vessel cooption, regression, and growth in tumors mediated by angiopoietins and VEGF. *Science* **284**, 1994-1998 (1999).
10. Y. Kienast, L. von Baumgarten, M. Fuhrmann, W. E. Klinkert, R. Goldbrunner, J. Herms, F. Winkler, Real-time imaging reveals the single steps of brain metastasis formation. *Nature medicine* **16**, 116-122 (2010).
11. M. Lorger, B. Felding-Habermann, Capturing changes in the brain microenvironment during initial steps of breast cancer brain metastasis. *The American journal of pathology* **176**, 2958-2971 (2010).
12. M. Valiente, A. C. Obenauf, X. Jin, Q. Chen, X. H. Zhang, D. J. Lee, J. E. Chaft, M. G. Kris, J. T. Huse, E. Brogi, J. Massague, Serpins promote cancer cell survival and vascular co-option in brain metastasis. *Cell* **156**, 1002-1016 (2014).
13. I. T. Gavrilovic, J. B. Posner, Brain metastases: epidemiology and pathophysiology. *Journal of neuro-oncology* **75**, 5-14 (2005).
14. E. A. Maher, J. Mietz, C. L. Arteaga, R. A. DePinho, S. Mohla, Brain metastasis: opportunities in basic and translational research. *Cancer research* **69**, 6015-6020 (2009).
15. K. J. Stelzer, Epidemiology and prognosis of brain metastases. *Surgical neurology international* **4**, S192-202 (2013).
16. P. D. Bos, X. H. Zhang, C. Nadal, W. Shu, R. R. Gomis, D. X. Nguyen, A. J. Minn, M. J. van de Vijver, W. L. Gerald, J. A. Foekens, J. Massague, Genes that mediate breast cancer metastasis to the brain. *Nature* **459**, 1005-1009 (2009).
17. A. E. Wiencken-Barger, J. Mavity-Hudson, U. Bartsch, M. Schachner, V. A. Casagrande, The role of L1 in axon pathfinding and fasciculation. *Cerebral cortex* **14**, 121-131 (2004).

18.   P. F. Maness, M. Schachner, Neural recognition molecules of the immunoglobulin superfamily: signaling transducers of axon guidance and neuronal migration. *Nature neuroscience* **10**, 19-26 (2007).

19.   Y. J. Boo, J. M. Park, J. Kim, Y. S. Chae, B. W. Min, J. W. Um, H. Y. Moon, L1 expression as a marker for poor prognosis, tumor progression, and short survival in patients with colorectal cancer. *Annals of surgical oncology* **14**, 1703-1711 (2007).

20.   M. Fogel, P. Gutwein, S. Mechtersheimer, S. Riedle, A. Stoeck, A. Smirnov, L. Edler, A. Ben-Arie, M. Huszar, P. Altevogt, L1 expression as a predictor of progression and survival in patients with uterine and ovarian carcinomas. *Lancet* **362**, 869-875 (2003).

21.   J. Hai, C. Q. Zhu, B. Bandarchi, Y. H. Wang, R. Navab, F. A. Shepherd, I. Jurisica, M. S. Tsao, L1 cell adhesion molecule promotes tumorigenicity and metastatic potential in non-small cell lung cancer. *Clinical cancer research : an official journal of the American Association for Cancer Research* **18**, 1914-1924 (2012).

22.   A. Thies, M. Schachner, I. Moll, J. Berger, H. J. Schulze, G. Brunner, U. Schumacher, Overexpression of the cell adhesion molecule L1 is associated with metastasis in cutaneous malignant melanoma. *European journal of cancer* **38**, 1708-1716 (2002).

23.   S. Tsutsumi, S. Morohashi, Y. Kudo, H. Akasaka, H. Ogasawara, M. Ono, K. Takasugi, K. Ishido, K. Hakamada, H. Kijima, L1 Cell adhesion molecule (L1CAM) expression at the cancer invasive front is a novel prognostic marker of pancreatic ductal adenocarcinoma. *Journal of surgical oncology* **103**, 669-673 (2011).

24.   C. Q. Zhu, K. Ding, D. Strumpf, B. A. Weir, M. Meyerson, N. Pennell, R. K. Thomas, K. Naoki, C. Ladd-Acosta, N. Liu, M. Pintilie, S. Der, L. Seymour, I. Jurisica, F. A. Shepherd, M. S. Tsao, Prognostic and predictive gene signature for adjuvant chemotherapy in resected non-small-cell lung cancer. *Journal of clinical oncology : official journal of the American Society of Clinical Oncology* **28**, 4417-4424 (2010).

25.   M. M. Winslow, T. L. Dayton, R. G. Verhaak, C. Kim-Kiselak, E. L. Snyder, D. M. Feldser, D. D. Hubbard, M. J. DuPage, C. A. Whittaker, S. Hoersch, S. Yoon, D. Crowley, R. T. Bronson, D. Y. Chiang, M. Meyerson, T. Jacks, Suppression of lung adenocarcinoma progression by Nkx2-1. *Nature* **473**, 101-104 (2011).

26.   C. T. Guy, M. A. Webster, M. Schaller, T. J. Parsons, R. D. Cardiff, W. J. Muller, Expression of the neu protooncogene in the mammary epithelium of transgenic mice induces metastatic disease. *Proceedings of the National Academy of Sciences of the United States of America* **89**, 10578-10582 (1992).

27.   D. X. Nguyen, A. C. Chiang, X. H. Zhang, J. Y. Kim, M. G. Kris, M. Ladanyi, W. L. Gerald, J. Massague, WNT/TCF signaling through LEF1 and HOXB9 mediates lung adenocarcinoma metastasis. *Cell* **138**, 51-62 (2009).

28.   E. Lim, N. U. Lin, Updates on the Management of Breast Cancer Brain Metastases. *Oncology* **28**,  (2014).

29.   S. Taimur, M. J. Edelman, Treatment options for brain metastases in patients with non-small-cell lung cancer. *Current oncology reports* **5**, 342-346 (2003).
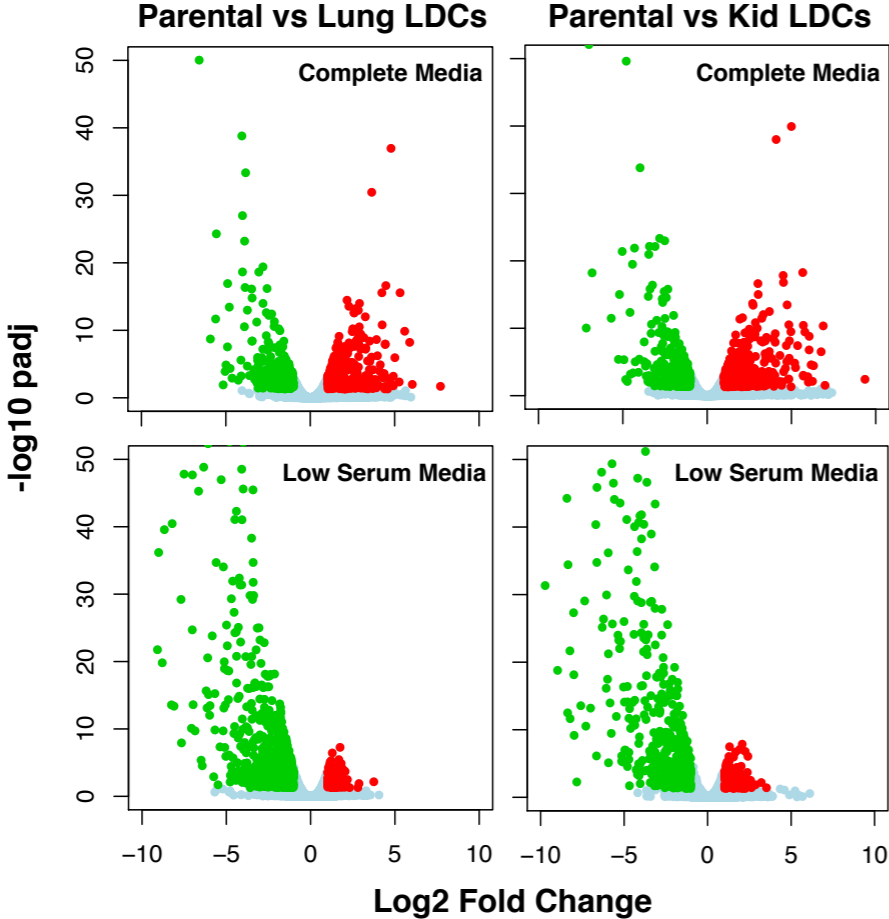
## APPENDICES

- **Figure 1. Genes and pathways activated in LMBC and LMLC lines - Progress 2.1**
  (A-B) Gene expression profile of lung and kidney LMLC lines. (A) Volcano blots showing differentially expressed genes in LMLC lines in comparison to parental population under conditions of stress. (B) Bar graph highlighting the differentially expressed genes under normal and stress conditions in LMLC lines. (C) Gene ontology analysis on the differentially down-regulated genes in LMLC lines. (D) Heat map highlighting the enriched expression of Sox transcription factors family members in LMLC lines. (E) Enrichment of CD44$^{high}$/CD24$^{low}$ surface marker expression in LMBCs.

- **Figure 2. Functional relevance of LMBC genes and pathways - Progress 4.1**
  (A) GFP positive H2030-BRM3 cells coopting the basal lamina rich in collagen IV of endothelial cells. bl, basal lamina, e, endothelium, cc, cancer cell. (B) Immuno-histochemical staining with anti-L1CAM antibodies and H&E counter staining of incipient lesions formed by H2030-BrM3 cancer cells. (C-E) The effect of L1CAM depletion on H2030-BrM3, MDA-231-BrM2 and PC9-BrM3 cells infiltrating brain 21 days post-intracardiac injection.

- **Figure 3. Functional relevance of LMBC genes and pathways - Progress 4.1**
  (A) Intracardiac injection of MDA231 BoM cells results in Bone metastasis, which is drastically reduced upon L1CAM knockdown. (B) MDA231-LM2 metastasis to lung following tail vain injection is reduced upon L1CAM knockdown. (C) Primary tumor growth and metastasis to lung and liver following mammary fat pad injection of MDA231 LM2 cells are inhibited upon L1CAM knockdown.

- **Figure 4. Functional relevance of LMBC genes and pathways - Progress 4.2**
  (A) Schematic illustration of luciferase complementary assay to detect the Cx43-PCDH7 interactions. NLuc: firefly luciferase N-terminal half; CLuc: luciferase C-terminal half. (B) Index of cell lines expressing split luciferase vector combinations for luciferase reconstitution assays. (C) Western immunoblotting analysis of Cx43 and PCDH7 in test cell lines. Samples are coded as indicated in (B). (D) Luciferase reconstitution assays of the cell lines described in (B). (E) Luciferase reconstitution and quantification of bioluminescence after co-culture of astrocytes with cancer cells expressing Cx43-CLuc and PCDH7-NLuc. (F) Schematic summary of Cx43-PCDH7 interactions.

- **Figure 5. Functional relevance of LMBC genes and pathways - Progress 4.2**
  (A) Experimental design for short-term brain metastasis assay. (B) Number of control (Ctrl), Cx43- or PCDH7-depleted MDA231-BrM2 cells in the brain parenchyma 7 days after cancer cell inoculation into mice. (C) Ki67 staining of 14-day brain lesions in the same experiments. Representative images shows GFP (green) and Ki67 (red) staining in cancer cells. (D) The cell content of brain metastatic colonies formed by control, Cx43- or PCDH7-depleted MDA231-BrM2 cells in (C) was determined and plotted based on lesion size range.
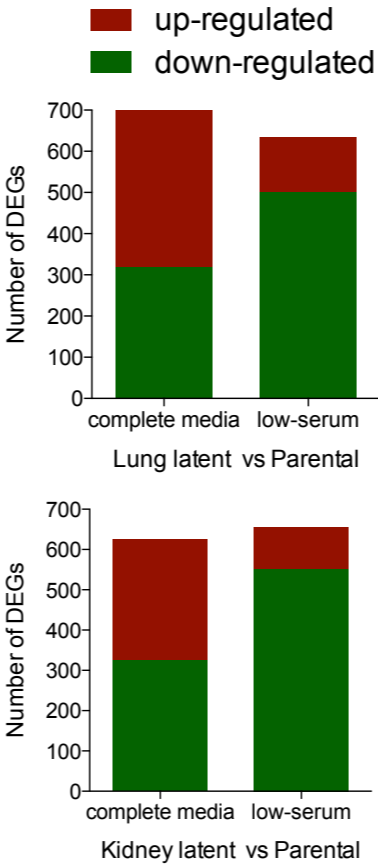
- **Figure 6. Functional relevance of LMBC genes and pathways - Progress 4.4**
  Heat map of signaling pathway classifiers highlighting the strength of each pathway in LMLC lines compared to parental populations.

- **Figure 7. Clinical relevance of LMLC genes and pathways - Progress 5.1**
  (A) Representative brain metastasis tissue microarray cores from NSCLC cases stained with anti-L1CAM antibodies. Arrowhead: cell interfaces. Scale bar, 100 mm. (B) Twenty-nine NSCLC brain metastasis samples were scored as ++ (high), + (low), or - (undetectable), according to the content of L1CAM-positive cells. The number of samples scoring in each level is indicated at the bottom of the panel.

- **Figure 8. Mechanism of action of LMBC genes and pathways - Progress 6.2**
  (A) Doxycycline-inducible L1CAM knockdown starting on day 14 following intracardiac injection of H2030 BrM cells inhibits metastasis. (B-C) Following the treatment regimens in the schema (B), brain metastasis burden was quantified by ex vivo BLI at day 35 after daily application of tonabersat (Tona) or meclofenamate (Meclo) in combination with carboplantin (C).

- **Valiente et al, Cell 156, 1002-1016 (2014)**

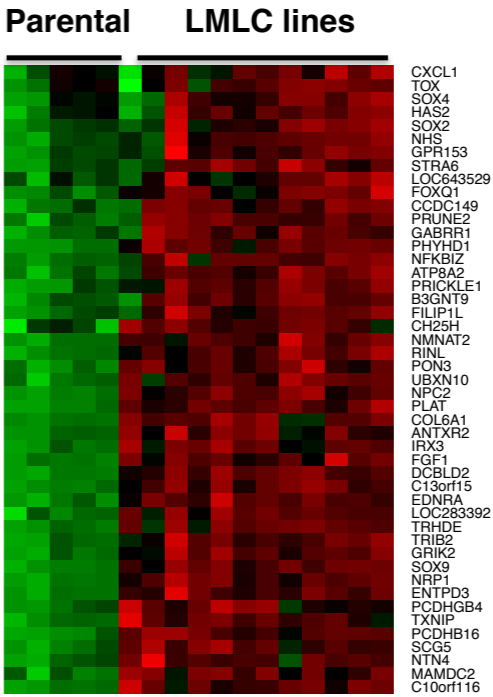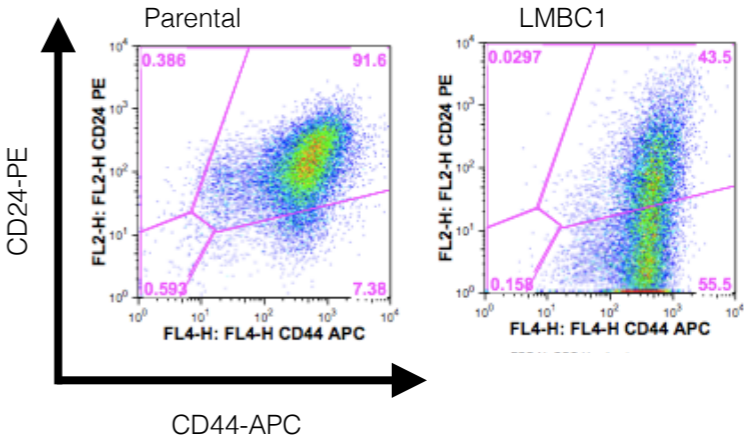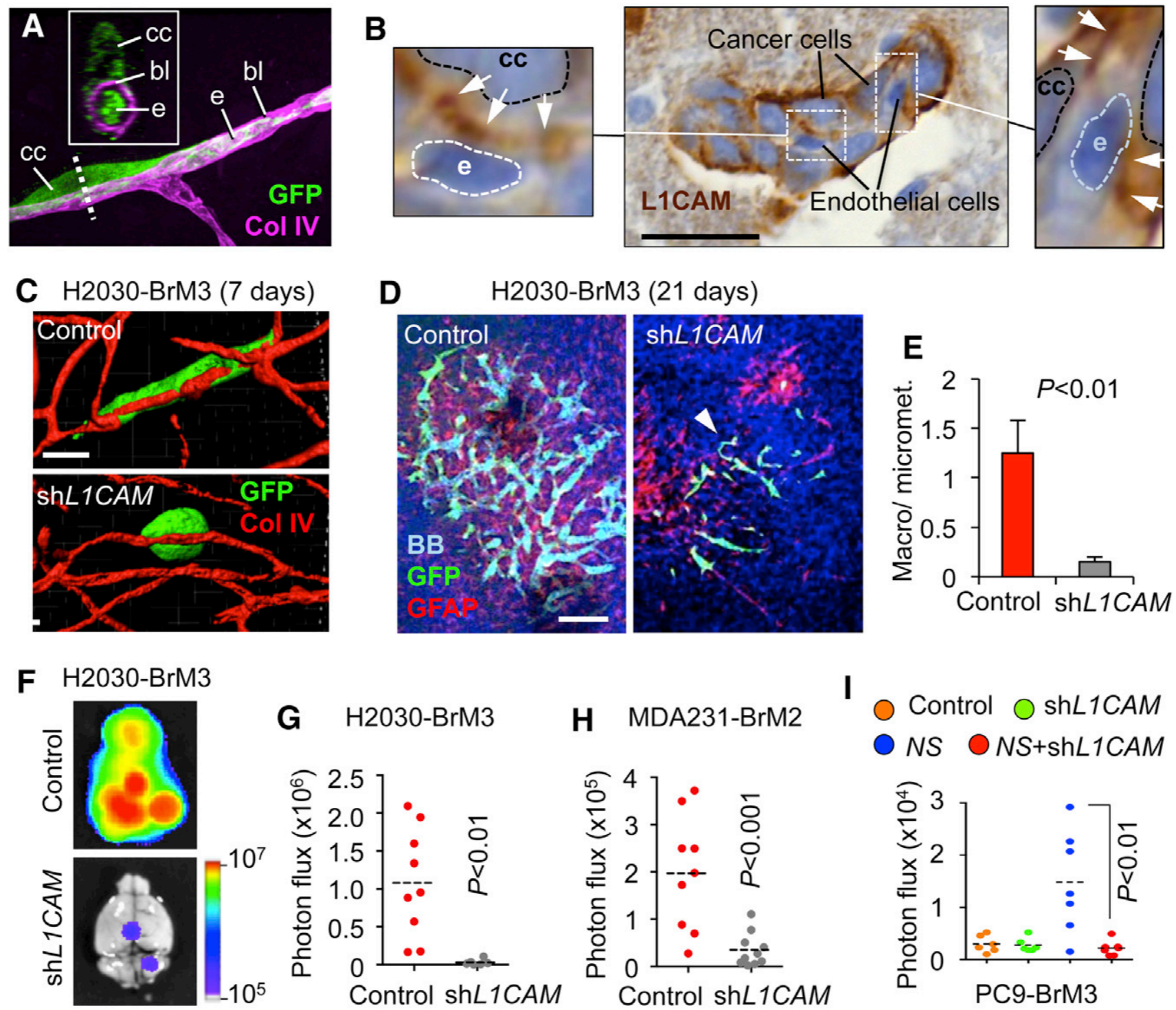- **Chen et al, manuscript submitted for publication.**

**Figure 1**

**A**

Parental vs Lung LDCs — Parental vs Kid LDCs

Complete Media / Low Serum Media

-log10 padj vs Log2 Fold Change

**B**

up-regulated
down-regulated

Number of DEGs — Lung latent vs Parental (complete media, low-serum)

Number of DEGs — Kidney latent vs Parental (complete media, low-serum)

**C**

| Category | Term | Gene ontology analysis | | Count | P Value |
|---|---|---|---|---|---|
| GOTERM_CC_FAT | GO:0031224~intrinsic to membrane | | | 199 | 2.82E-02 |
| GOTERM_CC_FAT | GO:0005886~plasma membrane | | **Cellular Component** | 164 | 1.21E-05 |
| GOTERM_CC_FAT | GO:0005576~extracellular region | | | 78 | 6.75E-02 |
| GOTERM_CC_FAT | GO:0005887~integral to plasma membrane | | | 62 | 2.15E-04 |
| GOTERM_BP_FAT | GO:0007166~cell surface receptor linked signal transduction | | | 77 | 8.98E-03 |
| GOTERM_BP_FAT | GO:0007242~intracellular signaling cascade | | **Biological Process** | 63 | 2.33E-04 |
| GOTERM_BP_FAT | GO:0042127~regulation of cell proliferation | | | 42 | 1.04E-03 |
| GOTERM_BP_FAT | GO:0006357~regulation of transcription from RNA polymerase II promoter | | | 37 | 4.75E-03 |
| GOTERM_BP_FAT | GO:0043067~regulation of programmed cell death | | | 37 | 2.33E-02 |
| GOTERM_MF_FAT | GO:0005509~calcium ion binding | | | 41 | 1.86E-02 |
| GOTERM_MF_FAT | GO:0003700~transcription factor activity | | **Molecular Function** | 39 | 8.53E-02 |
| GOTERM_MF_FAT | GO:0008092~cytoskeletal protein binding | | | 23 | 6.77E-02 |
| GOTERM_MF_FAT | GO:0046873~metal ion transmembrane transporter activity | | | 17 | 5.11E-02 |

**D**

Parental — LMLC lines

CXCL1, TOX, SOX4, HAS2, SOX2, NHS, GPR153, STRA6, LOC643529, FOXQ1, CCDC149, PRUNE2, GABRR1, PHYHD1, NFKBIZ, ATP8A2, PRICKLE1, B3GNT9, FILIP1L, CH25H, NMNAT2, RINL, PON3, UBXN10, NPC2, PLAT, COL6A1, ANTXR2, IRX3, FGF1, DCBLD2, C13orf15, EDNRA, LOC283392, TRHDE, TRIB2, GRIK2, SOX9, NRP1, ENTPD3, PCDHGB4, TXNIP, PCDHB16, SCG5, NTN4, MAMDC2, C10orf116

**E**

Parental — LMBC1

CD24-PE vs CD44-APC

Parental: 0.386, 91.6, 0.593, 7.38
LMBC1: 0.0297, 43.5, 0.158, 55.5

**Figure 2**



**A** cc, bl, e, GFP, Col IV

**B** cc, e, Cancer cells, Endothelial cells, L1CAM

**C** H2030-BrM3 (7 days) — Control, shL1CAM, GFP, Col IV

**D** H2030-BrM3 (21 days) — Control, shL1CAM, BB, GFP, GFAP

**E** Macro/micromet. — Control, shL1CAM, *P*<0.01

**F** H2030-BrM3 — Control, shL1CAM, 10^7, 10^5

**G** H2030-BrM3 — Photon flux (x10^6), Control, shL1CAM, *P*<0.01

**H** MDA231-BrM2 — Photon flux (x10^5), Control, shL1CAM, *P*<0.001

**I** Control, shL1CAM, NS, NS+shL1CAM — Photon flux (x10^4), PC9-BrM3, *P*<0.01

# Figure 3

**A**



MDA231-BoM2

$P<0.0001$

Normalized whole body photon flux ($\times 10^3$)

Control    sh*L1CAM*

Bone

$10^7$

$10^5$

**B**



MDA231-LM2

$P<0.0001$

Normalized lung photon flux

Control    sh*L1CAM*

$2\times10^5$

$2\times10^4$

**C**



MDA231-LM2 Fat pad

● Control
● sh*L1CA*M

Tumor volume ($\times 10^3$ mm$^3$)

$P<0.05$

Weeks

% animals with tumor

Lungs    80%    50%

Liver    50%    17%

Control    sh*L1CAM*

$2\times10^7$

$2\times10^5$

9 weeks

**Figure 4**



**A** Cx43  PCDH7

CLuc  NLuc

**B**

| | 1 | 2 | 3 | 4 | 5 | 6 |
|---|---|---|---|---|---|---|
| Cx43-Nluc | - | - | - | + | - | - |
| Cx43-CLuc | - | + | - | + | + | + |
| PCDH7-NLuc | - | - | + | - | Low | High |

**C**

MDA231  H2030

1 5 6 4  1 5 6 4

PCDH7

Cx43

tubulin

**D**

MDA231  H2030

**E**

Cancer cells ± Astrocytes $\xrightarrow{15min}$ BLI

MDA231  H2030

Astro: − +  − +

Normalized signal

Astro: − +  − +

MDA231 BrM2  H2030 BrM3

**F**

Astrocyte

PCDH7
Cx43
Split Luc

Cancer cell

# Figure 5

**A**

Cancer cells

5 weeks

Ex vivo brain
bioluminescence
analysis and
quantification

**B**

*Cx43*

*PCDH7*

Control    sh1    sh2    sh1    sh2

$x10^6$

1

4

**C**

MDA231-BrM2

*P<0.003*
*P<0.002*

Photon Flux ($10^6$)

Ctrl  sh1  sh2  sh1  sh2
      *Cx43*   *PCDH7*

H2030-BrM3

*P<0.006*
*P<0.002*

Ctrl  sh1  sh2  sh1  sh2
      *Cx43*   *PCDH7*

Kras/p53-393N1

*P=0.01*
*P=0.002*

Ctrl  sh1  sh1  sh2
      *Cx43*   *PCDH7*

**D**

Control    *Cx43* sh1    *PCDH7* sh1

1    2    3

1

2    3

# of lesions/brain

> 1 mm
0.1-1 mm
0.1 mm

Control    shCx43    shPCDH7

800000

600000

con+HA
sh1+HA
sh3+ha
sh7+ha
sh11+HA

**Figure 6**

Bioinformatic signaling pathway classifiers



| Parental | LMLC lines | Pathway | P Val |
|---|---|---|---|
| | | WNT_TCF | 4E-05 |
| | | MYC | 2E-04 |
| | | NFKB | 8E-03 |
| | | bCATININE | 7E-02 |
| | | TNC | 1E-02 |
| | | TGFb | 8E-02 |
| | | Src | 2E-01 |
| | | RAS | 2E-01 |
| | | AKT | 3E-01 |
| | | E2F1 | 6E-01 |

**Color Key**

−0.4    0    0.2
Value

**Figure 7**



**A** NSCLC brain metastasis

Ig control · L1CAM

**B** L1CAM

++ · + · −

n= 4 · n= 14 · n=13

Human NSCLC brain metastases

# Figure 8

**A**

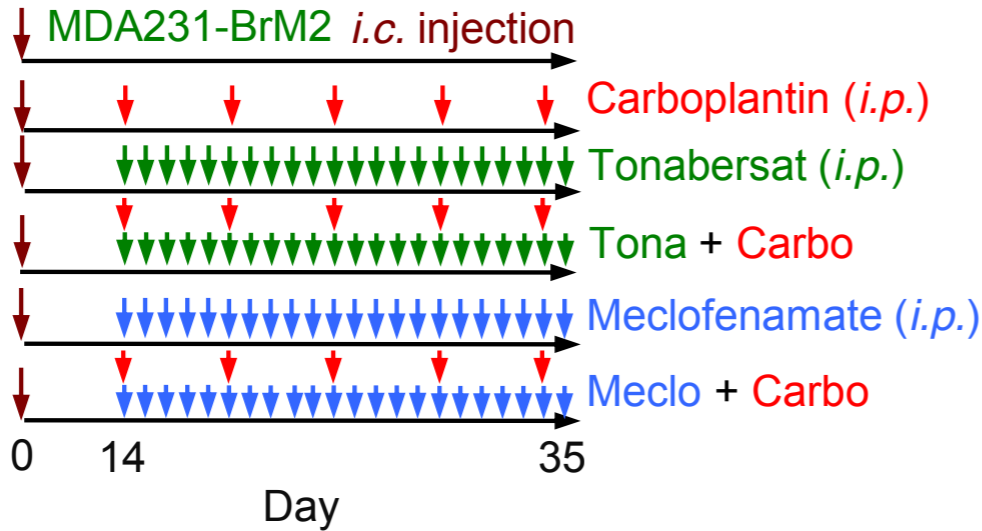Dox inducible shL1CAM
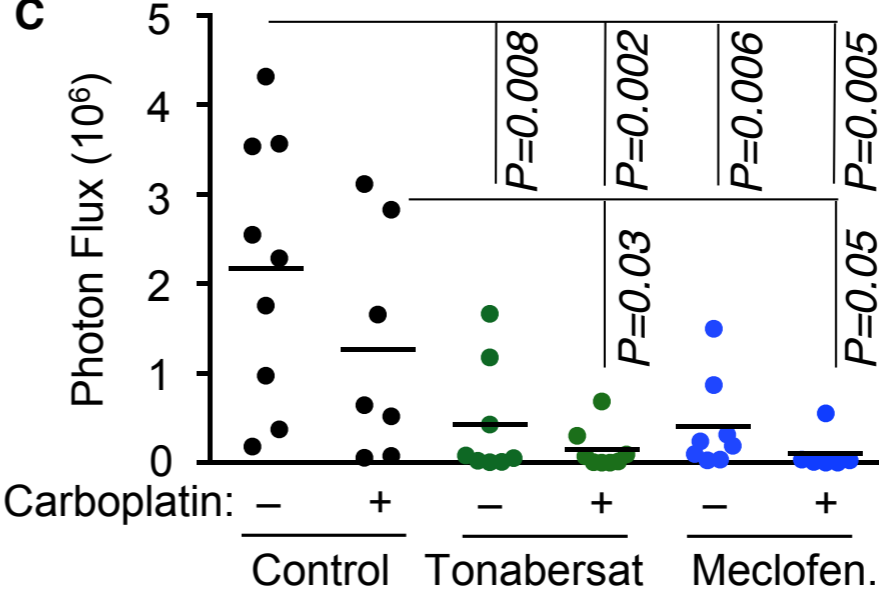Whole Animal Bioluminescence, Day 28



**B**



**C**

# Serpins Promote Cancer Cell Survival and Vascular Co-Option in Brain Metastasis

Manuel Valiente,[1] Anna C. Obenauf,[1] Xin Jin,[1] Qing Chen,[1] Xiang H.-F. Zhang,[1,8] Derek J. Lee,[1] Jamie E. Chaft,[2] Mark G. Kris,[2] Jason T. Huse,[3,4] Edi Brogi,[5] and Joan Massagué[1,4,6,7,*]

[1]Cancer Biology and Genetics Program
[2]Department of Medicine
[3]Human Oncology and Pathogenesis Program
[4]Brain Tumor Center
[5]Department of Pathology
[6]Metastasis Research Center
Memorial Sloan Kettering Cancer Center, New York, NY 10065, USA
[7]Howard Hughes Medical Institute, Chevy Chase, MD 21205, USA
[8]Present address: Lester and Sue Smith Breast Center, Baylor College of Medicine, One Baylor Plaza, Houston, TX 77030, USA
*Correspondence: j-massague@ski.mskcc.org
http://dx.doi.org/10.1016/j.cell.2014.01.040

## SUMMARY

**Brain metastasis is an ominous complication of cancer, yet most cancer cells that infiltrate the brain die of unknown causes. Here, we identify plasmin from the reactive brain stroma as a defense against metastatic invasion, and plasminogen activator (PA) inhibitory serpins in cancer cells as a shield against this defense. Plasmin suppresses brain metastasis in two ways: by converting membrane-bound astrocytic FasL into a paracrine death signal for cancer cells, and by inactivating the axon pathfinding molecule L1CAM, which metastatic cells express for spreading along brain capillaries and for metastatic outgrowth. Brain metastatic cells from lung cancer and breast cancer express high levels of anti-PA serpins, including neuroserpin and serpin B2, to prevent plasmin generation and its metastasis-suppressive effects. By protecting cancer cells from death signals and fostering vascular co-option, anti-PA serpins provide a unifying mechanism for the initiation of brain metastasis in lung and breast cancers.**

## INTRODUCTION

Metastasis is the main cause of death from cancer, but biologically, metastasis is a rather inefficient process. Most cancer cells that leave a solid tumor perish, and much of this attrition happens as circulating cancer cells infiltrate distant organs (Chambers et al., 2002). Although mechanisms for early steps of tumor cell dispersion and late stages of macrometastatic outgrowth are known (Valastyan and Weinberg, 2011; Vanharanta and Massagué, 2013), the factors that determine the survival and adapta-

tion of disseminated cancer cells in vital organs remain obscure. Identifying these factors is particularly critical in the case of brain metastasis. Brain relapse is the most devastating complication of cancer, with acute neurologic distress and high mortality being typical traits (Gavrilovic and Posner, 2005). The incidence of brain metastasis is ten times higher than that of all primary brain tumors combined (Maher et al., 2009). Lung cancer and breast cancer are the top sources of brain metastasis, together accounting for nearly two-thirds of total cases. However, it is in the brain that infiltrating cancer cells face a particularly high rate of attrition, as shown in experimental models (Kienast et al., 2010). Brain metastasis tends to be a late complication of cancer in the clinic (Feld et al., 1984; Karrison et al., 1999) and is rare in mice with genetically engineered tumors that readily metastasize to other organs (Francia et al., 2011; Winslow et al., 2011).

The severe attrition of metastatic cells in the brain and the late occurrence of brain metastasis in the clinic argue that circulating cancer cells face major hurdles in colonizing this organ. Cancer cells require specialized mechanisms to traverse the blood-brain barrier (BBB), and molecular mediators of this process were recently identified (Bos et al., 2009; Li et al., 2013). However, most cancer cells that pass the BBB die (Heyn et al., 2006; Kienast et al., 2010). Interestingly, cancer cells that succeed in infiltrating the brain present the striking feature of adhering to the surface of capillaries and growing as a sheath around the vessels, whereas those that fail to co-opt the vasculature also fail to thrive (Carbonell et al., 2009; Kienast et al., 2010; Lorger and Felding-Habermann, 2010). What kills most cancer cells that pass through the BBB, and what enables the few survivors to co-opt the vasculature are questions of biologic and clinical interest.

Seeking to define common mechanisms for metastatic colonization of the brain, we focused on a small set of genes whose expression is associated with brain metastatic phenotypes in

both lung and breast adenocarcinoma models. One of these genes, *SERPINI1*, encoding the plasminogen activator (PA) inhibitor neuroserpin (NS), is normally expressed mainly in the brain. Tissue PA (tPA) and urokinase PA (uPA) convert plasminogen into plasmin, an endopeptidase that mediates fibrinolysis in blood clot resolution and is also involved in the stromal response to brain injury (Benarroch, 2007; Sofroniew and Vinters, 2010). Reactive astrocytes are major sources of PAs in ischemia and neurodegenerative injury (Adhami et al., 2008; Ganesh and Chintala, 2011; Teesalu et al., 2001). To avert the deleterious action of plasmin, neurons express NS (Yepes et al., 2000). We found that by secreting PA inhibitory serpins, brain metastatic cells thwart the lethal action of plasmin from the reactive stroma. Moreover, suppression of Fas-mediated cancer cell killing and promotion of L1 cell adhesion molecule (L1CAM)-mediated vascular co-option lie downstream of anti-PA serpin action as critical requirements for the initiation of brain metastasis.

## RESULTS

### Association of PA-Inhibitory Serpins with the Brain Metastatic Phenotype

To identify shared mediators of brain metastasis, we compared the transcriptomic signatures of brain metastatic subpopulations (BrM) that were isolated from the lymph-node-derived human lung adenocarcinoma cell lines H2030 and PC9 (Nguyen et al., 2009) and the pleural-effusion-derived breast cancer cell lines MDA-MB-231 (MDA231 for short) and CN34 (Bos et al., 2009; Figure 1A). Seven genes were upregulated in brain metastatic cells compared with the source parental lines in at least three of the four models (Figure S1A available online). Among these genes, *LEF1* was previously defined as a mediator of WNT signaling in brain metastasis (Nguyen et al., 2009). Of the remaining genes, only *SERPINI1*, encoding NS, was associated with brain relapse in human primary tumors (see below). This was intriguing because NS expression is normally restricted to neurons, where it protects against PA cytotoxicity (Yepes et al., 2000).

The 36 serpin family members in human collectively target 18 proteases (Irving et al., 2000). Four serpins (NS and serpins B2, E1, and E2) selectively inhibit PA (Law et al., 2006). The mRNA levels for three of the four were upregulated >3-fold in brain metastatic cells (Figure 1A). Only one other serpin, *SERPIND1*, was also upregulated (Figure 1A). Serpin D1 inhibits thrombin, which cooperates with plasminogen in cerebral injury (Fujimoto et al., 2008). Bone metastatic derivatives (MDA231-BoM) (Kang et al., 2003) and lung metastatic derivatives (MDA231-LM2) (Minn et al., 2005) were available for comparisons with MDA231-BrM2, and showed little or no upregulation of the serpins (Figure 1B).

Additionally, we established the cell line ErbB2-P from a mouse mammary tumor driven by a mutant *ErbB2* transgene (Muller et al., 1988) and then isolated a brain metastatic derivative (ErbB2-BrM2) by selection of ErbB2-P in congenic mice. ErbB2-BrM2 cells showed a strong upregulation of serpins B2 and D1 compared with ErbB2-P (Figure 1A). We also screened four cell lines derived from lymph node metastases of genetically engineered *Kras*$^{G12D}$*;p53*$^{-/-}$ mouse lung adenocarcinomas (Winslow et al., 2011). All four lines were highly metastatic

to visceral organs but ranged widely in brain metastatic activity (Figures 1C and S1B), and brain metastasis was associated with high expression of serpins I1, B2, E2, and/or D1 (Figures 1C and 1D).

The upregulation of NS and serpin B2 in brain metastatic cells was confirmed at the protein level (Figures S1C and S1D). Moreover, conditioned media from brain metastatic cells inhibited the generation of plasmin activity from plasminogen (Figures 1E, 1F, and S1E). The only exception was PC9-BrM3, a cell line that is less aggressive in brain metastasis compared with H2030-BrM3 (Nguyen et al., 2009) and lacks upregulated anti-PA serpins (Figures 1A, S1C, and S1D).
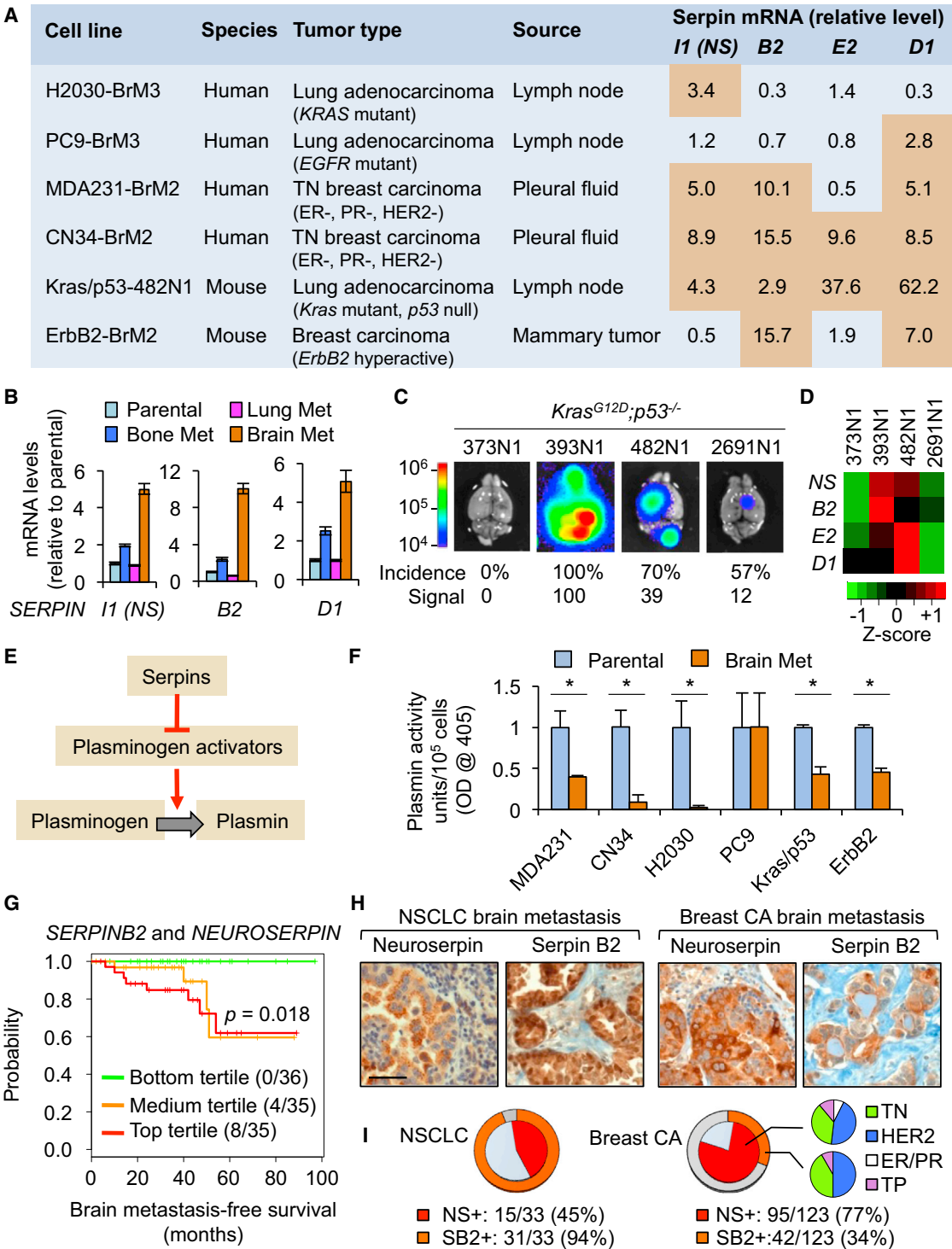
### NS and Serpin B2 in Human Brain Metastasis Tissues

Focusing on the two most frequently upregulated anti-PA serpins in these models, NS and serpin B2, we queried gene-expression data from 106 primary lung adenocarcinomas with relapse annotation (Nguyen et al., 2009). The expression level of *SERPINI1* and *SERPINB2* in the tumors was associated with brain relapse, both as individual genes (data not shown) and combined (p = 0.018, hazard ratio = 2.33 ± 0.3; Figure 1G). Expression of the two genes was not significantly associated with metastasis to bone or lungs (p = 0.89, hazard ratio = 0.91 ± 0.33; p = 0.36, hazard ratio = 0.76 ± 0.27; Figures S1F and S1G). *SERPINI1* and *SERPINB2* expression in breast tumors was not a predictor of brain metastasis (p = 0.21, hazard ratio = 0.96 ± 0.16; Figure S1H), though in most of these cases brain relapse was a late event that might have been seeded from metastases in other organs.

We performed an immunohistochemical analysis of NS and serpin B2 in human brain metastasis tissue using mouse brain lesions formed by serpin-expressing human cancer cells as a reference (Figure S1I). Among 33 metastases of non-small-cell lung carcinomas (NSCLCs), 45% scored positive for NS and 94% scored positive for serpin B2. Among 123 metastases from various subtypes of breast cancer, 77% scored positive for NS and 34% scored positive for serpin B2 (Figures 1H, 1I, S1I, and S1J). The immunoreactivity was distributed diffusely in the cytoplasm of carcinoma cells and only minimally in the scant extracellular stroma. Positivity for NS and serpin B2 in the inflammatory infiltrate was limited.

### Plasmin Is Lethal to Cancer Cells that Invade the Brain Parenchyma

The MDA231-BrM2 and H2030-BrM3 models are metastatic to the brain from orthotopic tumors and the arterial circulation (Bos et al., 2009; Nguyen et al., 2009). We inoculated these cells into the arterial circulation of immunodeficient mice via the left cardiac ventricle and fixed the tissue to count cancer cells lodged in the brain capillary network at different time points (Figures 2A–2C and S2A). One day after inoculation, we observed isolated cancer cells trapped within brain capillaries (Figure 2B, and H2030-BrM3 data not shown). Cells passing through the BBB were observed between days 2 and 7 after inoculation (Figures 2B and S2B). All cells that remained within capillaries on day 7 stained positive for the apoptosis marker, cleaved caspase-3 (Figures S2C and S2D). No intravascular cells were observed thereafter. In parental MDA231, the number of extravasated cells

**A**

| Cell line | Species | Tumor type | Source | Serpin mRNA (relative level) | | | |
|---|---|---|---|---|---|---|---|
| | | | | I1 (NS) | B2 | E2 | D1 |
| H2030-BrM3 | Human | Lung adenocarcinoma (*KRAS* mutant) | Lymph node | 3.4 | 0.3 | 1.4 | 0.3 |
| PC9-BrM3 | Human | Lung adenocarcinoma (*EGFR* mutant) | Lymph node | 1.2 | 0.7 | 0.8 | 2.8 |
| MDA231-BrM2 | Human | TN breast carcinoma (ER-, PR-, HER2-) | Pleural fluid | 5.0 | 10.1 | 0.5 | 5.1 |
| CN34-BrM2 | Human | TN breast carcinoma (ER-, PR-, HER2-) | Pleural fluid | 8.9 | 15.5 | 9.6 | 8.5 |
| Kras/p53-482N1 | Mouse | Lung adenocarcinoma (*Kras* mutant, *p53* null) | Lymph node | 4.3 | 2.9 | 37.6 | 62.2 |
| ErbB2-BrM2 | Mouse | Breast carcinoma (*ErbB2* hyperactive) | Mammary tumor | 0.5 | 15.7 | 1.9 | 7.0 |

**Figure 1. Association of PA-Inhibitory Serpins with the Brain Metastatic Phenotype**

(A) Serpin mRNA levels in brain metastatic cell lines relative to the levels in counterparts not metastatic to brain. TN, triple negative; ER−, estrogen receptor negative; PR−, progesterone receptor negative.

(B) mRNA levels of the indicated serpins in the parental MDA231 cell line and derivatives with different metastatic tropisms. Error bars, 95% confidence interval.

(C) Representative ex vivo bioluminescence images of brains from syngeneic mice inoculated with $Kras^{G12D};p53^{-/-}$ mouse lung cancer cell lines. The percentage of mice that developed brain metastasis and the mean BLI photon flux signal are indicated. n = 10.

(D) Heatmap of serpin mRNA expression in $Kras^{G12D};p53^{-/-}$ derivatives.

*(legend continued on next page)*

dropped sharply after day 5 and rarely recovered (Figure S2B). In line with previous reports (Kienast et al., 2010; Lorger and Feld-ing-Habermann, 2010), >90% of cancer cells that entered the brain disappeared within days. In MDA231-BrM2, the number of extravasated cells increased until day 7 and then dropped sharply by day 10, but recovered by day 16. The survivors were bound to and stretched over the abluminal surface of brain capillaries (Figures 2A and 2B). Outgrowth occurred mainly on co-opted vessels (Figure 2C; summarized in Figure 2D).

In the brain, metastatic cells were in close proximity to astro-cytes (Figures 2E, S2E, and S2F), microglia, and neurons (Figures S2G–S2J). Reactive astrocytes, identified by high glial fibrillary acidic protein (GFAP) expression and a stellate morphology, were associated with cancer cells right after extrav-asation and thereafter (Figures 2E, S2E, and S2F). Reactive astrocytes are a major source of PA in brain injury (Adhami et al., 2008; Ganesh and Chintala, 2011). Indeed, mouse brain sections harboring metastatic cells showed tPA and uPA immu-noreactivity associated with astrocytes (Figures 2F and 2G). Mouse astrocytes cultures were superior to microglia for con-verting plasminogen to plasmin (Figure S2K). Neurons produce plasminogen for neurite and synapse formation (Gutiérrez-Fer-nández et al., 2009). Plasminogen immunoreactivity was associ-ated with NeuN+ neurons near metastatic cells in mouse brain (Figure 2H). Thus, the brain metastasis microenvironment con-tains the necessary components for plasmin production.

To determine whether plasmin is harmful to metastatic cells in the brain parenchyma, we used mouse brain slice cultures (Fig-ure 2I). When placed on top of brain slices, H2030-BrM3 cells migrated into the tissue, targeted blood capillaries, and spread on the surface of the vessels (Figure 2J). H2030-BrM3 cells proliferated under these conditions (Figures 2K and 2L), whereas parental H2030 did not proliferate (Figures 2K and 2L) and under-went apoptosis (Figures 2M and 2N). Similar results were ob-tained with MDA231 cells (Figure S2N). In cocultures of cancer cells with astrocytes and microglia, plasminogen addition trig-gered apoptosis in parental H2030, but not in H2030-BrM3 (Fig-ures S2L and S2M). The brain slices contained endogenous plasmin activity, and addition of a plasmin inhibitor, α2-antiplas-min (Bajou et al., 2008), inhibited this activity (Figures S2O and S2P) and increased the survival of parental H2030 cells in the slices (Figures 2K–2N). Of note, addition of plasmin to cancer cell monolayer cultures did not trigger apoptosis (Figure S2Q). These results suggested that plasmin acting through unknown substrates kills infiltrating cancer cells in the brain, whereas highly metastatic cells are shielded from this threat (Figure 2O).

## NS Protects Metastatic Cells from Plasmin-Mediated Attrition

To investigate the role of NS in brain metastasis, we first used the H2030-BrM3 model, in which only this serpin is upregulated (refer to Figure 1A). Brain lesions formed by H2030-BrM3 cells showed strong NS immunoreactivity (Figure S3A). Two small hairpin RNAs (shRNAs) that decreased NS expression and secretion by >85% (Figures S3B and S3C) did not affect the growth of H2030-BrM3 cells in culture (Figure S3D) but inhibited the metastatic activity of these cells, as shown by bioluminescence imaging (BLI) of marker luciferase in vivo (Figures 3A–3D), BLI ex vivo (Figure 3B), and marker GFP expression in brain sections (Figure 3E). NS depletion in H2030-BrM3 decreased the number and size of brain lesions (Figures 3F and S3E), with a >90% overall reduction in brain tumor burden (Figure 3G). The few macroscopic lesions that developed were rich in NS (Figure S3F), suggesting escape from the knockdown.

NS knockdown did not inhibit the entry of H2030-BrM3 cells into the brain parenchyma (Figure S3G) or their ability to cross an endothelial/astrocyte BBB-like barrier in vitro, whereas the knockdown of ST6GalNaC5, a mediator of BBB extravasation, did (Bos et al., 2009; Figures S3H and S3I). In brain slice assays, NS knockdown in H2030-BrM3 cells decreased the number of infiltrated cells (Figures 3H and 3I) and increased apoptosis (Fig-ures 3H and 3J), whereas overexpression of NS in parental H2030 and MDA231 cells had the opposite effects (Figures 3K and 3L).

## Brain Metastasis Mediated by the PA Inhibitory Function of NS

PC9-BrM3 can infiltrate the brain but are less aggressive than H2030-BrM3 in colonizing it (Nguyen et al., 2009) and show no upregulation of anti-PA serpins (refer to Figure 1A). PC9-BrM3 cells were stably transduced with vectors encoding the wild-type NS or a mutant (NSΔloop) that is devoid of PA inhibitory function (Takehara et al., 2009; Figures S3J–S3M). Wild-type NS significantly increased the brain metastatic activity of PC9-BrM3, whereas the mutant did not (Figures 3M and 3N). PC9-BrM3 cells are also metastatic to bone (Nguyen et al., 2009), and NS overexpression did not markedly affect this activity (Figures 3M and 3N). NS$^{\Delta loop}$ was also ineffective at protecting the parental H2030 and MDA231 cells from apoptosis in brain tissue (Figures 3K and 3L). These results suggest that NS mediates brain metastatic activity in cancer cells by inhibiting PA.

(E) Summary of the serpin-PA-plasmin cascade.

(F) Inhibition of plasminogen conversion into plasmin by cell culture supernatants of the indicated cell lines. Plasmin activity was determined by a chromogenic assay. Data are averages ± SEM from triplicate experiments.

(G) Kaplan-Meier analysis of brain-metastasis-free survival in 106 cases of lung adenocarcinoma classified based on SERPINB2 and SERPINI1 mRNA levels in the primary tumor. The p value was calculated from a Cox proportional hazard model, with SERPINB2 and SERPINI1 expression treated as a continuous variable.

(H) Representative human brain metastasis samples from lung and breast cancer stained with antibodies against NS or serpin B2.

(I) Proportion of metastasis samples that scored positive for NS immunostaining (red) or serpin B2 immunostaining (orange) in 33 cases of NSCLC and 123 cases of breast carcinoma. Small diagrams in the breast cancer set represent the primary tumor subtype (HER2, HER2+; ER/PR, hormone-receptor positive; TP, triple positive) of the serpin-positive samples for which this information was available. Brain metastases that scored positive for both serpins comprised 42% and 34% of the lung cancer and breast cancer cases, respectively. Samples scored as positive had >80% of neoplastic cells showing positive reactivity.

Scale bar, 100 μm. See also Figure S1.
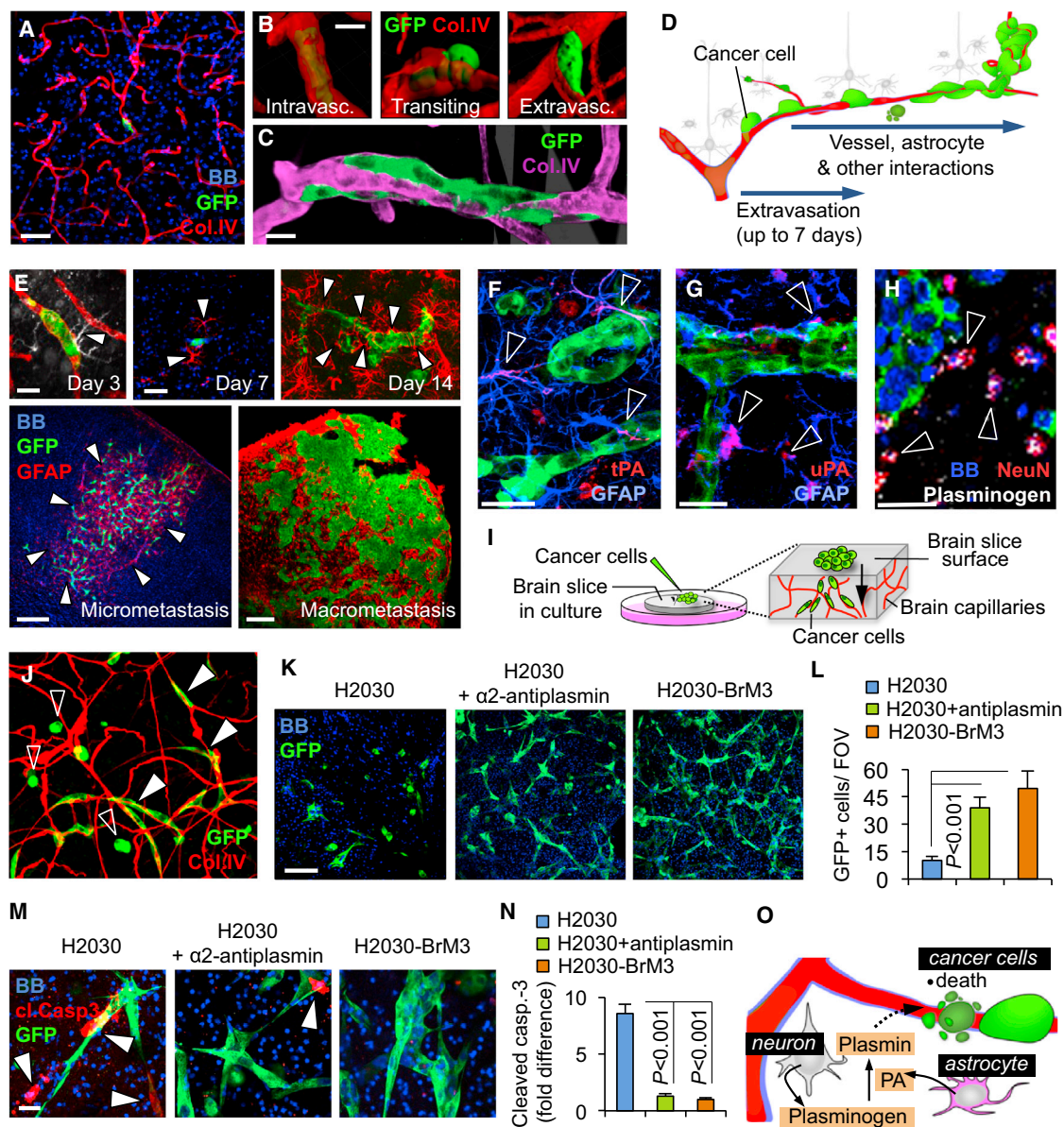
**Figure 2. Vascular Co-Option, Outgrowth, and Escape from Stromal Plasmin Action**

(A) Metastatic cell interactions with brain capillaries. MDA231-BrM2 cells (green) remain bound to brain capillaries (red) after completing extravasation.

(B) Confocal analysis of the extravasation steps showing a GFP+ MDA231-BrM2 cell.

(C) Cluster of extravasated MDA231-BrM2 cells forming a sheath around a brain capillary. All extravasated cells initially grew in this manner. Blue, nuclear staining.

(D) Schema representing the initial steps and interactions during metastatic colonization of the brain.

(E) Exposure of metastatic H2030-BrM3 cells to GFAP+ reactive astrocytes (arrowheads) in the brain parenchyma at different time points after inoculation of cancer cells into the circulation. Day 3: red, collagen IV; white, GFAP; green, GFP+ cancer cells; blue, nuclear staining.

(F and G) tPA and uPA immunofluorescence staining (arrowheads) associated with GFAP+ astrocytes in a mouse brain harboring GFP+ H2030-BrM3 cells (green).

(H) Plasminogen immunofluorescence staining (white, arrowheads) is associated with NeuN+ neuron bodies (red) near a cluster of GFP+ metastatic cells (green) in a mouse brain. Blue, nuclei.

(I) Schema of brain slice organotypic cultures. Cancer cells placed on the surface of slices migrate into the tissue and seek microcapillaries.

(J) Representative image of a brain slice harboring infiltrated H2030-BrM3 cells that are still round (open arrowheads) or already spread over brain capillaries (closed arrowheads).

(K) Representative confocal images of brain slice tissue infiltrated with the indicated cancer cells. α2-antiplasmin was added to the indicated cultures. Note the lower density and disorganized aspect of parental cells compared with the stretched morphology of BrM3 cells or parental cells with α2-antiplasmin.

(L) Quantification of GFP+ cancer cells in the experiments of (K). The numbers of cells per field of view (FOV) are averages ± SEM, n = 6–10 brain slices, scoring at least two fields per slice, in at least two independent experiments.

*(legend continued on next page)*

## Role of Anti-PA Serpins in Brain Metastatic Breast Cancer Cells

Unlike the H2030-BrM3 cells, most other brain metastatic models and a large proportion of human brain metastatic tissues overexpressed not one but multiple anti-PA serpins (refer to Figures 1A and 1I). In MDA231-BrM2, a triple knockdown of the three upregulated serpins (B2, D1, and NS; Figures S4A–S4C) inhibited the brain metastatic activity of the cells more than did the knockdown of any individual serpin (Figures 4A, 4B, S4G, and S4H). The knockdown of serpin B2 (Figures S4D and S4E) partially inhibited the brain metastatic activity of MDA231-BrM2, and the lost activity could be rescued by enforced overexpression of NS (Figures 4A, 4B, and S4F). Clonal cell lines isolated from the MDA231-BrM2 population showed heterogeneity in the overexpression of anti-PA serpins. Compared with the parental MDA231 population, we observed upregulation of NS in nine out of ten clones, serpin B2 in five out of ten, and serpin D1 in eight out of ten (Figures 4C and S4I). As a trend, clones with high levels of the three serpins were more metastatic to brain than were clones with lower levels (Figures 4D and S4J). Clones with high levels of NS and serpin D1 lost brain metastatic activity when transduced with *NS* shRNA (Figure 4E). In the ErbB2-BrM2 model, the knockdown of its only upregulated anti-PA serpin, serpin B2 (refer to Figure 1A), strongly decreased the brain metastatic activity in immunocompetent mice (Figures 4F–4H). In sum, the evidence indicated that expression of one or more anti-PA serpins provides lung cancer and breast cancer cells with a critical advantage in the formation of brain metastases.

## Metastatic Cells Face FasL in the Brain

We searched plasmin substrate databases (MEROPS and CutDB) for proteins whose cleavage might affect brain metastasis (Bajou et al., 2008; Chen and Strickland, 1997; Nayeem et al., 1999; Pang et al., 2004). We focused first on FasL, a proapoptotic cytokine. FasL is a membrane-anchored homotrimeric protein that binds to Fas, a receptor that activates proapoptotic caspases through the adaptor protein FADD (Ashkenazi and Dixit, 1998). FasL is highly expressed in reactive astrocytes in ischemia, brain trauma, Alzheimer's disease, encephalomyelitis, and multiple sclerosis (Choi and Benveniste, 2004). Astrocytes are the main source of FasL against invading T cells in encephalomyelitis (Wang et al., 2013). Plasmin cleaves FasL at Arg144, releasing sFasL as a diffusible cell death signal (Bajou et al., 2008; Fang et al., 2012). Therefore, we asked whether anti-PA serpins shield cancer cells from the lethal action of plasmin-mobilized sFasL (Figure 5A).

FasL immunoreactivity in brain sections harboring H2030-BrM3 lesions was concentrated on reactive astrocytes (Figures 5B and S5A). Human and mouse astrocytes expressed FasL in culture (Figures 5C and S5B). Addition of plasminogen decreased the level of cell-bound FasL in these cultures and increased sFasL in the supernatants (Figures 5C, 5D, and S5C–S5E). Addition of anti-PA serpins or antiplasmin decreased the level of sFasL in mouse brain slices (Figure 5E). These results showed that the PA-plasmin system can mobilize stromal FasL in response to metastatic invasion of the brain.

H2030, PC9, MDA231, and CN34 expressed Fas, as did their BrM derivatives (Figure S5F). Addition of sFasL caused apoptosis in BrM cells in monolayer cultures (Figures S5G–S5I) and in brain tissue (Figures 5F–5H), even in the presence of α2-antiplasmin (Figure S5J). Conversely, addition of anti-FasL blocking antibody protected parental H2030 cells against apoptosis in brain tissue (Figures 5G–5I). Thus, brain metastatic cells are susceptible to apoptosis if they are exposed to sFasL in the brain parenchyma, and this occurs downstream of plasmin.

## NS Shields Brain Metastatic Cells from Fas-Mediated Killing

To determine whether Fas signaling caused the death of cancer cells that infiltrated the brain, we used a FADD truncation mutant that lacks the death effector domain (FADD-DD construct) and acts as a dominant-negative inhibitor of Fas signaling (Chinnaiyan et al., 1996; Figure 5J). Transduction of FADD-DD in the H2030-BrM3 cell line (Figure 5K) prevented the activation of caspase 3 by sFasL (Figure 5L). The apoptosis that anti-PA serpin-depleted BrM cells suffer in brain tissue (refer to Figures 3H–3J and S5L) could be prevented by adding anti-FasL blocking antibodies to the tissue cultures, as well as by enforcing the expression of FADD-DD in the cancer cells (Figures 5M, 5N, and S5L). Moreover, FADD-DD partially rescued the metastatic activity of NS-depleted H2030-BrM3 (Figure 5O). Collectively, these results showed that anti-PA serpin activity shields metastatic cells from FasL attack in the brain.

## The Plasmin Target L1CAM Mediates Cancer Cell Adhesion

Although inhibition of Fas signaling with FADD-DD protected NS-depleted cancer cells from death in the brain, it did not fully restore their metastatic activity (Figure 5O). The NS-depleted, FADD-DD-expressing H2030-BrM3 cells formed smaller lesions that were less well organized (Figure S6A). Therefore, we postulated that anti-PA serpins promote brain metastasis by doing more than just preventing FasL action.
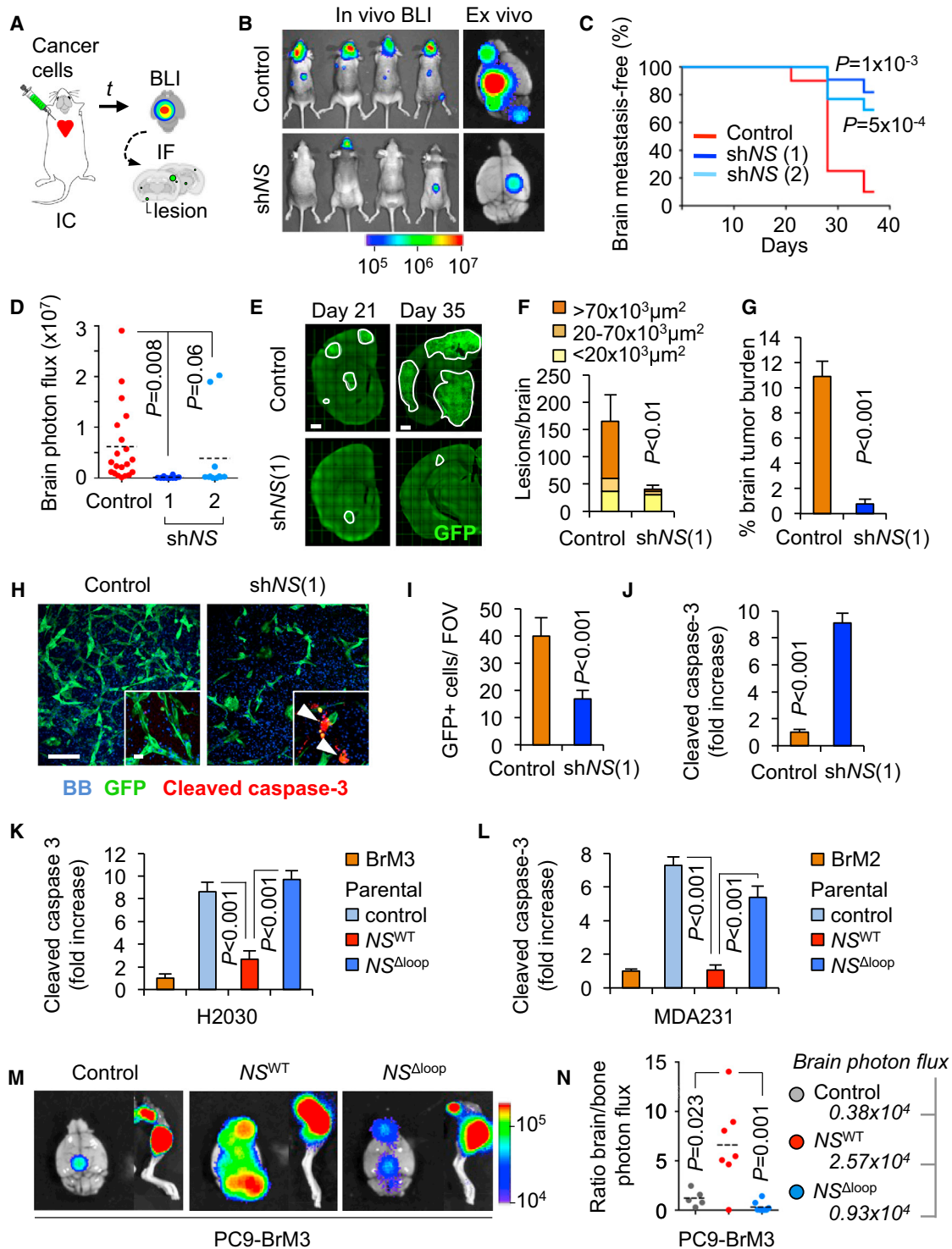
Several clues led us to consider L1CAM as a relevant mediator of metastasis in this context. L1CAM is mainly expressed in neural tissues and in tumors (Schäfer and Altevogt, 2010). It consists of six immunoglobulin-like (Ig) domains, five fibronectin-like (FN) domains, a transmembrane region, and

---

(M) Cleaved caspase-3 immunofluorescence staining in brain slices harboring the indicated cells and additions.
(N) Quantification of cleaved caspase-3-positive cancer cells in the experiments of (M). Values are quantified as (L), normalized to H2030-BrM3, and are averages ± SEM.
(O) Schematic summary showing neurons and astrocytes as sources of plasminogen and PA, respectively, and the lethal effect of the resulting plasmin on infiltrating cancer cells.
All p values by Student's t test. Scale bars, 25 μm (A), 5 μm (B and C), 5 μm (day 3), 15 μm (day 7), 25 μm (day 14), 70 μm (micrometastasis), 100 μm (macrometastasis) (D), 10 μm (F–H), 100 μm (K), and 5 μm (M). See also Figure S2.

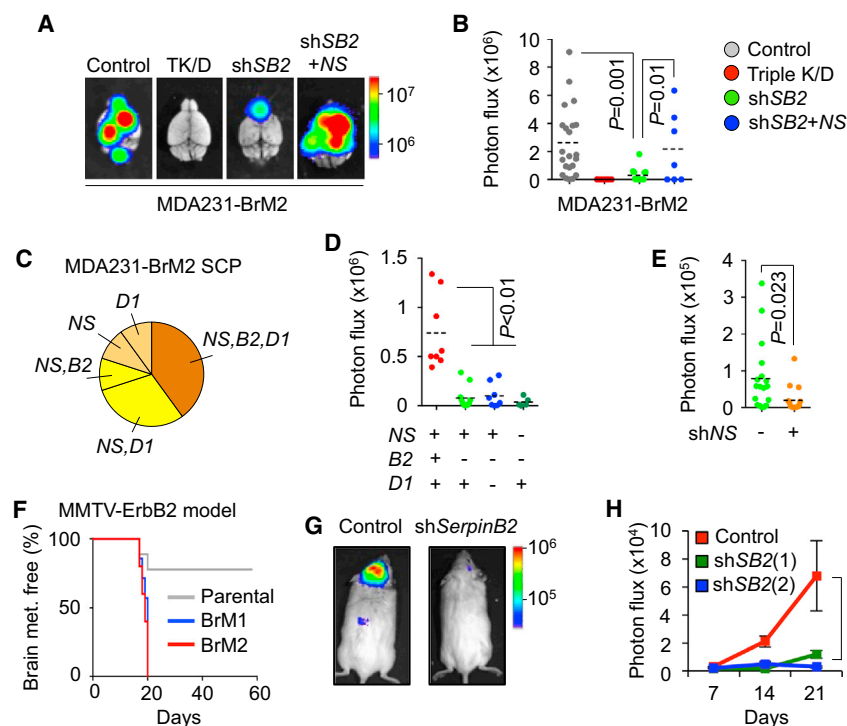**Figure 3. NS Mediates Brain Metastasis**

(A) Schema of the experimental design.

(B) Representative images of whole-body BLI and brain ex vivo BLI 5 weeks after inoculation of H2030-BrM3 cells transduced with control shRNA or *NS* shRNA (sh*NS*).

(C) Kaplan-Meier plot of brain-metastasis-free survival in the experiment of (B). Control (n = 20) and two different sh*NS* (sh*NS* (1), n = 11; sh*NS* (2), n = 13) were analyzed; p values were obtained with the log rank Mantel-Cox test.

(D) Quantification of ex vivo BLI in brains from (B).

*(legend continued on next page)*

**Figure 4. Anti-PA Serpins Mediate Brain Metastasis by Breast Cancer Cells**

(A and B) MDA231-BrM2 cells transduced with control vector; shRNA vectors targeting *NS*, *SERPINB2*, and *SERPIND1* (triple K/D); *SERPINB2* shRNA (sh*SB2*); or sh*SB2* plus an NS-expressing vector were inoculated into the arterial circulation of immunodeficient mice. Brain metastasis burden was visualized by ex vivo brain BLI (A) and quantitated (B). Control n = 22, triple K/D n = 9, sh*SB2* n = 14, sh*SB2* and NS n = 8.

(C) Distribution of clones (single-cell progenies [SCPs]) overexpressing one, two, or three of the indicated serpins among ten clonal cell lines isolated from the MDA231-BrM2 population.

(D) Ex vivo brain BLI quantification from different MDA231-BrM2 SCPs injected. Red dots, SCP (high levels of all serpins), n = 8; light green dots, SCP (low levels of serpin B2), n = 11; blue dots, SCP (low levels of serpin B2 and D1), n = 8; dark green dots, SCP (low levels of serpin B2 and NS), n = 5. The p value was determined by Student's t test.

(E) SCPs with high levels of NS and serpin D1 were subjected to *NS* knockdown and tested for brain metastatic activity.

(F) Kaplan-Meier survival curves for brain-metastasis-free survival in syngeneic mice inoculated with parental ErbB2-P cells (n = 9) or brain metastatic derivatives ErbB2-BrM1 (n = 7) and ErbB2-BrM2 (n = 5). Survival curves were compared using the log rank Mantel-Cox test. ErbB2-P versus ErbB2-BrM1, p = 0.0045; ErbB2-P versus ErbB2-BrM2, p = 0.0053.

(G and H) Representative images (G) and quantification (H) of brain metastasis BLI photon flux formed by ErbB2-BrM2 or these cells expressing two different serpin *B2* shRNAs (sh*SB2*). Control, n = 10; sh*SB2* (1), n = 10; sh*SB2* (2), n = 6.

Data are averages ± SEM. All p values were determined by Student's t test, except in (F). See also Figure S4.

an intracellular domain (Figure 6A). The L1CAM Ig-like repeats mediate homo- and heterophilic interactions for axon guidance (Maness and Schachner, 2007). L1CAM binds to itself, to integrins (Felding-Habermann et al., 1997), and to other proteins (Castellani et al., 2002; Donier et al., 2012; Kulahin et al., 2008). L1CAM expression in tumors is implicated in invasion (Voura et al., 2001) and associated with poor prognosis (Doberstein et al., 2011; Schröder et al., 2009). Plasmin cleaves L1CAM at dibasic motifs (Lys860/Lys863), disrupting the capacity for cell adhesion (Nayeem et al., 1999; Silletti et al., 2000; Figure 6A).

Hence, we postulated that L1CAM mediates plasmin-sensitive vascular co-option by metastatic cells in the brain. L1CAM was expressed in the cancer cell lines regardless of their metastatic activity, tumor type, or species of origin (Figures S6B and S6C). H2030-BrM3 cells readily adhered to monolayers of human brain microvascular endothelial cells (HBMECs; Figures 6B and 6C) and to monolayers of their own (Figure 6D). RNAi-mediated knockdown of L1CAM (Figure S6B) inhibited these cell-cell binding activities (Figures 6C and 6D). Addition of plasmin to cancer cell monolayers caused a decrease in cell-associated L1CAM levels, as shown by flow cytometry (Figure 6E) and by the accumulation of a 150 kDa fragment in the media (Figure 6F; Mechtersheimer et al., 2001). Moreover, plasmin-treated H2030-BrM3 cells lost cell adhesion capacity (Figures 6G and 6H).

(E) Representative images of coronal brain sections analyzed with immunofluorescence (IF) against GFP at 21 or 35 days after inoculation of H2030-BrM3 cells into mice. Lesion contours are marked.

(F) Quantification of brain lesions according to size at the 21 day time point in (E). Control n = 5, sh*NS* n = 6 brains; p value refers to size distribution. For the total number of lesions, p < 0.05.

(G) Quantification of brain tumor burden in the experiment of (E). Control n = 5, sh*NS* n = 6.

(H) Representative images of control and *NS*-depleted H2030-BrM3 cells in brain slice assays. Insets show cleaved caspase-3 IF.

(I and J) Quantification of GFP+ cells (I) and cleaved caspase-3 (J) in the experiment of (H). Data are averages ± SEM; n = 6–10 slices, scoring at least two fields per slice, in at least two independent experiments.

(K and L) Quantification of cells that were positive for cleaved caspase-3, comparing parental and BrM cell lines, and the effect of overexpressing NS wild-type (NS$^{WT}$) or a mutant form unable to target PA (NS$^{\Delta loop}$) in parental cell lines H2030 (K) and MDA231 (L). Data are averages ± SEM, quantified as (J).

(M) Representative ex vivo BLI images of brains and hindlimbs from mice 21 days after inoculation with PC9-BrM3. Cells were transduced with empty vector (n = 5), NS$^{WT}$ (n = 7), or NS$^{\Delta loop}$ mutant (n = 8).

(N) Ratio of photon flux in brain versus bone in the experiment of (M). Ex vivo brain mean BLI values are also shown.

All p values were calculated by Student's t test, except in (C). Scale bars, 250 μm (E), 100 μm, and 5 μm (inset) (H). See also Figure S3.
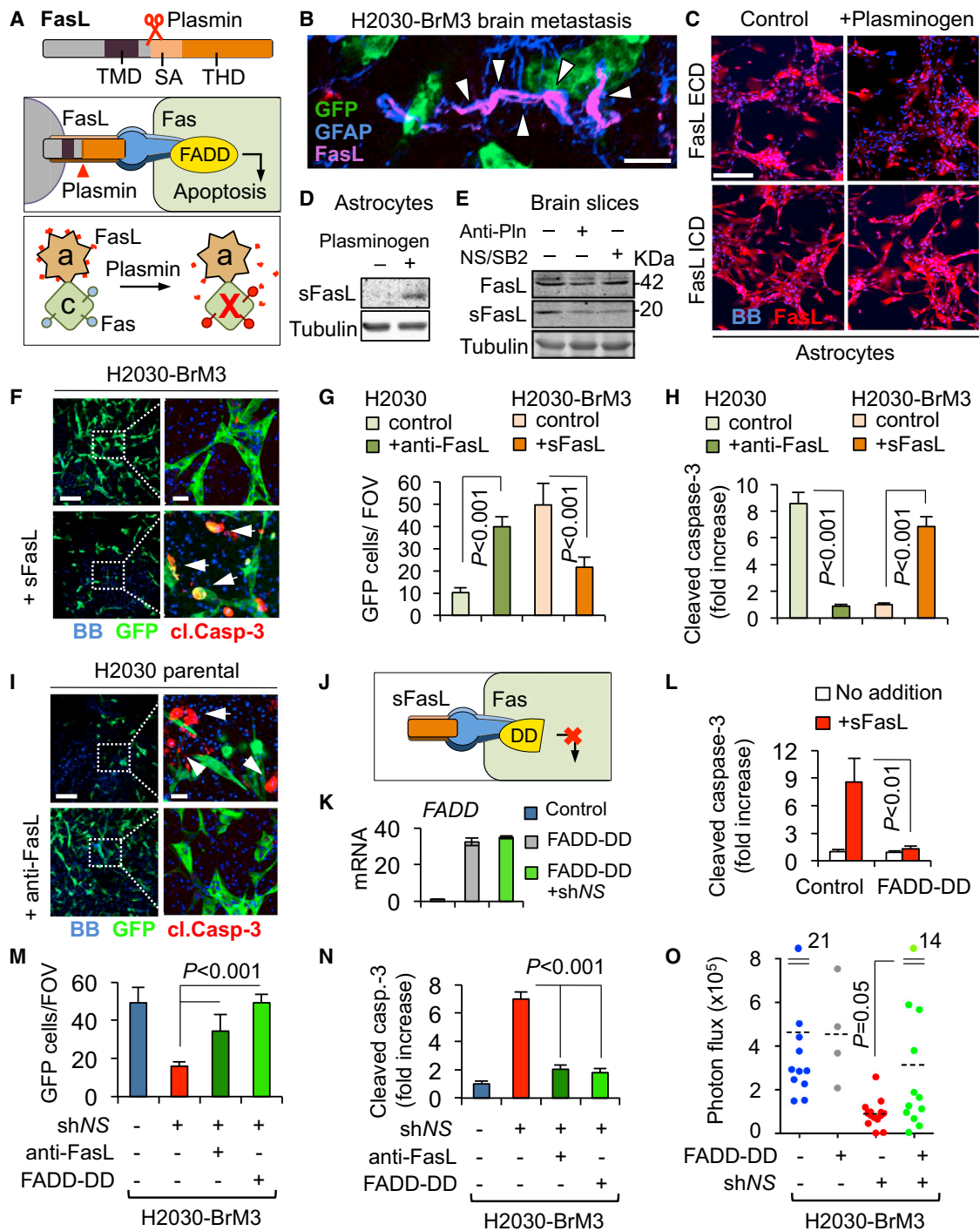
**Figure 5. NS Shields Cancer Cells from FasL Death Signals**

(A) Schema of FasL and its conversion by plasmin into sFasL, a diffusible trigger of apoptosis through Fas-FADD signaling. TMD, transmembrane domain; SA, trimeric self-assembly domain; THD, tumor necrosis factor-homology domain; red crosses, apoptotic cells; a, astrocyte; c, cancer cell.

(B) IF with antibodies against GFP (cancer cells), GFAP (reactive astrocytes), and FasL in a mouse brain harboring metastatic cells 21 days after arterial inoculation of H2030-BrM3.

(C) Images of astrocyte cultures incubated with exogenous plasminogen (1 μM) or no additions. Staining was performed with antibodies against the extracellular domain (ECD) or intracellular domain (ICD) of FasL.

(D) Western immunoblotting of supernatants from cultures shown in (C) using anti-FasL ECD antibodies.

(E) Mouse brain slices were incubated with α2-antiplasmin, NS, and serpin B2, or no additions. sFasL in tissue lysates was detected by western immunoblotting with anti-FasL ECD. Quantification of band density relative to tubulin (left to right) yielded sFasL:FasL ratios of 1, 0.51, and 0.28.

*(legend continued on next page)*

## L1CAM Mediates Vascular Co-Option and Metastatic Outgrowth

The molecular basis for vascular co-option in cancer remains unknown. To address this issue, we asked whether L1CAM participates in vascular co-option by metastatic cells in the brain. L1CAM depletion in H2030-BrM3 cells did not affect their ability to grow in culture (Figure S6D), infiltrate brain tissue, or seek capillaries (Figures 6I and S6E). Notably, L1CAM depletion significantly reduced the ability of H2030-BrM3 and MDA231-BrM2 cells to spread on the abluminal surface of the capillaries (Figures 6I, 6J, and S6G). This was accompanied with a marked decrease in the proliferation marker Ki67 in vessel-associated cancer cells (Figure 6K), without changes in apoptosis markers (Figure S6F).

PC9-BrM3 cells, which do not overexpress endogenous anti-PA serpins, had a limited ability to spread on brain capillaries (Figures 6L and 6M). Enforced expression of NS in these cells not only augmented their metastatic activity (see Figure 3N) but also increased their spreading on brain capillaries (Figures 6L and 6M) and their proliferation on the co-opted vessels (Figure 6N). L1CAM depletion in PC9-BrM3-NS cells (Figures S6H and S6I) abrogated these NS-dependent gains (Figures 6L–6N).

## L1CAM Supports Metastasis Initiation Downstream of NS

L1CAM immunostaining was clearly detectable on carcinoma cells in a majority of the human NSCLC brain metastasis samples examined, and tended to be concentrated at cell interfaces (Figures S7A and S7B). L1CAM-positive cells were present in clusters. In the brain of inoculated mice, extravasated H2030-BrM3 cells were spread over the basal lamina of capillaries, without discernible contacts with the endothelial cells (Figure 7A). L1CAM immunostaining in micrometastases was concentrated at the interfaces of cancer cells with capillaries and adjacent cancer cells (Figure 7B). In recently extravasated H2030-BrM3 cells, L1CAM-depletion allowed cell contact with capillaries but prevented cell spreading over the capillaries (Figure 7C). Twenty-one days later, L1CAM-depleted cells remained mostly as single cells or small clusters, whereas the wild-type cells readily expanded over the capillary network and formed large colonies (Figures 7D and 7E). L1CAM knockdown markedly decreased the overall brain metastatic activity of H2030-BrM3 and MDA231-BrM2 cells (Figures 7F–7H). Moreover, L1CAM

depletion abrogated the gain in metastatic activity of PC9-BrM3 cells imparted by enforced NS overexpression (Figure 7I). These results argued that L1CAM expression in metastatic cells acts downstream of NS to mediate co-option of brain capillaries and metastatic outgrowth.

## DISCUSSION

The growing incidence of brain metastasis warrants a better understanding of the molecular mechanisms that underlie this condition. Our findings illuminate two critical requisites for metastatic colonization of the brain, namely, the escape of infiltrating cancer cells from killing by reactive stromal signals, and the striking ability of the surviving cancer cells to co-opt brain capillaries for metastatic expansion. We show that a stromal PA-plasmin pathway and its inhibition by carcinoma serpins control both of these processes in brain metastasis from lung and breast cancers, suggesting a unified mechanism for metastatic colonization of the brain.

### Anti-PA Serpins as Common Mediators of Brain Metastasis

Brain metastasis involves close and sustained interactions of cancer cells with brain capillaries and reactive astrocytes. Previous work (Carbonell et al., 2009; Kienast et al., 2010; Lorger and Felding-Habermann, 2010) and our own studies show that circulating cancer cells interact with capillary walls not only during extravasation but also thereafter, by attaching to the abluminal surface and growing as a sheath along the co-opted vessels. Cancer cells that infiltrate the brain are immediately exposed to astrocytes that abound in the perivascular space and produce deleterious signals to repel invading cells. Cancer cells must be shielded from such signals in order to survive and to extract benefits from the stroma, including benefits from astrocytes (Lin et al., 2010; Seike et al., 2011). We show that the expression of anti-PA serpins in cancer cells provides such a shield. Serpin D1 and three out of four known anti-PA serpins are expressed in our six brain metastasis models. The most prominent of these serpins, NS and B2, are expressed in a majority of brain metastases from lung cancer and breast cancer patients. The PA-plasmin system is well characterized in connection with its role in blood clot resolution, but its role in cancer has remained paradoxical. Although

---

(F) GFP+ H2030-BrM3 cells (green) were allowed to infiltrate brain slices in media containing added sFasL or no additions and scored for cleaved caspase-3 (red, inset).

(G and H) Quantification of total GFP+ cells (G) and apoptotic GFP+ cells (H) in the experiments of (F) (orange bars) and (I) (green bars). Data are averages ± SEM, n = 6–10 slices, scoring at least two fields per slice, from at least two independent experiments.

(I) GFP+ H2030 cells (green) were allowed to infiltrate brain slices in media containing anti-FasL blocking antibody or no additions. Anti-FasL prevented endogenous signals from triggering caspase-3 activation (red, inset).

(J) Depiction of FADD-DD overexpression (yellow shape) to suppress proapoptotic Fas signaling in cancer cells.

(K) *FADD* expression in H2030-BrM3 transduced with a FADD-DD vector.

(L) Quantification of apoptotic cells following sFasL addition to H2030-BrM3 cells transduced with the indicated vectors.

(M and N) Quantification of total GFP+ cells (M) and apoptotic GFP+ cells (N) in brain slices harboring the indicated GFP+ H2030-BrM3 transfectants and/or additions. Data are averages ± SEM and quantitated as (G) and (H).

(O) Brain metastatic activity of H2030-BrM3 cells transduced with the indicated vectors and inoculated into the arterial circulation of mice. BLI photon flux was quantitated in cells transduced with control shRNA (n = 11), FADD-DD (n = 4), *NS* shRNA (n = 14), or *NS* shRNA and FADD-DD (n = 12).

All p values were determined by Student's t test. Scale bars, 25 μm (B), 200 μm (C), 100 μm (F and I), and 5 μm (insets in F and I).

See also Figure S5.
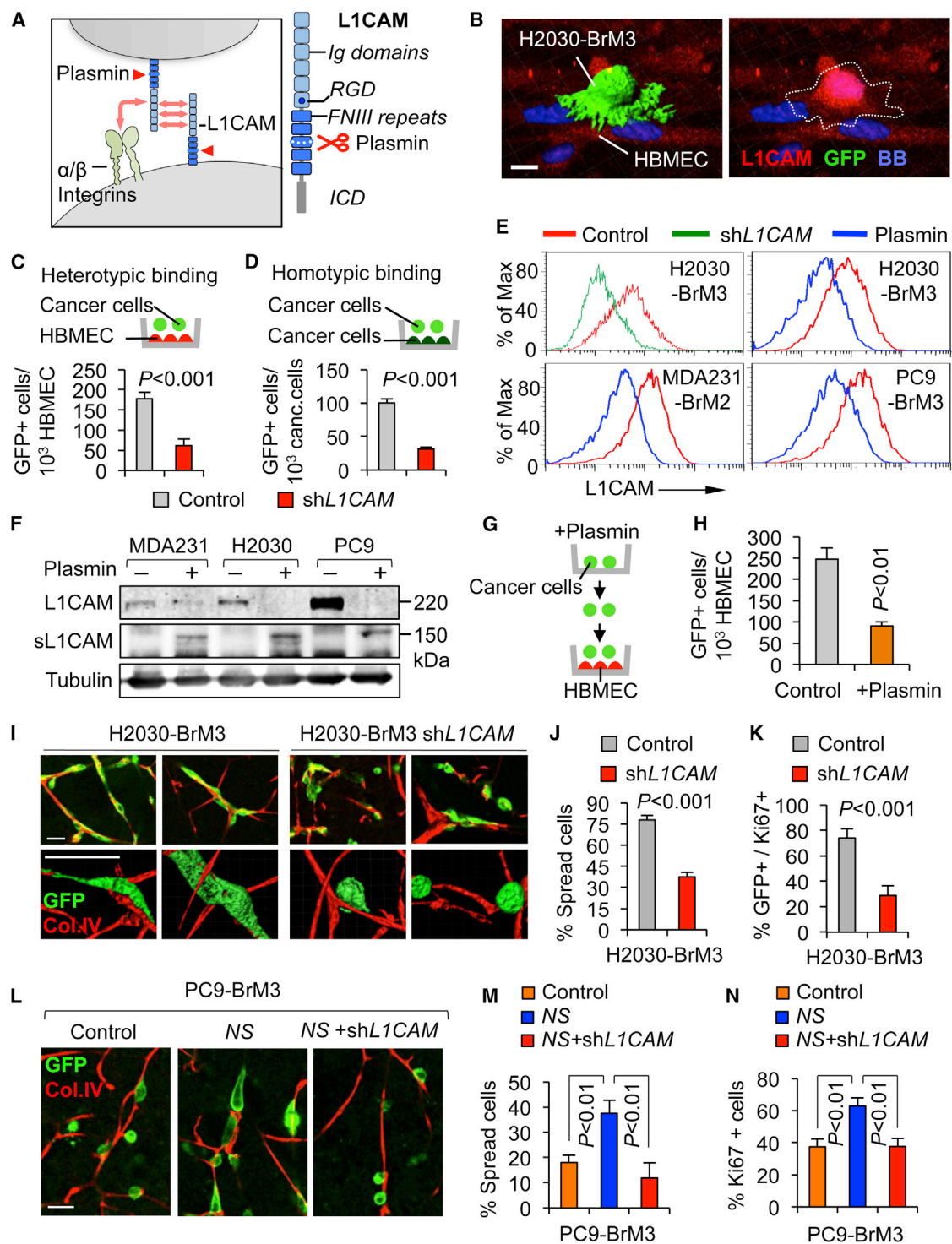
**Figure 6. The Plasmin Target L1CAM Mediates Vascular Co-Option by Brain Metastatic Cells**

(A) Schema of L1CAM as a mediator of homophilic and heterophilic (e.g., integrins) cell adhesive interactions, and its conversion by plasmin into an adhesion-defective fragment. Ig and fibronectin type III (FNIII) domain repeats, the ICD, and an integrin-binding RGD sequence are indicated.

(B) Suspensions of GFP+ H2030-BrM3 cells were placed on top of a monolayer of HBMECs.

(C and D) Analysis of H2030-BrM3 binding to HBMEC monolayers (C) or H2030-BrM3 monolayers (D), and the effect of L1CAM knockdown. Data are averages ± SEM, n = 5, scoring at least ten fields per coverslip.

(E) Flow cytometry of cell-surface L1CAM in the indicated brain cells expressing *L1CAM* shRNA or incubated with plasmin, compared with untreated controls.

*(legend continued on next page)*

plasmin can promote cancer cell proliferation and invasion by cleaving growth factor precursors and extracellular matrix proteins (McMahon and Kwaan, 2008), anti-PA serpin levels in tumors and blood are associated with poor outcome in many cancers (Berger, 2002; Foekens et al., 1995; Harbeck et al., 1999). Here we show that anti-PA serpins shield metastatic cells from PA-plasmin in the brain, providing a clear prometastatic advantage.

### Averting Fas Killing and Protecting L1CAM Vascular Co-Option

Although FasL plays important roles in immune homeostasis (Krammer, 2000) and is present in tumors (Baldini et al., 2009), its expression is particularly acute in reactive astrocytes (Beer et al., 2000). Astrocytes are the main source of FasL in response to infiltrating leukocytes, and of PAs in response to brain injury. We show that metastasis-associated astrocytes express both PA and FasL. Plasmin releases membrane-bound FasL from astrocytes, and sFasL levels in brain tissue depend on plasmin. Brain metastatic cells from lung or breast cancers suffer Fas-dependent death in the brain unless they are protected by anti-PA serpins. We conclude that Fas signaling mediates and anti-PA serpins prevent the attrition of infiltrating cancer cells in the brain.

We show that L1CAM mediates the spread of metastatic cells on the vasculature and additionally mediates interactions between cancer cells. When cancer cells are experimentally depleted of L1CAM, they fail to co-opt brain capillaries and metastatic outgrowth stalls. Cancer cell-derived anti-PA serpins prevent plasmin destruction of L1CAM, providing yet another benefit besides averting Fas-mediated cancer cell killing. L1CAM expression is normally restricted to neurons, where it mediates axonal guidance through highly plastic interactions of the growth cone with surrounding components (Wiencken-Barger et al., 2004). The dynamic nature of L1CAM adhesive interactions might be particularly advantageous to cancer cells in their quest to co-opt the vasculature while invading tissue. Although the molecular basis for vascular co-option in cancer is largely unknown, the present identification of L1CAM as a mediator provides an opening for a mechanistic dissection of this process.

### Implications beyond Brain Metastasis

The molecular mechanisms defined here protect metastatic cells against selective pressures that are particularly acute in the brain. However, a high mortality of infiltrating cancer cells is characteristic of metastasis in general (Gupta and Massagué, 2006; Valastyan and Weinberg, 2011), and vascular co-option occurs in metastasis to other organs and by other types of cancer (Donnem et al., 2013). Vascular co-option also provides cancer cells with an escape from therapy-induced hypoxia (Leenders et al., 2004). The anti-PA serpins that are upregulated in our brain metastatic models are also expressed, albeit at lower levels, in counterparts that are metastatic to other organs. Moreover, L1CAM expression in primary tumors is associated with poor prognosis in various types of cancer, as are PA, plasmin, and FasL. The reactive brain stroma, with its high capacity to generate PA-plasmin and FasL, may be more challenging to infiltrating cancer cells than is the stroma in other organs, and as a result, it may select for accentuated versions of otherwise general metastatic traits. Although anti-PA serpins, plasmin, FasL, and L1CAM have not previously been connected to metastatic cell survival and vascular co-option, their repeated clinical association with poor prognosis and the mechanistic links exposed in the present work may reflect a wider role in cancer than is shown here.

### EXPERIMENTAL PROCEDURES

#### Animal Studies

All animal experiments were done in accordance with a protocol approved by the MSKCC Institutional Animal Care and Use Committee. Athymic NCR nu/nu, Cr:NIH bg-nu-xid, FVB/NCr (all from NCI-Frederick), and B6129SF1/J (The Jackson Laboratory) female mice 4–6 weeks of age were used. Brain metastatic derivatives of a syngeneic ErbB2 model (ErbB2-BrM2) were established according to a previous protocol (Bos et al., 2009; Nguyen et al., 2009) and are detailed in the Extended Experimental Procedures. Brain colonization assays were performed as follows: We injected 100 μl of PBS into the left ventricle containing 50,000 cells (for long-term experiments) or 500,000 cells (for short-term experiments) in the case of MDA231-BrM2a, CN34BrM-2c, H2030-BrM3, and PC9-BrM3, and 100,000 cells in the case of 373N1, 393N1, 482N1, 2691N1, and ErbB2-BrM2. Brain colonization was analyzed in vivo and ex vivo by BLI. Anesthetized mice (ketamine 100 mg/kg/xylazine 10 mg/kg) were injected retro-orbitally with D-Luciferin (150 mg/kg) and imaged with an IVIS Spectrum Xenogen machine (Caliper Life Sciences). Bioluminescence analysis was performed using Living Image software, version 2.50.

#### Brain Slice Assays

Organotypic slice cultures from adult mouse brain were prepared by adapting previously described methods (Polleux and Ghosh, 2002). Brains from 4- to 6-week-old athymic NCR nu/nu mice were dissected in Hank's balanced salt solution (HBSS) supplemented with HEPES (pH 7.4, 2.5 mM), D-glucose (30 mM), $CaCl_2$ (1 mM), $MgSO_4$ (1 mM), $NaHCO_3$ (4 mM), and embedded in low-melting agarose (Lonza) preheated at 42°C. The embedded brains were cut into 250 μm slices using a vibratome (Leica). Brain slices (bregma −1 mm to +3 mm) were placed with flat spatulas on top of 0.8 μm pore membranes (Millipore) in slice culture media (Dulbecco's modified Eagle's medium [DMEM], supplemented HBSS, fetal bovine serum 5%, L-glutamine (1 mM), 100 IU/ml penicillin, 100 μg/ml streptomycin). The brain slices were incubated at 37°C and 5%

(F) Anti-L1CAM western immunoblotting of cells and culture supernatants after incubation with or without plasmin.

(G and H) Cancer cells were treated with plasmin and subjected to HBMEC adhesion assays. Data are averages ± SEM, n = 3, scoring at least five fields per coverslip.

(I) Control or L1CAM-depleted H2030-BrM3 cells after infiltrating brain tissue slices. GFP+ cancer cells (green) and vasculature (collagen IV immunostaining, red) were visualized after 2 days. Two representative images are shown per condition. Bottom: high magnification.

(J and K) Quantification of cells that were spread on capillaries (J) and Ki67+ cells (K) in the experiments of (I). Data are averages ± SEM, n = 6 slices, scoring at least three fields per slice, from two independent experiments.

(L) Effect of NS overexpression and L1CAM depletion on the interaction of PC9-BrM3 cells with capillaries in brain slices.

(M and N) Quantification of cells that were spread on capillaries (M) and Ki67+ cells (N) in the experiments shown in (L).

Data are averages ± SEM and quantitated as (J) and (K). All p values by Student's t test. Scale bars, 10 μm (B) and 50 μm (I and L). See also Figure S6.
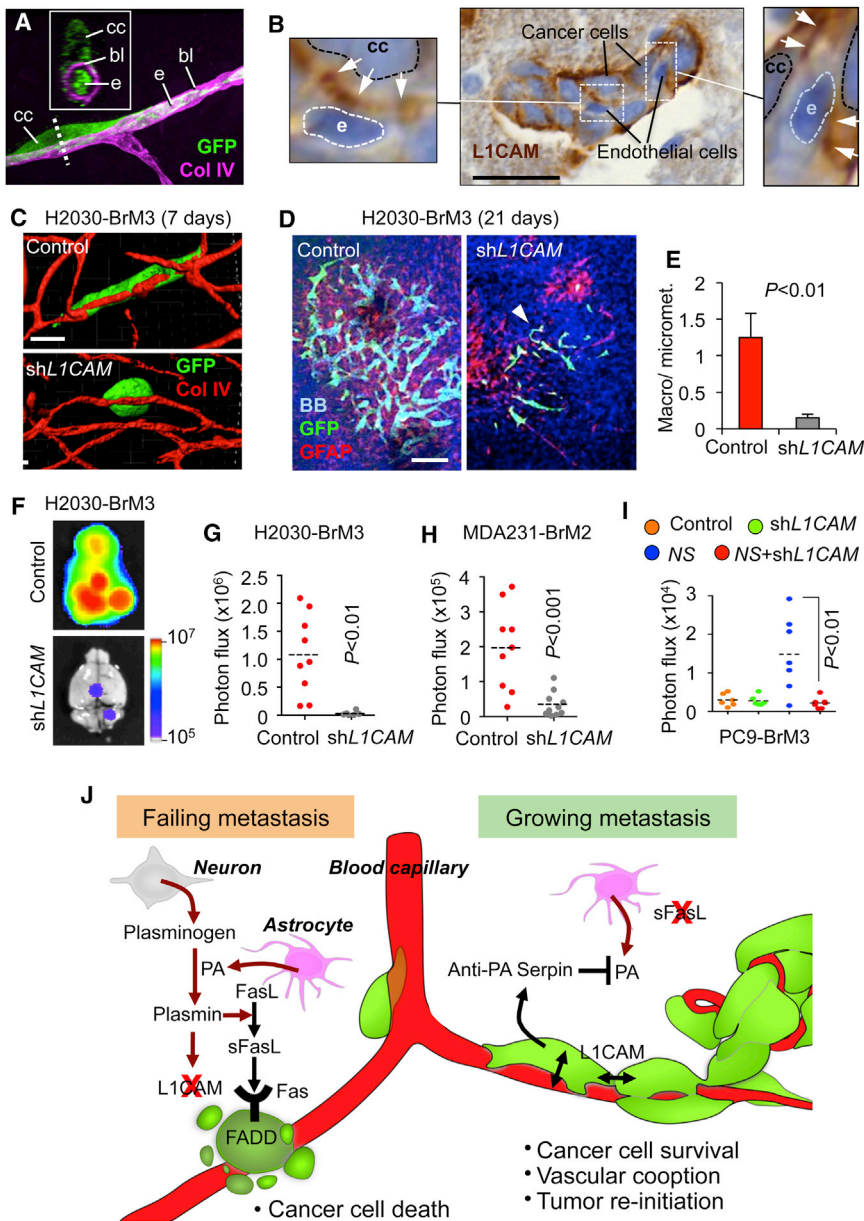
**Figure 7. L1CAM Mediates Metastatic Outgrowth in the Brain**

(A) GFP+ H2030-BrM3 co-opting the basal lamina rich in collagen IV of endothelial cells labeled with VE-cadherin in brain slices. bl, basal lamina; e, endothelium; cc, cancer cell.

(B) Immunohistochemical staining with anti-L1CAM antibodies and hematoxylin and eosin (H&E) counterstaining of incipient brain colonies formed by H2030-BrM3. Cancer cells (cc, pale blue nuclei) remain close to each other and interact with endothelial cells (e, dark blue nuclei). Insets: higher magnification of cell-cell contact areas.

(C) H2030-BrM3 cells infiltrating the brain 7 days after intracardiac injection, and the effect of *L1CAM* depletion.

(D) Representative images of GFP+ metastatic lesions from brains at 21 days.

(E) Relative abundance of macrometastasis over micrometastasis (as defined in Figure 3F) in brains shown in (D). Number of lesions: control = 283.2 ± 84.8, sh*L1CAM* = 69.8 ± 11.5. Data are averages ± SEM, n = 3 brains.

(F and G) Representative images (F) and quantification (G) of ex vivo brain BLI from mice inoculated with the indicated H2030-BrM3 cells. Control shRNA, n = 9; sh*L1CAM*, n = 6.

(H) Quantification of ex vivo brain BLI from mice that were arterially inoculated with indicated MDA231-BrM2 cells. Control shRNA, n = 9; sh*L1CAM*, n = 10.

(I) Quantification of ex vivo brain BLI from mice that were arterially inoculated with the indicated PC9-BrM3 cells (n = 5–7). All p values were determined by Student's t test. Scale bar, 25 μm (B), 30 μm (C), and 200 μm (D).

(J) Model of the action of the stromal PA-plasmin system against cancer cells that infiltrate the brain, and the role of anti-PA serpins in protecting brain metastatic cells from stromal PA-plasmin. Reactive astrocytes produce PAs in the presence of extravasated cancer cells. Left side: metastasis fails when PAs generate plasmin from neuron-derived plasminogen and plasmin mobilizes FasL from astrocytes to kill cancer cells. Additionally, plasmin cleaves and inactivates L1CAM, a cell adhesion molecule that cancer cells express for vascular co-option. Right side: metastasis proceeds when brain metastatic cells express anti-PA serpins that prevent the generation of plasmin and its deleterious effects on the survival and vascular attachment of the cancer cells.
See also Figure S7.

$CO_2$ for 1 hr, and then $3 \times 10^4$ cancer cells suspended in 2 μl of culture media were placed on the surface of the slice and incubated for 48–72 hr. Brain slices could be maintained under these conditions for up to 5 days without apparent alterations in tissue architecture. α2-antiplasmin (2.5 μg/ml; Molecular Innovations), NS, and serpin B2 (0.5 μg/ml each; Peprotech) were added to the medium. sFasL (500 ng/ml; Peprotech) or FasL blocking antibodies (12.5 μg/ml; BD) were added to the medium, and slices were preincubated for 24 hr before addition of cancer cells. Brain slices were fixed in paraformaldehyde (4%) overnight, and then free-floating immunofluorescence was performed for GFP (1:1,000, ref. GFP-1020; Aves Labs), cleaved caspase-3 (1:500, ref. 9661; Cell Signaling), collagen IV (1:500, ref. AB756P; Millipore). Nuclei were stained with Bis-Benzamide (1 μg/ml; Sigma). Slices were mounted with ProLong Gold anti-fade reagent (Invitrogen).

## SUPPLEMENTAL INFORMATION

Supplemental Information includes Extended Experimental Procedures and seven figures and can be found with this article online at http://dx.doi.org/10.1016/j.cell.2014.01.040.

## REFERENCES

Adhami, F., Yu, D., Yin, W., Schloemer, A., Burns, K.A., Liao, G., Degen, J.L., Chen, J., and Kuan, C.Y. (2008). Deleterious effects of plasminogen activators in neonatal cerebral hypoxia-ischemia. Am. J. Pathol. *172*, 1704–1716.

Ashkenazi, A., and Dixit, V.M. (1998). Death receptors: signaling and modulation. Science *281*, 1305–1308.

Bajou, K., Peng, H., Laug, W.E., Maillard, C., Noel, A., Foidart, J.M., Martial, J.A., and DeClerck, Y.A. (2008). Plasminogen activator inhibitor-1 protects endothelial cells from FasL-mediated apoptosis. Cancer Cell *14*, 324–334.

Baldini, E., Ulisse, S., Marchioni, E., Di Benedetto, A., Giovannetti, G., Petrangeli, E., Sentinelli, S., Donnorso, R.P., Reale, M.G., Mottolese, M., et al. (2009). Expression of Fas and Fas ligand in human testicular germ cell tumours. Int. J. Androl. *32*, 123–130.

Beer, R., Franz, G., Schöpf, M., Reindl, M., Zelger, B., Schmutzhard, E., Poewe, W., and Kampfl, A. (2000). Expression of Fas and Fas ligand after experimental traumatic brain injury in the rat. J. Cereb. Blood Flow Metab. *20*, 669–677.

Benarroch, E.E. (2007). Tissue plasminogen activator: beyond thrombolysis. Neurology *69*, 799–802.

Berger, D.H. (2002). Plasmin/plasminogen system in colorectal cancer. World J. Surg. *26*, 767–771.

Bos, P.D., Zhang, X.H., Nadal, C., Shu, W., Gomis, R.R., Nguyen, D.X., Minn, A.J., van de Vijver, M.J., Gerald, W.L., Foekens, J.A., and Massagué, J. (2009). Genes that mediate breast cancer metastasis to the brain. Nature *459*, 1005–1009.

Carbonell, W.S., Ansorge, O., Sibson, N., and Muschel, R. (2009). The vascular basement membrane as "soil" in brain metastasis. PLoS ONE *4*, e5857.

Castellani, V., De Angelis, E., Kenwrick, S., and Rougon, G. (2002). Cis and trans interactions of L1 with neuropilin-1 control axonal responses to semaphorin 3A. EMBO J. *21*, 6348–6357.

Chambers, A.F., Groom, A.C., and MacDonald, I.C. (2002). Dissemination and growth of cancer cells in metastatic sites. Nat. Rev. Cancer *2*, 563–572.

Chen, Z.L., and Strickland, S. (1997). Neuronal death in the hippocampus is promoted by plasmin-catalyzed degradation of laminin. Cell *91*, 917–925.

Chinnaiyan, A.M., Tepper, C.G., Seldin, M.F., O'Rourke, K., Kischkel, F.C., Hellbardt, S., Krammer, P.H., Peter, M.E., and Dixit, V.M. (1996). FADD/MORT1 is a common mediator of CD95 (Fas/APO-1) and tumor necrosis factor receptor-induced apoptosis. J. Biol. Chem. *271*, 4961–4965.

Choi, C., and Benveniste, E.N. (2004). Fas ligand/Fas system in the brain: regulator of immune and apoptotic responses. Brain Res. Brain Res. Rev. *44*, 65–81.

Doberstein, K., Wieland, A., Lee, S.B., Blaheta, R.A., Wedel, S., Moch, H., Schraml, P., Pfeilschifter, J., Kristiansen, G., and Gutwein, P. (2011). L1-CAM expression in ccRCC correlates with shorter patients survival times and confers chemoresistance in renal cell carcinoma cells. Carcinogenesis *32*, 262–270.

Donier, E., Gomez-Sanchez, J.A., Grijota-Martinez, C., Lakomá, J., Baars, S., Garcia-Alonso, L., and Cabedo, H. (2012). L1CAM binds ErbB receptors through Ig-like domains coupling cell adhesion and neuregulin signalling. PLoS ONE *7*, e40674.

Donnem, T., Hu, J., Ferguson, M., Adighibe, O., Snell, C., Harris, A.L., Gatter, K.C., and Pezzella, F. (2013). Vessel co-option in primary human tumors and metastases: an obstacle to effective anti-angiogenic treatment? Cancer Med. *2*, 427–436.

Fang, H., Placencio, V.R., and DeClerck, Y.A. (2012). Protumorigenic activity of plasminogen activator inhibitor-1 through an antiapoptotic function. J. Natl. Cancer Inst. *104*, 1470–1484.

Feld, R., Rubinstein, L.V., and Weisenberger, T.H. (1984). Sites of recurrence in resected stage I non-small-cell lung cancer: a guide for future studies. J. Clin. Oncol. *2*, 1352–1358.

Felding-Habermann, B., Silletti, S., Mei, F., Siu, C.H., Yip, P.M., Brooks, P.C., Cheresh, D.A., O'Toole, T.E., Ginsberg, M.H., and Montgomery, A.M. (1997). A single immunoglobulin-like domain of the human neural cell adhesion molecule L1 supports adhesion by multiple vascular and platelet integrins. J. Cell Biol. *139*, 1567–1581.

Foekens, J.A., Look, M.P., Peters, H.A., van Putten, W.L., Portengen, H., and Klijn, J.G. (1995). Urokinase-type plasminogen activator and its inhibitor PAI-1: predictors of poor response to tamoxifen therapy in recurrent breast cancer. J. Natl. Cancer Inst. *87*, 751–756.

Francia, G., Cruz-Munoz, W., Man, S., Xu, P., and Kerbel, R.S. (2011). Mouse models of advanced spontaneous metastasis for experimental therapeutics. Nat. Rev. Cancer *11*, 135–141.

Fujimoto, S., Katsuki, H., Ohnishi, M., Takagi, M., Kume, T., and Akaike, A. (2008). Plasminogen potentiates thrombin cytotoxicity and contributes to pathology of intracerebral hemorrhage in rats. J. Cereb. Blood Flow Metab. *28*, 506–515.

Ganesh, B.S., and Chintala, S.K. (2011). Inhibition of reactive gliosis attenuates excitotoxicity-mediated death of retinal ganglion cells. PLoS ONE *6*, e18305.

Gavrilovic, I.T., and Posner, J.B. (2005). Brain metastases: epidemiology and pathophysiology. J. Neurooncol. *75*, 5–14.

Gupta, G.P., and Massagué, J. (2006). Cancer metastasis: building a framework. Cell *127*, 679–695.

Gutiérrez-Fernández, A., Gingles, N.A., Bai, H., Castellino, F.J., Parmer, R.J., and Miles, L.A. (2009). Plasminogen enhances neuritogenesis on laminin-1. J. Neurosci. *29*, 12393–12400.

Harbeck, N., Thomssen, C., Berger, U., Ulm, K., Kates, R.E., Höfler, H., Jänicke, F., Graeff, H., and Schmitt, M. (1999). Invasion marker PAI-1 remains a strong prognostic factor after long-term follow-up both for primary breast cancer and following first relapse. Breast Cancer Res. Treat. *54*, 147–157.

Heyn, C., Ronald, J.A., Ramadan, S.S., Snir, J.A., Barry, A.M., MacKenzie, L.T., Mikulis, D.J., Palmieri, D., Bronder, J.L., Steeg, P.S., et al. (2006). In vivo MRI of cancer cell fate at the single-cell level in a mouse model of breast cancer metastasis to the brain. Magn. Reson. Med. *56*, 1001–1010.

Irving, J.A., Pike, R.N., Lesk, A.M., and Whisstock, J.C. (2000). Phylogeny of the serpin superfamily: implications of patterns of amino acid conservation for structure and function. Genome Res. *10*, 1845–1864.

Kang, Y., Siegel, P.M., Shu, W., Drobnjak, M., Kakonen, S.M., Cordón-Cardo, C., Guise, T.A., and Massagué, J. (2003). A multigenic program mediating breast cancer metastasis to bone. Cancer Cell *3*, 537–549.

Karrison, T.G., Ferguson, D.J., and Meier, P. (1999). Dormancy of mammary carcinoma after mastectomy. J. Natl. Cancer Inst. *91*, 80–85.

Kienast, Y., von Baumgarten, L., Fuhrmann, M., Klinkert, W.E., Goldbrunner, R., Herms, J., and Winkler, F. (2010). Real-time imaging reveals the single steps of brain metastasis formation. Nat. Med. *16*, 116–122.

Krammer, P.H. (2000). CD95's deadly mission in the immune system. Nature *407*, 789–795.

Kulahin, N., Li, S., Hinsby, A., Kiselyov, V., Berezin, V., and Bock, E. (2008). Fibronectin type III (FN3) modules of the neuronal cell adhesion molecule L1 interact directly with the fibroblast growth factor (FGF) receptor. Mol. Cell. Neurosci. *37*, 528–536.

Law, R.H., Zhang, Q., McGowan, S., Buckle, A.M., Silverman, G.A., Wong, W., Rosado, C.J., Langendorf, C.G., Pike, R.N., Bird, P.I., and Whisstock, J.C. (2006). An overview of the serpin superfamily. Genome Biol. *7*, 216.

Leenders, W.P., Küsters, B., Verrijp, K., Maass, C., Wesseling, P., Heerschap, A., Ruiter, D., Ryan, A., and de Waal, R. (2004). Antiangiogenic therapy of cerebral melanoma metastases results in sustained tumor progression via vessel co-option. Clin. Cancer Res. 10, 6222–6230.

Li, B., Wang, C., Zhang, Y., Zhao, X.Y., Huang, B., Wu, P.F., Li, Q., Li, H., Liu, Y.S., Cao, L.Y., et al. (2013). Elevated PLGF contributes to small-cell lung cancer brain metastasis. Oncogene 32, 2952–2962.

Lin, Q.B., Balasubramanian, K., Fan, D., Kim, S.J., Guo, L., Wang, H., Bar-Eli, M., Aldape, K.D., and Fidler, I.J. (2010). Reactive astrocytes protect melanoma cells from chemotherapy by sequestering intracellular calcium through gap junction communication channels. Neoplasia 12, 748–754.

Lorger, M., and Felding-Habermann, B. (2010). Capturing changes in the brain microenvironment during initial steps of breast cancer brain metastasis. Am. J. Pathol. 176, 2958–2971.

Maher, E.A., Mietz, J., Arteaga, C.L., DePinho, R.A., and Mohla, S. (2009). Brain metastasis: opportunities in basic and translational research. Cancer Res. 69, 6015–6020.

Maness, P.F., and Schachner, M. (2007). Neural recognition molecules of the immunoglobulin superfamily: signaling transducers of axon guidance and neuronal migration. Nat. Neurosci. 10, 19–26.

McMahon, B., and Kwaan, H.C. (2008). The plasminogen activator system and cancer. Pathophysiol. Haemost. Thromb. 36, 184–194.

Mechtersheimer, S., Gutwein, P., Agmon-Levin, N., Stoeck, A., Oleszewski, M., Riedle, S., Postina, R., Fahrenholz, F., Fogel, M., Lemmon, V., and Altevogt, P. (2001). Ectodomain shedding of L1 adhesion molecule promotes cell migration by autocrine binding to integrins. J. Cell Biol. 155, 661–673.

Minn, A.J., Gupta, G.P., Siegel, P.M., Bos, P.D., Shu, W., Giri, D.D., Viale, A., Olshen, A.B., Gerald, W.L., and Massagué, J. (2005). Genes that mediate breast cancer metastasis to lung. Nature 436, 518–524.

Muller, W.J., Sinn, E., Pattengale, P.K., Wallace, R., and Leder, P. (1988). Single-step induction of mammary adenocarcinoma in transgenic mice bearing the activated c-neu oncogene. Cell 54, 105–115.

Nayeem, N., Silletti, S., Yang, X., Lemmon, V.P., Reisfeld, R.A., Stallcup, W.B., and Montgomery, A.M. (1999). A potential role for the plasmin(ogen) system in the posttranslational cleavage of the neural cell adhesion molecule L1. J. Cell Sci. 112, 4739–4749.

Nguyen, D.X., Chiang, A.C., Zhang, X.H., Kim, J.Y., Kris, M.G., Ladanyi, M., Gerald, W.L., and Massagué, J. (2009). WNT/TCF signaling through LEF1 and HOXB9 mediates lung adenocarcinoma metastasis. Cell 138, 51–62.

Pang, P.T., Teng, H.K., Zaitsev, E., Woo, N.T., Sakata, K., Zhen, S., Teng, K.K., Yung, W.H., Hempstead, B.L., and Lu, B. (2004). Cleavage of proBDNF by tPA/plasmin is essential for long-term hippocampal plasticity. Science 306, 487–491.

Polleux, F., and Ghosh, A. (2002). The slice overlay assay: a versatile tool to study the influence of extracellular signals on neuronal development. Sci. STKE 2002, p19.

Schäfer, M.K., and Altevogt, P. (2010). L1CAM malfunction in the nervous system and human carcinomas. Cell. Mol. Life Sci. 67, 2425–2437.

Schröder, C., Schumacher, U., Fogel, M., Feuerhake, F., Müller, V., Wirtz, R.M., Altevogt, P., Krenkel, S., Jänicke, F., and Milde-Langosch, K. (2009). Expression and prognostic value of L1-CAM in breast cancer. Oncol. Rep. 22, 1109–1117.

Seike, T., Fujita, K., Yamakawa, Y., Kido, M.A., Takiguchi, S., Teramoto, N., Iguchi, H., and Noda, M. (2011). Interaction between lung cancer cells and astrocytes via specific inflammatory cytokines in the microenvironment of brain metastasis. Clin. Exp. Metastasis 28, 13–25.

Silletti, S., Mei, F., Sheppard, D., and Montgomery, A.M. (2000). Plasmin-sensitive dibasic sequences in the third fibronectin-like domain of L1-cell adhesion molecule (CAM) facilitate homomultimerization and concomitant integrin recruitment. J. Cell Biol. 149, 1485–1502.

Sofroniew, M.V., and Vinters, H.V. (2010). Astrocytes: biology and pathology. Acta Neuropathol. 119, 7–35.

Takehara, S., Onda, M., Zhang, J., Nishiyama, M., Yang, X., Mikami, B., and Lomas, D.A. (2009). The 2.1-A crystal structure of native neuroserpin reveals unique structural elements that contribute to conformational instability. J. Mol. Biol. 388, 11–20.

Teesalu, T., Hinkkanen, A.E., and Vaheri, A. (2001). Coordinated induction of extracellular proteolysis systems during experimental autoimmune encephalomyelitis in mice. Am. J. Pathol. 159, 2227–2237.

Valastyan, S., and Weinberg, R.A. (2011). Tumor metastasis: molecular insights and evolving paradigms. Cell 147, 275–292.

Vanharanta, S., and Massagué, J. (2013). Origins of metastatic traits. Cancer Cell 24, 410–421.

Voura, E.B., Ramjeesingh, R.A., Montgomery, A.M., and Siu, C.H. (2001). Involvement of integrin alpha(v)beta(3) and cell adhesion molecule L1 in transendothelial migration of melanoma cells. Mol. Biol. Cell 12, 2699–2710.

Wang, X., Haroon, F., Karray, S., Martina Deckert, and Schlüter, D. (2013). Astrocytic Fas ligand expression is required to induce T-cell apoptosis and recovery from experimental autoimmune encephalomyelitis. Eur. J. Immunol. 43, 115–124.

Wiencken-Barger, A.E., Mavity-Hudson, J., Bartsch, U., Schachner, M., and Casagrande, V.A. (2004). The role of L1 in axon pathfinding and fasciculation. Cereb. Cortex 14, 121–131.

Winslow, M.M., Dayton, T.L., Verhaak, R.G., Kim-Kiselak, C., Snyder, E.L., Feldser, D.M., Hubbard, D.D., DuPage, M.J., Whittaker, C.A., Hoersch, S., et al. (2011). Suppression of lung adenocarcinoma progression by Nkx2-1. Nature 473, 101–104.

Yepes, M., Sandkvist, M., Wong, M.K., Coleman, T.A., Smith, E., Cohan, S.L., and Lawrence, D.A. (2000). Neuroserpin reduces cerebral infarct volume and protects neurons from ischemia-induced apoptosis. Blood 96, 569–576.

# Assembly and Targeting of Cancer Cell-Astrocyte

# Gap Junctions in Brain Metastasis

Qing Chen[1], Adrienne Boire[1,2], Manuel Valiente[1], Xin Jin[1†], Ekrem Emrah Er[1], Ruzeen Patwa[1], Ke Xu[3] and Joan Massagué[1]

[1] Cancer Biology and Genetics Program,

[2] Department of Neurology,

[3] Molecular Cytology Core Facility

Memorial Sloane-Kettering Cancer Center, New York, NY 10065, USA

[†] Current address: Cancer Program, The Eli and Edythe L. Broad Institute, Cambridge, Massachusetts 02142, USA.

Correspondence:

Joan Massagué, PhD

Box 116, Memorial Sloan Kettering Cancer Center

1275 York Avenue, New York, NY 10065 USA

Phone: 646-888-2044 Email: j-massague@ski.mskcc.org

# SUMMARY

Brain metastases represent a substantial source of morbidity and mortality. The role of the most abundant cell type in the brain, the astrocyte, in brain metastasis has remained ambiguous. Cancer cells within the brain parenchyma are killed by astrocytes. However, growing brain metastases display marked astrocytic infiltrate. We resolve this paradox by demonstrating that breast and lung cancer cells express protocadherin 7 (PCDH7), to direct assembly of functional carcinoma-astrocyte gap junctions composed of connexin 43 (Cx43). Depleted of PCDH7 or Cx43, brain metastatic cells traverse the blood-brain barrier and co-opt brain capillaries, but fail to form overt metastatic lesions. Treatment of mice with modulators of gap junction signaling suppresses the progression of established brain metastases. The evidence supports a model whereby PCDH7 directs brain metastatic cells to engage the protective astrocyte network to withstand physiologic and chemotherapeutic stresses. Cancer cell-astrocyte gap junction function represents a promising therapeutic target for treatment of brain metastases.

Brain metastases occur in 20-40% of advanced stage cancers and represent the most prevalent intracranial malignancy in adults[1,2]. Improvements in modern imaging and more effective systemic therapies together with increased life expectancy have led to increased diagnosis of brain metastasis, most strikingly in the case of Her-2 breast cancer[3,4]. Despite treatment advances at other metastatic sites, current clinical management of brain metastases affords limited disease control and most patients succumb to tumour progression less than twelve months after diagnosis[1,5].

Recent work has begun to uncover the complex cellular and molecular interactions responsible for initiation and progression of brain metastases. Circulating cancer cells first traverse the reinforced vessel walls that constitute the blood-brain barrier (BBB)[6], aided by a number of factors[7-9]. Within the brain parenchyma, metastatic cells remain associated with the microvasculature[10], tightly adherent to the abluminal capillary basal lamina via L1CAM[11]. However, the vast majority of cancer cells that infiltrate the brain perish[10,12], rejected by the most abundant cell type in the brain, the astrocyte[11]. The astrocyte network, coupled together via gap junctions, serves a protective, homeostatic role in the CNS[13,14]. In the setting of brain metastasis, reactive astrocytes generate the protease plasmin and subsequent cytotoxic cytokines[11]. To counter this attack, brain metastatic cells express serpin inhibitors of plasminogen activator[11]. However, astrocyte may not be uniformly antagonistic to invading cancer cells. Growing metastatic lesions contain abundant astrocytes[14], and astrocytes can have protective effects on cancer cell co-cultures *in vitro*[15].

In this report, we disambiguate the dual role of the astrocyte in brain metastasis. We identify the neural member of the cadherin family protocadherin 7 (PCDH7) as a component that brain metastatic cells employ to selectively engage astrocytes in the formation of protective gap junctions. We show that, once thus engaged with astrocytes, cancer cells are able to withstand physiologic as well as chemotherapeutic stresses. Based on these insights, and using existing modulators of gap junction function, we provide proof-of-principle for the applicability of these drugs to treat established brain metastasis.

## Brain Metastasis Linked to PCDH7 Expression

Lung and breast cancers are the most common sources of brain metastasis[1]. We employed four brain metastatic models derived from mammary (MDA231-BrM2, ErbB2-BrM) or lung adenocarcinomas (H2030-BrM3, Kras/p53-BrM), of either human or murine origin that represent major disease subtypes (Extended Data Table 1)[7,11,16,17]. When implanted as tumours in the orthotopic site or inoculated into the arterial circulation of mice these cells form brain lesions that replicate key features of the human disease, including marked astrocytosis (Fig. 1a) and edema[7,11,16]. In all these models, the brain metastatic cells produce anti-PA serpins to prevent the generation of lethal plasmin by reactive astrocytes[11]. Congruent with previous *in vitro* observations[15], co-culture of these brain metastatic derivatives with astrocytes protected cancer cells from chemotherapy and the proapoptotic cytokine FasL (Extended Data Fig. 1). To assess the effect of astrocytes on tumour growth independent of other components of the brain microenvironment, we co-implanted astrocytes and BrM cells subcutaneously. The admixture of astrocytes in these ectopic tumours increased tumour outgrowth (Fig. 1b). These results suggested a possible dual role of astrocytes in brain metastasis.

As enforcers of homeostasis in the brain parenchyma, astrocytes interact with their adjacent astrocytes, endothelial cells and neurons through gap junctions[18]. Connexin 43 (Cx43, also known as gap junction protein α1, GJA1) is integral to these interactions. Beyond its role in the brain, Cx43 can mediate cancer cell-endothelial cell interactions[19] and cancer cell-astrocyte interactions[20]. It is unclear whether these interactions are pro-metastatic[21,22], anti-metastatic[23,24], or chemoprotective[15]. In our models, some brain metastatic derivatives expressed higher levels of Cx43 than the parental cancer cell population (Fig. 1c, Extended Data Fig. 2a). However, the correlation was imperfect: The lung cancer H2030 cell line expressed high level of Cx43 without further upregulation in the brain metastatic derivative H2030-BrM3 (Fig. 1c, Extended Data Fig. 2a). Moreover, Cx43 expression in the metastatic cells was lower than, or similar to that in astrocytes, neurons and brain microvascular endothelial cells (Fig. 1d, Extended Data Fig. 2c). Because astrocyte, neurons and endothelium are engaged in gap junctions through Cx43[25], these observations raised the questions of whether and how metastatic cells compete for gap junction formation with astrocytes and other brain parenchymal cells.

3

Reasoning that cancer cells must use another component besides Cx43 to engage astrocytes in the brain, we investigated protocadherin 7 (PCDH7), one of a small group of genes that are upregulated in brain metastatic cells from both breast tumours and lung tumours[7,16]. Protocadherins are integral membrane proteins with seven cadherin repeats thought to mediate cell-cell contacts by homophilic interaction. PCDH7 (also known as cadherin-related neuronal receptor) is singular among protocadherins for being expressed predominantly in brain[26,27]; its function is unknown. PCDH7 levels were higher in all our brain metastatic models than in corresponding parental cell lines (Fig. 1c, Extended Data Fig. 2b) or in matched derivatives that are highly metastatic to bone or lung but not brain (Fig. 1e; refer to Extended Data Table 1). The PCDH7 level in brain metastatic cells was higher than in astrocytes, neurons, microglia or endothelial cells (Fig. 1d, Extended Data Fig. 2c).

In clinical cohorts of triple-negative breast cancer with site of relapse annotation, the combined expression of *PCDH7* and *Cx43* in primary tumours was associated with brain metastasis, but not bone or lung metastasis (Fig. 1f). Although most lung adenocarcinoma datasets are not annotated with site-specific metastasis information, a large proportion (up to 70%) of relapses in these patients include brain metastases[28]. Due to the profound morbidity and mortality associated with brain metastases[29], these contribute disproportionately to metastasis-free survival. Indeed, *Cx43* and *PCDH7* expression were associated with decreased metastasis-free survival of lung adenocarcinoma patients in three cohorts (Fig. 1g, Extended Data Fig. 2d). Taken together, these results support the hypothesis that PCDH7 and Cx43 are relevant in brain metastasis.

**PCDH7 Directs Carcinoma-Astrocyte Gap Junctions**

Gap junctions are formed by hexameric connexin hemi-channels. Pairwise interactions between hemi-channels on adjacent cells create junctions that allow the traffic of many small cytosolic molecules[30-32]. Anti-Cx43 immunostaining of brain metastatic lesions in mice demonstrated Cx43 accumulation at carcinoma-astrocyte interfaces (Fig. 2a). Certain cancer cell gap junctions are capable of junctional coupling[33], and others are not[24,34]. To assay junctional activity, we undertook dye transfer assays (Extended Data Fig. 3). Calcein AM transfer from MDA231-BrM2 cells to astrocytes, or vice versa, occurred in a time-dependent manner, as demonstrated by time-lapse fluorescent microscopy (Extended Data Fig. 3a; Supplementary Video 1) or flow cytometry (Extended Data Fig. 3b). Dye transfer from astrocytes occurred more readily with

brain metastatic cancer cells than with their parental counterparts (Fig. 2b). Consistent with the known role of Cx43, dye transfer was dependent on Cx43, as shown by the suppression of the transfer in Cx43-depleted cells using independent shRNA hairpins (Fig. 2c,d, Extended Data Fig. 4a-c). Notably, depletion of PCDH7 by either of two independent shRNA hairpins also suppressed the dye transfer (Fig. 2c,d, Extended Data Fig. 4a-c). Given the ability of cadherins to establish homophilic binding between molecules on adjacent cells[35], we determined whether astrocytic PCDH7 also participates in the formation of gap junctions with cancer cells. Indeed, PCDH7 depletion in astrocytes (Fig. 2e, Extended Data Fig. 4d) inhibited dye transfer from MDA231-BrM2 cells (Fig. 2f). Thus, brain-metastatic cells and astrocytes require both PCDH7 and Cx43 to form functional carcinoma-astrocyte gap junctions.

Compared to astrocytes, human brain microvascular endothelilal cells (HBMECs) had no detectable PCDH7 expression and much lower Cx43 expression (Fig. 1d). Gap junction communication between endothelial cells and cancer cells in dye transfer assays was weak compared to astrocyte-carcinoma communication, and was independent of PCDH7 (Fig. 2g). Moreover, when similar numbers of astrocytes and endothelial cells were allowed to compete for cancer cells, dye transfer between cancer cell and astrocyte was vastly favored over dye transfer between cancer cell and endothelial cell (Fig. 2h). Therefore, PCDH7 directs cancer cells to selectively form Cx43 based gap junctions with astrocytes.

**PCDH7 Interacts with Cx43**

To investigate the mechanism of PCDH7-mediated gap junction formation we employed a split luciferase complementation assay[36] for the detection of PCDH7 interactions with Cx43 in live cells. Constructs encoding PDCH7 and Cx43 fused to the N-terminal (NLuc) and C-terminal (CLuc) halves of firefly luciferase, respectively, were expressed in relevant combinations in test cells (Fig. 3a,b). To avoid pitfalls inherent in overexpression, we generated cell lines with levels of PCDH7 and Cx43 that were somewhat higher than the endogenous levels in the parental cells and lower or comparable to those in BrM derivatives (Fig. 3c and data not shown). Because Cx43 self-assembles into hexameric semi-channels in the cell membrane, transduction of cells with Cx43-NLuc and Cx43-CLuc vectors served as positive control (Fig. 3d).

Using this approach we detected specific luciferase activity in cells expressing both Cx43-CLuc and PCDH7-NLuc (Fig. 3d). No activity was detected when N-cadherin or E-cadherin were fused with NLuc and co-expressed with Cx43-CLuc (Extended Data Fig. 5a-c). Moreover, co-culture with astrocytes generated a higher level of luciferase signal in the transduced cancer cells (Fig. 3e). In contrast to astrocytes, human dermal fibroblasts, which do not express Cx43 or PCDH7 (Extended Data Fig. 5d), did not increase luciferase activity of Cx43-CLuc/PCDH7-NLuc expressing cancer cells (Extended Data Fig. 5e). Together, these observations support a model in which PCDH7 directly and specifically interacts with Cx43 to promote gap junction formation between tumour cells and astrocytes (Fig. 3f).

**Cx43 and PCDH7 Mediate Brain Metastatic Colonization**

RNAi-mediated depletion of either Cx43 or PCDH7 strongly inhibited the formation of brain metastases by breast cancer and lung cancer cells in both immunodeficient (MDA231-BrM2, H2030-BrM3) and immunocompetent (Kras/p53-393N1) models (Fig. 4a-c). Immunohistologic staining for GFP in brain sections confirmed this result and indicated a marked reduction in lesion size as a result of Cx43 or PCDH7 depletion (Fig. 4d). These effects were specific to brain metastasis as depletion of Cx43 or PCDH7 did not affect the formation of lung lesions by MDA231-BrM2 cells after tail vein injection (Extended Data Fig. 6a).

To obviate the possible confounding effects of gap interactions between the cancer cells and other cells within the brain parenchyma, we used the astrocyte-dependent ectopic tumour formation assay (refer to Fig. 1c). Congruent with our model, astrocyte facilitation of tumour growth in these assays also required Cx43 and PCDH7 expression in the cancer cells (Fig. 4e). When co-injected with human brain microvascular endothelial cells, tumour growth neither enhanced nor dependent on Cx43 and PCDH7 (Extended Data Fig. 6b).

To isolate the stage at which PCDH7 and Cx43 in the cancer cells contribute to the formation of brain metastases, we assessed metastatic activity at two time points after arterial inoculation of cancer cells. The first time point was at 7 days post-inoculation, which in these models corresponds to the point when extravasation of cancer cells across BBB into the brain parenchyma has been completed and colony outgrowth is starting[11]. Cx43 or PCDH7 depletion in MDA231-BrM2 did not significantly diminish the number of GFP+ cancer cells in the brain

parenchyma 7 days after inoculation (Extended Data Fig. 7a). Vascular endothelial cells and astrocytes grown on opposite sides of a microporous membrane reconstitute a BBB surrogate *in vitro* that brain metastatic cells can trespass[7]. In this assay, the knockdown of Cx43 or PCDH7 in the cancer cells did not inhibit the BBB transmigration activity (Extended Data Fig. 7b). These results suggested that Cx43 or PCDH7 are not required for the entry of circulating cancer cells into the brain parenchyma.

Fourteen days after inoculation into the circulation of mice, cancer cells that were depleted of Cx43 or PCDH7 showed a significant decrease in the size distribution of micrometastases (Extended Data Fig. 8a,b). The colonies that were formed by Cx43- or PCDH7-depleted cells displayed decreased proliferation, as determined by Ki67 staining of brain sections (Figure Extended Data Fig. 8c). Of note, these Cx43- or PCDH7-depleted cells retained close interactions with vascular structures *in vivo* (Extended Data Fig. 8d). These cells also retained ability to coopt vasculature in *in vitro* assays employing 3D-cultured brain microvascular endothelial cells, a key step in the initiation of metastatic colonization (Extended Data Fig. 8e). To assess cancer cell apoptosis within the brain parenchyma, we employed brain-slice assays[11]. We detected increased apoptosis in Cx43 or PCDH7-depleted cells, as determined by cleaved caspase 3 staining (Extended Data Fig. 9a). In carcinoma-astrocyte co-culture experiments, the protective effect of astrocytes also depended on Cx43 and PCDH7 (Extended Data Fig. 9b).

**Pharmacologic Inhibition of Gap Junction Activity**

Our results provided a rationale for testing pharmacologic suppressors of gap junction activity in combination with chemotherapy against brain metastasis. To this end, we selected two compounds for pre-clinical trials. Tonabersat is an orally bioavailable benzopyran derivative that inhibits gap-junction mediated pathophysiological processes including cortical spreading depression[37-39] and trigeminal ganglion neuronal-satellite cell signaling in animal models[40]. It binds to a unique stereoselective binding site in astrocytes[41-43]. Tonabersat was employed as anti-migraine therapy[44] When administered systemically, tonabersat negatively modulates neuron-astrocyte gap junction activity[41,44] without altering human blood vessels or myocardium function[45]. In clinical trials, the effective does of tornabersat, 10 mg/kg, was well-tolerated and safe in patients with migraine, though less effective for migraine pain than anticipated[46-48].

In addition to their anti-inflammatory properties, the fenamate class of non-steroid anti-inflammatory drugs (NSAID) possess anti-gap junction activity, as shown by inhibition of Ca+ action potential propagation in normal rat kidney fibroblasts[49]. Meclofenamate has a distinct structure within the class[50], and inhibits epileptogenesis in animal models[51,52]. Meclofenamate inhibits Cx43 gap junction gating, as measured by voltage-clamp step response[49,53]. It is well tolerated systemically[54] and is an FDA-approved NSAID in use for arthritic pain.

The gap junction modulatory properties of tonabersat and meclofenamate *in vivo* and their biosafety made them attractive candidates for testing our hypothesis. Mice were treated with either vehicle or with these compounds from day 1 following inoculation with breast cancer MDA231-BrM2 cells, or with lung cancer H2030-BrM3 cells in immunodefiecent mice and Kras/p53-393N1 cells in immunocompetent mice (Fig. 4f). In this early treatment protocol, both drugs prevented the emergence of brain metastases, which was consistent with our evidence that gap junction activity supports metastatic outgrowth (Fig. 4g,h). Similar inhibition of tumour growth by both drugs was observed in the astrocyte-dependent ectopic tumour formation assay (Fig. 4i). In contrast, the growth of MDA231-BrM2 cells as lung metastatic lesions, or as tumours in mammary fat pads, was resistant to this treatment (Extended Data Fig. 10a,b).

**Gap Junction Directed Suppression of Overt Brain Metastasis**

To test the effect of Cx43 or PCDH7 depletion once the brain metastases were established, we transduced MDA231-BrM2 cells with Tet-inducible shRNA expression vectors. A red fluorescence protein under the control of the same promoter provided a marker of hairpin expression (Extended Data Fig. 11a). Cells transduced with inducible *Cx43* or *PCDH7* shRNA vectors showed doxycycline-dependent depletion of Cx43 or PCDH7, respectively, after 48h (Extended Data Fig. 11a,b). Thus engineered, the cells were inoculated into the arterial circulation of mice and allowed to form brain metastatic colonies for 14 days, at which point brain lesions were apparent by BLI in all the mice (Extended Data Fig. 11c). At this stage, the lesions were growing aggressively, engulfing the microvasculature and forming multilayered tumours (Fig. 5a), which will cause the demise of the animals within another 2-3 weeks[7,11]. Administration of doxycycline starting on day 14 resulted in a significant decrease in brain metastatic burden generated by Cx43 or PCDH7 knockdown cells three weeks later, compared to controls (Fig. 5b).

Brain metastases are distinguished by pronounced resistance to chemotherapy[55-57]. Carboplatin crosses the blood brain barrier[58], and has shown modest improvements in overall survival in patients with breast cancer[59] and non-small cell lung cancer[60]. Administration of carboplatin alone (50 mg/kg/5 days) starting on day 14 inhibited brain metastasis to an extent similar to that of depleting Cx43 or PCDH7 (Fig. 5b). When carboplatin was combined with doxycycline, the brain metastatic burden generated by Cx43- or PCDH7-depleted cells was further reduced (Fig. 5b). PCDH7 or Cx43 depletion also significantly increased the susceptibility of the cancer cells to carboplatin in ectopic astrocyte-dependent tumour formation assays (Extended Data Fig. 11d).

Next we assessed the effectiveness of chemotherapy in combination with gap junction modulatory therapy. Treatment with carboplatin minimally inhibited brain metastasis growth (Fig. 5c). Daily administration of tonabersat (10 mg/kg) or meclofenamate (20 mg/kg) as single agents (Fig. 5c) significantly inhibited the progression of metastatic lesions as determined at the 35-day end point. The combination of carboplatin with either tonabersat or meclofenamate profoundly inhibited brain metastasis (Fig. 5c).

**DISCUSSION**

The brain represents a unique and formidable metastatic target, with astrocytes a predominant feature of the metastatic microenvironment. Taken together, our results suggest that brain metastatic cells that have infiltrated the brain and withstood deleterious effect of astrocytes can employ the gap junction components PCDH7 and Cx43 to engage astrocytes for protection against microenvironmental stresses and exogenous chemotherapeutic agents (Fig. 5d). Cadherin family members are important mediators of cell-cell communication in embryo development and tissue homeostasis[35], including many roles in the developing nervous system[61]. It is remarkable that brain metastatic cells adopt a particular member of this family whose normal expression is largely restricted to the brain[26]. PCDH7 therefore joins ST6GALNAC5[7], and neuroserpin[11] as brain-restricted components that brain metastatic cells from breast and lung carcinomas selectively express to colonize the brain.

In our brain metastasis models, PCDH7 and Cx43 contribute to colony expansion and chemoresistance once metastatic colonies initiate robust proliferation. PCDH7 and Cx43 were not required for the earlier events of extravasation or vascular cooption of cancer cells in the brain. Our results provide *in vivo* evidence and mechanistic underpinnings for a previously observed chemoprotective effect of astrocytes on cancer cells *in vitro*[15]. The present evidence suggests that cancer cells protect themselves from astrocytic attack in two distinct ways: first, through generation of plasmin inhibitors such as serpins, and second, by engaging astrocytes through gap junctions. This duality is reminiscent of the complex role of tumour-associated macrophages in cancer[62,63].

Brain metastases are a major contributor to cancer patient morbidity and mortality, with few therapeutic options available. Early steps in the brain metastatic cascade, including cancer cell dissemination from source tumours and extravasation through the BBB, have not been amenable to therapy[2,6]. However, cancer cell dependency on PCDH7 and Cx43 for the survival and outgrowth of metastatic lesions suggests an opportunity that could be therapeutically exploited for the treatment of brain metastasis. Our pre-clinical results using combinations of chemotherapy and gap junction modulators provide proof of principle for the therapeutic potential of these interventions against brain metastasis.

**METHODS**

**Cell Culture.** MDA-MD-231, MMTV-neu parental and metastatic derivative cell lines and 373N1, 393N1, 482N1, 2691N1 cells were cultured in DMEM with 10% fetal bovine serum (FBS) and 2mM L-Glutamine. H2030 parental and metastatic derivative cell lines cells were cultured in RPMI 1640 medium with 10% FBS and 2 mM L-Glutamine. For lentivirus production, 293T cells were cultured in DME media supplemented with 10% fetal bovine serum and 2 mM L-Glutamine. Human primary astrocytes, human brain microvascular endothelial cells (HBMEC) and human adult dermal fibroblasts (ScienCell) were cultured in complete astrocyte medium, endothelial cell medium and fibroblast medium (ScienCell) and used between passages 2-6.

**Animal Studies.** All experiments using animals were done in accordance to a protocol approved by MSKCC Institutional Animal Care and Use Committee (IACUC). Athymic NCR nu/nu (NCI-Frederick), Cr:NIH bg-nu-xid (NCI-Frederick) and B6129SF1/J (Jackson Laboratory) mice between 5-6 weeks old were used for all animal experiments. For long-term brain metastasis assays, we followed previously described procedures[64]. In brief, 10,000 MDA BrM, 50,000 H2030 BrM and 100,000 393N1 cells in 100 μl PBS were injected in the left ventricle. At the experimental endpoint, anesthetized mice (ketamine100 mg/kg and xylazine 10 mg/kg) were injected retro-orbitally with D-Luciferin (150 mg/kg) and brain colonization was quantified by *ex vivo* BLI. In short-term brain metastasis experiments (7- and 14-days), 500,000 cancer cells were injected in the left ventricle and brain tissues were harvested for further analysis. In selected experiments, TRITC dextran (70 KD) (Life technology) was intravenously injected to indicate vascular structures. For inducible knockdown experiments, the experimental mice were fed with doxycycline hyclate (Sigma-Aldrich) containing water (2 mg/mL) and diet (Harlan) 14 days after initial injection. For lung colonization assays, 200,000 MDA BrM cells in 100 μL PBS were injected into the lateral tail vein, and lung colonization was quantified using BLI. For co-injection experiments, 5,000 cancer cells and 10,000 astrocytes or HBMEC were subcutaneously injected in the experimental mice. For the primary tumour implantation, 5,000 cells in 50 μL of 1:1 mix of PBS/growth factor reduced matrigel (BD Biosciences) were injected into the 4th right mammary fat pad of mice. In the indicated experiments, the experimental mice were

intraperitoneally injected with carboplatin (Hospira)(50 mg/kg/5 days), tonabersat (MedChem Express)(10 mg/kg/day) or meclofenamic acid sodium salt (Sigma-Aldrich) (20 mg/kg/day) while the vehicle (10% DMSO in Poly ethynol glycol, 400) was injected into control mice. BLI was done by IVIS Spectrum Xenogen machine (Caliper Life Sciences) and analysis was performed using Living Image software, version 2.50.

**Knockdown and Overexpression Constructs.** In human cancer cells, stable knockdown of Cx43 and PCDH7 were generated using shRNAs in pLKO.1 lentiviral vectors (Open Biosystems): TRCN0000059773 (Cx43 sh1), TRCN0000059775 (Cx43 sh2), TRCN0000055744 (PCDH7 sh1) and TRCN0000291663 (PCDH7 sh2). Virus-infected cells were selected with 5 μg/ml puromycin. For inducible knockdown system, shRNAs in TRIPZ lentivial vector were used (Open Biosystems): V3THS_411733 (Cx43 sh1), V3THS_411729 (Cx43 sh2), V3THS_338930 (PCDH7 sh1) and V3THS_152694 (PCDH7 sh2). 1μg/mL doxycycline hyclate (Sigma-Aldrich) were added to induce the expression of shRNA. In mouse cancer cells, stable knockdown of Cx43 and PCDH7 were generated using shRNAs in GIPZ lentiviral vectors (Open Biosystems): V3LHS_411730 (Cx43 sh), V3LMM_510718 (PCDH7 sh1) and V2LMM_11270 (PCDH7 sh2). To set up luciferase complementation assay[36], fusion cDNA was generated by deleting stop codon in human Cx43 (Origene), PCDH7 (Origene), E-cadherin (Addgene) or N-cadherin (Addgene) cDNA and connecting the N terminal or C terminal fragment of firefly luciferase (Addgene). The constructs were cloned into PLVX lentiviral expression vector to stably express the fusion proteins in unmodified MDA-MB-231 or H2030 cells.

**mRNA and Protein Levels.** Total RNA was extracted using the PrepEase RNA spin kit (USB). 1 micrograms of total RNA was subjected to Transcriptor First Strand cDNA synthesis kit (Roche). Cx43 expression was quantified by Taqman gene expression assay primers (Hs00748445_s1, Mm00439105_m1, Applied Biosystems). Relative gene expression was normalized to the *β2M* (Hs99999907_m1, Mm00437762_m1). Primer pair is designed to detect all PCDH7 isoforms: 5'-agttcaacgtggtcatcgtg-3'(sense), 5'-acaatcagggagttgttgctc-3'(antisense); and reactions were performed using SYBR Green I Master Mix (Applied Biosystems). Expression data was acquired using an ABI Prism 7900HT Sequence Detection System (Applied Biosystems). Quantitative expression data were acquired and analyzed using an ABI Prism 7900HT Sequence Detection System (Applied Biosystems). For western immunoblotting, cancer

cell pellets were lysed with RIPA buffer and protein concentrations determined by BCA Protein Assay Kit (Pierce). Protein lysates of primary human astrocytes, neurons, microglia and HBMEC were purchased from Sciencell. Proteins were separated by SDS-PAGE and transferred to nitrocellulose membranes (Bio-Rad). Membranes were immunoblotted with monoclonal antibodies against PCDH7, α-tublulin (Sigma-Aldrich), or Cx43, E-cadherin, N-cadherin (Cell Signaling).

**Dye Transfer Assays.** Monolayer of cancer cells or astrocytes was labelled with 2.5 μg/ml Calcein Red-Orange AM dye (Life Technology) at 37°C for 30 minutes. Single cell suspensions of labelled cells and cells were mixed at a ratio of 2 (labelled): 1 (unlabelled). In the selected experiments, 3 cell populations were mixed: MDA231-BrM (GFP-positive), HBMEC (prlabelled with Cell Proliferating Dye eFluor@670 (eBioscience)) and unlabelled astrocytes. Dye transfer was either directly observed by Zeiss LSM 5 Live confocal microscope (20-minute time lapse) or quantified by FACSCalibur flow cytometer (BD Biosciences) at different time points.

*In Vitro* **Coculture Experiments.** Single cell suspensions of astrocytes and cancer cells were mixed at ratio of 2 (astrocyte): 1 (cancer cell). After overnight incubation, the co-cultured cells were treated with 500 ng/ml sFasL in serum free media (Peprotech), 500 nM carboplatin (Sigma-Aldrich) or 25 nM Paclitaxel (Sigma-Aldrich) for 24 hours. Single cells suspensions were stained with APC-conjugated cleaved caspase 3 antibody (Cell Signaling) and apoptotic GFP$^+$ cancer cells were detected by flow cytometer.

**Immunohistochemical Staining.** To visualize metastatic lesions, brains were fixed with 4% paraformaldehyde and sectioned by vibratome (Leica) or cryostat (Leica). Cryosections were used for GFP (Aves Labs)/Ki67 (Novus) or GFP/GFAP (Dako) dual staining. Following the established protocol [11], brain slides (80 μm) were stained with GFP (Aves Labs), GFAP (Dako and Millipore), Col.IV (Millipore), Cx43 (Cell Signaling). Brain slides were used to detect cancer cell apoptosis [11]. In brief, adult mouse brains were sliced at 250um using a vibratome (Leica) and slices were placed on top of 0.8um pore membranes (Millipore) in Slice Culture Medium (DMEM, complete HBSS, FBS 5%, L-Glutamine (1mM), 100 IU/mL penicillin, 100 μg/mL streptomycin). 3x10$^5$ cancer cells were plated on the surface of the brain slice. 48 hours after incubation, brain slices were fixed 4% paraformaldehyde and stained with GFAP and

cleaved caspase 3 (Cell Signaling). Images were acquired with Zeiss Axio Imager.Z1 microscope or Leica SP5 up-right confocal microscope. Images analyzed with ImageJ, Imaris and Metamorph softwares.

**Trans-BBB Assays.** This assay was performed as previously described[7]. Briefly, primary human brain microvessel endothelial cells (HBMEC, ScienCell) were co-cultured with human primary astrocytes (ScienCell), on opposite sides of a polylysine-treated, gelatin-coated tissue culture transwell insert (3 μm pore, Fisher) for 3 days. Cancer cells were prelabelled with green CMFDA (5-chloromethylfluorescein diacetate, Invitrogen) and $5 \times 10^5$ cancer cells were seeded on the upper chamber and incubated for 18 h. Inserts were washed with PBS and fixed with 4% PFA. Transmigrated cells was quantified by green fluorescent signals.

**Statistical analysis**

Statistical analysis was performed using GraphPad software (Prism) using Student's *t*-test (two-tailed). *P* value of <0.05 was considered statistically significant. Graphs present the mean value ± standard error of the mean (s.e.m.).

**Analysis of Clinical Data Sets.** *Cx43 and PCDH7* transcript levels were analysed in the microarray data of primary breast cancer (EMC-MSK) and adenocarcinoma (MSKCC set2, GSE3141 and GSE8893). Multiple probes mapping to the same gene were combined by selecting the probe with maximal variance across samples. Triple negative breast cancer subtypes were determined either using the clinical annotation associated with the data set (if applicable) or by the transcript levels of ESR1 and ERBB2. The hazard ratio of the values of Cx43 and PCDH7 was computed based on Cox Proportional Hazards Models, as implemented by the "coxph" command in R. *P* values were calculated from a Cox proportional hazard model, with Cx43 and PCDH7 expression treated as a continuous variable.

**ACKNOWLEDGEMENTS**

## AUTHOR CONTRIBUTIONS

J.M. conceptualized the project and supervised the work. Q.C. conceptualized, designed and performed the experiments. A.B. designed and performed the preclinical treatment experiments. M.V., E.E.E. and R.P. assisted with the experiments. X.J. performed bioinformatics analysis. K.X. assisted the time-lapse confocal imaging. Q.C., A.B. and J.M. wrote the paper.

## REFERENCES

1       Gavrilovic, I. T. & Posner, J. B. Brain metastases: epidemiology and pathophysiology. *Journal of neuro-oncology* **75**, 5-14 (2005).

2       Maher, E. A., Mietz, J., Arteaga, C. L., DePinho, R. A. & Mohla, S. Brain metastasis: opportunities in basic and translational research. *Cancer research* **69**, 6015-6020 (2009).

3       Patel, R. R. & Mehta, M. P. Targeted therapy for brain metastases: improving the therapeutic ratio. *Clinical cancer research : an official journal of the American Association for Cancer Research* **13**, 1675-1683 (2007).

4       Stemmler, H. J. *et al.* Characteristics of patients with brain metastases receiving trastuzumab for HER2 overexpressing metastatic breast cancer. *Breast* **15**, 219-225 (2006).

5       Stelzer, K. J. Epidemiology and prognosis of brain metastases. *Surgical neurology international* **4**, S192-202 (2013).

6       Eichler, A. F. *et al.* The biology of brain metastases-translation to new therapies. *Nature reviews. Clinical oncology* **8**, 344-356 (2011).

7       Bos, P. D. *et al.* Genes that mediate breast cancer metastasis to the brain. *Nature* **459**, 1005-1009 (2009).

8       Li, B. *et al.* Elevated PLGF contributes to small-cell lung cancer brain metastasis. *Oncogene* **32**, 2952-2962 (2013).

9       Sevenich, L. *et al.* Analysis of tumour- and stroma-supplied proteolytic networks reveals a brain-metastasis-promoting role for cathepsin S. *Nature cell biology* **16**, 876-888 (2014).

10      Kienast, Y. *et al.* Real-time imaging reveals the single steps of brain metastasis formation. *Nature medicine* **16**, 116-122 (2010).

11      Valiente, M. *et al.* Serpins promote cancer cell survival and vascular co-option in brain metastasis. *Cell* **156**, 1002-1016 (2014).

12      Heyn, C. *et al.* In vivo MRI of cancer cell fate at the single-cell level in a mouse model of breast cancer metastasis to the brain. *Magnetic resonance in medicine : official journal of the Society of Magnetic Resonance in Medicine / Society of Magnetic Resonance in Medicine* **56**, 1001-1010 (2006).

13      Verkhratsky, A. *et al.* Neurological diseases as primary gliopathies: a reassessment of neurocentrism. *ASN neuro* **4** (2012).

14      Sofroniew, M. V. Molecular dissection of reactive astrogliosis and glial scar formation. *Trends in neurosciences* **32**, 638-647 (2009).

15      Kim, S. J. *et al.* Astrocytes upregulate survival genes in tumor cells and induce protection from chemotherapy. *Neoplasia* **13**, 286-298 (2011).

16      Nguyen, D. X. *et al.* WNT/TCF signaling through LEF1 and HOXB9 mediates lung adenocarcinoma metastasis. *Cell* **138**, 51-62 (2009).

17      Winslow, M. M. *et al.* Suppression of lung adenocarcinoma progression by Nkx2-1. *Nature* **473**, 101-104 (2011).

18      Theis, M. & Giaume, C. Connexin-based intercellular communication and astrocyte heterogeneity. *Brain research* **1487**, 88-98 (2012).

19      Cai, J., Jiang, W. G. & Mansel, R. E. Gap junctional communication and the tyrosine phosphorylation of connexin 43 in interaction between breast cancer and endothelial cells. *International journal of molecular medicine* **1**, 273-278 (1998).

20      Lin, Q. *et al.* Reactive astrocytes protect melanoma cells from chemotherapy by sequestering intracellular calcium through gap junction communication channels. *Neoplasia* **12**, 748-754 (2010).

21      Elzarrad, M. K. *et al.* Connexin-43 upregulation in micrometastases and tumor vasculature and its role in tumor cell attachment to pulmonary endothelium. *BMC medicine* **6**, 20 (2008).

22      Pollmann, M. A., Shao, Q., Laird, D. W. & Sandig, M. Connexin 43 mediated gap junctional communication enhances breast tumor cell diapedesis in culture. *Breast cancer research : BCR* **7**, R522-534 (2005).

23     Stuhlmann, D. *et al.* Modulation of homologous gap junctional intercellular communication of human dermal fibroblasts via a paracrine factor(s) generated by squamous tumor cells. *Carcinogenesis* **24**, 1737-1748 (2003).

24     Li, Z., Zhou, Z., Welch, D. R. & Donahue, H. J. Expressing connexin 43 in breast cancer cells reduces their metastasis to lungs. *Clinical & experimental metastasis* **25**, 893-901 (2008).

25     Eugenin, E. A. *et al.* The role of gap junction channels during physiologic and pathologic conditions of the human central nervous system. *Journal of neuroimmune pharmacology : the official journal of the Society on NeuroImmune Pharmacology* **7**, 499-518 (2012).

26     Yoshida, K., Yoshitomo-Nakagawa, K., Seki, N., Sasaki, M. & Sugano, S. Cloning, expression analysis, and chromosomal localization of BH-protocadherin (PCDH7), a novel member of the cadherin superfamily. *Genomics* **49**, 458-461 (1998).

27     Kim, S. Y., Chung, H. S., Sun, W. & Kim, H. Spatiotemporal expression pattern of non-clustered protocadherin family members in the developing rat brain. *Neuroscience* **147**, 996-1021 (2007).

28     Gaspar, L. E. *et al.* Time from treatment to subsequent diagnosis of brain metastases in stage III non-small-cell lung cancer: a retrospective review by the Southwest Oncology Group. *Journal of clinical oncology : official journal of the American Society of Clinical Oncology* **23**, 2955-2961 (2005).

29     Gaspar, L. E., Scott, C., Murray, K. & Curran, W. Validation of the RTOG recursive partitioning analysis (RPA) classification for brain metastases. *International journal of radiation oncology, biology, physics* **47**, 1001-1006 (2000).

30     Oshima, A. Structure and closure of connexin gap junction channels. *FEBS letters* **588**, 1230-1237 (2014).

31     Bennett, M. V. & Goodenough, D. A. Gap junctions, electrotonic coupling, and intercellular communication. *Neurosciences Research Program bulletin* **16**, 1-486 (1978).

32     Holder, J. W., Elmore, E. & Barrett, J. C. Gap junction function and cancer. *Cancer research* **53**, 3475-3485 (1993).

33    Stoletov, K. *et al.* Role of connexins in metastatic breast cancer and melanoma brain colonization. *Journal of cell science* **126**, 904-913 (2013).

34    Miekus, K., Czernik, M., Sroka, J., Czyz, J. & Madeja, Z. Contact stimulation of prostate cancer cell migration: the role of gap junctional coupling and migration stimulated by heterotypic cell-to-cell contacts in determination of the metastatic phenotype of Dunning rat prostate cancer cells. *Biology of the cell / under the auspices of the European Cell Biology Organization* **97**, 893-903 (2005).

35    Yagi, T. & Takeichi, M. Cadherin superfamily genes: functions, genomic organization, and neurologic diversity. *Genes & development* **14**, 1169-1180 (2000).

36    Luker, K. E. *et al.* Kinetics of regulated protein-protein interactions revealed with firefly luciferase complementation imaging in cells and living animals. *Proceedings of the National Academy of Sciences of the United States of America* **101**, 12288-12293 (2004).

37    Bradley, D. P. *et al.* Diffusion-weighted MRI used to detect in vivo modulation of cortical spreading depression: comparison of sumatriptan and tonabersat. *Experimental neurology* **172**, 342-353 (2001).

38    Smith, M. I. *et al.* Repetitive cortical spreading depression in a gyrencephalic feline brain: inhibition by the novel benzoylamino-benzopyran SB-220453. *Cephalalgia : an international journal of headache* **20**, 546-553 (2000).

39    Read, S. J., Smith, M. I., Hunter, A. J., Upton, N. & Parsons, A. A. SB-220453, a potential novel antimigraine agent, inhibits nitric oxide release following induction of cortical spreading depression in the anaesthetized cat. *Cephalalgia : an international journal of headache* **20**, 92-99 (2000).

40    Damodaram, S., Thalakoti, S., Freeman, S. E., Garrett, F. G. & Durham, P. L. Tonabersat inhibits trigeminal ganglion neuronal-satellite glial cell signaling. *Headache* **49**, 5-20 (2009).

41    Chan, W. N. *et al.* Identification of (-)-cis-6-acetyl-4S-(3-chloro-4-fluoro-benzoylamino)-3,4-dihydro-2,2-dimethyl-2H-benzo[b]pyran-3S-ol as a potential antimigraine agent. *Bioorganic & medicinal chemistry letters* **9**, 285-290 (1999).

42 Herdon, H. J. *et al.* Characterization of the binding of [3H]-SB-204269, a radiolabelled form of the new anticonvulsant SB-204269, to a novel binding site in rat brain membranes. *British journal of pharmacology* **121**, 1687-1691 (1997).

43 Upton, N. *et al.* Profile of SB-204269, a mechanistically novel anticonvulsant drug, in rat models of focal and generalized epileptic seizures. *British journal of pharmacology* **121**, 1679-1686 (1997).

44 Sarrouilhe, D., Dejean, C. & Mesnil, M. Involvement of gap junction channels in the pathophysiology of migraine with aura. *Frontiers in physiology* **5**, 78 (2014).

45 MaassenVanDenBrink, A. *et al.* Craniovascular selectivity of eletriptan and sumatriptan in human isolated blood vessels. *Neurology* **55**, 1524-1530 (2000).

46 Goadsby, P. J. *et al.* Randomized, double-blind, placebo-controlled, proof-of-concept study of the cortical spreading depression inhibiting agent tonabersat in migraine prophylaxis. *Cephalalgia : an international journal of headache* **29**, 742-750 (2009).

47 Silberstein, S. D. *et al.* Tonabersat, a gap-junction modulator: efficacy and safety in two randomized, placebo-controlled, dose-ranging studies of acute migraine. *Cephalalgia : an international journal of headache* **29 Suppl 2**, 17-27 (2009).

48 Dahlof, C. G., Hauge, A. W. & Olesen, J. Efficacy and safety of tonabersat, a gap-junction modulator, in the acute treatment of migraine: a double-blind, parallel-group, randomized study. *Cephalalgia : an international journal of headache* **29 Suppl 2**, 7-16 (2009).

49 Harks, E. G. *et al.* Fenamates: a novel class of reversible gap junction blockers. *The Journal of pharmacology and experimental therapeutics* **298**, 1033-1041 (2001).

50 Bartzatt, R. Anti-inflammatory drugs and prediction of new structures by comparative analysis. *Anti-inflammatory & anti-allergy agents in medicinal chemistry* **11**, 151-160 (2012).

51 Jin, M. *et al.* Effects of meclofenamic acid on limbic epileptogenesis in mice kindling models. *Neuroscience letters* **543**, 110-114 (2013).

52    Nilsen, K. E., Kelso, A. R. & Cock, H. R. Antiepileptic effect of gap-junction blockers in a rat model of refractory focal cortical epilepsy. *Epilepsia* **47**, 1169-1175 (2006).

53    Juszczak, G. R. & Swiergiel, A. H. Properties of gap junction blockers and their behavioural, cognitive and electrophysiological effects: animal and human studies. *Progress in neuro-psychopharmacology & biological psychiatry* **33**, 181-198 (2009).

54    Holmes, E. L. Experimental observations on flufenamic, mefenamic, and meclofenamic acids. IV. Toleration by normal human subjects. *Annals of physical medicine* **Suppl**, 36-49 (1966).

55    Deeken, J. F. & Loscher, W. The blood-brain barrier and cancer: transporters, treatment, and Trojan horses. *Clinical cancer research : an official journal of the American Association for Cancer Research* **13**, 1663-1674 (2007).

56    Loscher, W. & Potschka, H. Drug resistance in brain diseases and the role of drug efflux transporters. *Nature reviews. Neuroscience* **6**, 591-602 (2005).

57    Zhang, R. D., Price, J. E., Fujimaki, T., Bucana, C. D. & Fidler, I. J. Differential permeability of the blood-brain barrier in experimental brain metastases produced by human neoplasms implanted into nude mice. *The American journal of pathology* **141**, 1115-1124 (1992).

58    Pitz, M. W., Desai, A., Grossman, S. A. & Blakeley, J. O. Tissue concentration of systemically administered antineoplastic agents in human brain tumors. *Journal of neuro-oncology* **104**, 629-638 (2011).

59    Lim, E. & Lin, N. U. Updates on the Management of Breast Cancer Brain Metastases. *Oncology (Williston Park)* **28** (2014).

60    Taimur, S. & Edelman, M. J. Treatment options for brain metastases in patients with non-small-cell lung cancer. *Current oncology reports* **5**, 342-346 (2003).

61    Hirano, S., Suzuki, S. T. & Redies, C. The cadherin superfamily in neural development: diversity, function and interaction with other molecules. *Frontiers in bioscience : a journal and virtual library* **8**, d306-355 (2003).

62    Noy, R. & Pollard, J. W. Tumor-Associated Macrophages: From Mechanisms to Therapy. *Immunity* **41**, 49-61 (2014).

63    Joyce, J. A. & Pollard, J. W. Microenvironmental regulation of metastasis. *Nature reviews. Cancer* **9**, 239-252 (2009).

64    Bos, P. D., Nguyen, D. X. & Massague, J. Modeling metastasis in the mouse. *Current opinion in pharmacology* **10**, 571-577 (2010).

**FIGURE LEGENDS**

**Figure 1 | Brain Metastasis Linked to Protocadherin 7 Expression.**

**a**, GFP+ H2030-BrM3 cells (green) are surrounded by GFAP+ activated astrocytes (red) in the brain parenchyma at early (7 days) and later (21 days) time points after inoculating cancer cells into the circulation. Blue, vessels stained by collagen IV (ColIV). Scale bar, 10 μm. **b,** 3 weeks after subcutaneous co-injection of MDA231-BrM2 cells and astrocytes, the growth of cancer cells were quantified by bioluminescent imaging. **c,** Cx43 and PCDH7 expression in parental (Par) and metastatic derivatives of brain (BrM) by western immunoblotting. **d,** Comparison of Cx43 and PCDH7 expression in BrM cells and different cell types in brain. **e,** Cx43 and PCDH7 expression in MDA231 parental cells (Par) and the metastatic derivatives of brain (BrM2), lung (LM) and bone (BoM). **f,** Kaplan-Meier plot illustrates the probability of cumulative brain metastasis (met) free survival in 189 cases of triple negative breast cancer according to Cx43/PCDH7 expression in the primary tumours. Similar assay was done for lung and bone metastasis survival and *P* values are indicated in the table. **g,** Kaplan-Meier plot illustrates the probability of cumulative metastasis free survival in 129 cases (MSKCC set2) of lung adenocarcinoma according to Cx43/PCDH7 expression in the primary tumours.

**Figure 2 | PCDH7 Enhances Carcinoma-Astrocyte Gap Junction Communications.**

**a,** Cx43 staining (red) at H2030-BrM3 (green) and astrocytes (blue) interfaces (arrow head). Scale bar, 10 μm. **b,** Quantification of dye transfer from astrocytes to cancer cells. Histograms show red fluorescent signals in parental (Par) and BrM cells. **c,** Knockdown of Cx43 and PCDH7 in MDA231-BrM2 cells with short hairpin RNAs (shRNA) as assessed by immunoblotting. Ctrl, control. **d,** Quantification of dye transfer from astrocytes to Cx43- or PCDH7-depleted BrM cells. **e,** Knockdown of PCDH7 in astrocytes with shRNAs. **f,** Quantification of dye transfer from MDA231-BrM2 cells to PCDH7-depleted astrocytes. **g,** Quantification of dye transfer from MDA231-BrM2 cells to Cx43- or PCDH7-depleted human brain microvascular endothelial cells (HBMEC). **h,** Dye transfer from MDA231-BrM2 cells to a mixed population of astrocytes and HBMEC. All graphs shown are mean ± s.e.m. (n = 3 in each group).

**Figure 3 | Cx43 and PCDH7 Interaction.**

**a,** Schematic illustration of luciferase complementary assay to detect the Cx43-PCDH7 interactions. Nluc: N-terminal fragments of firefly luciferase; Cluc: C-terminal fragments of

firefly luciferase. **b,** Index of the cell lines generated to express different combinations of fusion protein. **c,** Western immunoblotting indicating the Cx43 and PCDH7 levels after overexpressing the fusion proteins. Lane loading is according to table in **b**. **d,** Bioluminescent imaging (BLI) to detect luciferase activities of cell lines according to table in **b**. **e,** Quantification of BLI after co-culture of the cancer cells and astrocytes for 15 minutes. **f,** Schematic summary of Cx43-PCDH7 interactions.

**Figure 4 | Inhibition of Gap Junction Activity Prevents Brain Metastatic Outgrowth.**
**a,** Experimental design for brain metastasis assay. **b,** Bioluminescent imaging (BLI) of brain metastatic lesions formed by control, Cx43- or PCDH7-depleted MDA231-BrM2 cells. **c,** BLI quantification of brain metastatic lesions. **d,** Quantification of the brain metastatic lesions formed by control, Cx43- or PCDH7-depleted MDA231-BrM2 cells. Representative images are the GFP+ cancer cells in the coronal brain sections. Brain lesions were classified based on their sizes and quantified in each group. All graphs shown are mean ± s.e.m. (n = 3 brains in each group). Scale bar, 200 μm. **e,** Control, Cx43- or PCDH7-depleted MDA231-BrM2 cells were subcutaneously co-injected with or without astrocytes, the growth of cancer cells were measured by BLI. **f,** Schematic illustration of treatment regimens. **g,** BLI quantification of brain metastatic lesions from by MDA231-BrM after daily application of tonabersat (Tona) or meclofemamate (Meclo). **h,** BLI quantification of brain metastatic lesions following the treatment regimens showing in **f**. **i,** MDA231-BrM2 cells were subcutaneously co-injected with astrocytes, the growth of cancer cells were measured by BLI following the treatment regimens showing in **f**.

**Figure 5 | Targeting Gap Junction Activity Controls Established Brain Metastases.**
**a,** GFP staining (green) of 14 day brain metastatic lesions. Representative images show large, progressive lesions. Blue, DAPI nuclear staining. Bar, 40μm. **b,** 14 days after inoculation with MDA231-BrM2 cells transduced with inducible control, *Cx43* or *PCDH7* shRNA, experimental mice were treated with doxycycline and carboplatin. Brain metastatic lesions were quantified by bioluminescent imaging (BLI). Representative images are the brain *ex vivo* BLI and red fluorescent images of the same brain. **c,** 14 days after inoculation with MDA231-BrM2 cells, mice were treated with tonabersat (Tona), meclofenamate (Meclo) and carboplatin (Carbo). Following the illustrated regimens, brain metastasis lesions were quantified by BLI. **d,** Summary dual functions of astrocytes to invaded cancer cells: (1) killing factors released by astrocytes and

(2) prometastatic effect of PCDH7 mediated gap junction communications between cancer cells and astrocytes.

## EXTENDED DATA FIGURE LEGENDS

**Extended Data Figure 1 | Astrocytes Co-culture Protects Cancer Cells.**
GFP+ BrM cells were co-cultured with or without astrocytes. 24 hours after sFasL- or chemo-treatments, apoptotic BrM cells were detected by cleaved caspase 3 (Casp3) staining.

**Extended Data Figure 2 | Elevated Expression of Cx43 and PCDH7 in Brain Metastatic Cancer Cells and Astrocytes.**
**a,** Cx43 expression in parental (Par) and BrM cells by RT-PCR. **b,** PCDH7 expression in parental and BrM cells by RT-PCR. **c,** Comparison of the Cx43 expression in BrM cells and different cell types in brain by RT-PCR. **d,** Kaplan-Meier plot illustrates the probability of cumulative metastasis free survival in 58 cases (GSE3141) and 63 cases (GSE8893) of lung adenocarcinoma according to Cx43/PCDH7 expression in the primary tumours. *P* value was calculated from a Cox proportional hazard model.

**Extended Data Figure 3 | Gap Junction Communications between Astrocytes and BrM cells.**
**a,** Dye transfer from MDA231-BrM2 cells to astrocytes. As illustrated in the schema, time-lapse images were captured. See also Supplementary Video 1. Scale bars, 100μm. **b,** Dye transfer between MDA231-BrM2 cells and astrocytes. Schema illustrates the experimental setup. The percentage of Calcein AM (red) positive cells in GFP+ BrM cells was quantified by flow cytometry over time.

**Extended Data Figure 4 | PCDH7 Facilitates Gap Junction Communications.**
**a,b,** Knockdown of Cx43 and PCDH7 in BrM cells with short hairpin RNAs (shRNA), as assessed by RT-PCR (**a**) and westernblotting (**b**). Ctrl, control. **c,** Quantification of dye transfer from astrocytes to Cx43- or PCDH7-depleted Kras/p53-393N1 cells. Graphs shown are mean ± s.e.m. (n = 3 in each group). **d,** Knockdown of PCDH7 in astrocytes with shRNA, as assessed by RT-PCR.

**Extended Data Figure 5 | Cx43 Does Not Interact with E cadherin or N cadherin.**
**a,** Index of the cell lines generated to express different combinations of fusion protein. **b,** Western immunoblotting indicating the E cadherin or N cadherin levels after overexpressing the

fusion proteins. Lane loading is according to table in **a**. **c,** BLI to detect luciferase activities of indicated cell lines according to table in **a**. **d,** Comparison of the Cx43 and PCDH7 expression in astrocytes and fibroblast by RT-PCR. **e,** Quantification of BLI signal after co-culture of the cancer cells and fibroblasts. Schema illustrates the experimental setup.

**Extended Data Figure 6 | Cx43 and PCDH7 Does Not Mediate Lung Metastasis or Endothelial Cell Co-Implanted Tumour Growth.**

**a,** Lung metastatic lesions were quantified by BLI 5 weeks after intravenously injecting MDA231-BrM2 cells. Graphs shown are mean ± s.e.m. (n = 5 mice in each group). **b,** 3 weeks after subcutaneous co-injection of MDA231-BrM2 cells and human brain microvascular endothelial cells (HBMEC), the growth of cancer cells were quantified by bioluminescent imaging.

**Extended Data Figure 7 | Cx43 and PCDH7 Do Not Mediate Trans-BBB Migration.**

**a,** 7 days after cancer cell inoculation, numbers of control, Cx43- or PCDH7-depleted MDA231-BrM2 cells in the brain parenchyma were quantified. Graphs shown are mean ± s.e.m.  (n = 5 brains in each group). **b,** Trans-BBB migration assay. Cancer cells (green) migrated through the artificial BBB were quantified. Graphs shown are mean ± s.e.m.  (n = 3  in each group).

**Extended Data Figure 8 | Cx43 and PCDH7 Mediate Cancer Cell colonization *in Vivo*.**

**a,** Ki67 staining of 14-day brain lesions.  Representative images shows GFP (green) and Ki67 (red) staining in cancer cells. **b,** Sizes of the brain metastatic lesions formed by control, Cx43- or PCDH7-depleted MDA231-BrM2 cells were analyzed. Brain lesions were classified based on their sizes and quantified in each group. Graphs shown are mean ± s.e.m.  (n = 5 brains in each group). **c,** The proportion of Ki67+ cancer cells was quantified. Graphs shown are mean ± s.e.m. (n = 5 brains in each group). **d,e,** Cx43 or PCDH7 depletion does not affect vascular cooption of cancer cells. **d,** 14 days after inoculation of contol, Cx43- or PCDH7-depleted MDA231-BrM2 cells. The interactions between GFP+ cancer cells (green) and vascular structure filled with TRITC dextran (red) were indicated in the representative images. Scale bar, 20 μm. **e,** Contol, Cx43- or PCDH7-depleted MDA231-BrM2 cells were applied to the *in vitro* 3D cultured vascular structure. Our previous work indicated that LICAM in cancer cells is required for BrM cell vascular cooption[11].  Thus, LICAM-depleted cells were used as a control. Scale bar, 100 μm.

**Extended Data Figure 9 | Cx43 and PCDH7 Mediate Cancer Cell Survival.**

**a,** Brain slice assays. Apoptotic cancer cells (green) were detected by cleaved caspase 3 (Casp3) staining (red). The proportion of apoptotic cancer cells was quantified. Graphs shown are mean ± s.e.m. (n = 5 brain slices in each group). Scale bars, 30μm. **b,** GFP+ H2030-BrM3 cells were co-cultured with or without astrocytes. Apoptotic cells were detected by cleaved caspase 3 (Casp3) staining 24 hours after Taxol or soluble Fas ligand (sFasL) treatments. The proportions of apoptotic cancer cells after treatment were quantified. Graphs shown are mean ± s.e.m. (n = 3 in each group).

**Extended Data Figure 10 | Inhibition of Gap Junction Activity Does Not Affect Lung Metastasis or Primary Tumour Growth.**

**a,** Following the treatment regiment, lung metastatic lesions were quantified by BLI 5 weeks after intravenously injecting MDA231-BrM2 cells. Graphs shown are mean ± s.e.m. (n = 5 mice in each group). **b,** Following the treatment regiment, primary tumour growth were quantified by BLI 5 weeks after injecting MDA231-BrM2 cells in mammary fat pads (MFP) of the experimtnal mice. Graphs shown are mean ± s.e.m. (n = 5 mice, 10 tumours in each group).

**Extended DatamFigure 11 | Inhibition of Gap Junction Activity Prevents Brain Metastatic Outgrowth.**

**a,b,** Knockdown of Cx43 and PCDH7 in MDA BrM cells with tet-on inducible short hairpin RNAs (shRNA), as assessed by RT-PCR (**a**) and western immunoblotting (**b**), after doxycycline treatment *in vitro*. **c,** 14 days after inoculation of MDA231-BrM2 cells, brain *ex vivo* BLI was quantified. **d,** Astrocytes were subcutaneously co-implanted with MDA231-BrM2 cells transduced with inducible control, *Cx43* or *PCDH7* shRNA. 2 weeks after the implantation, experimental mice were treated with doxycycline and carboplatin. The growth of cancer cells was measured by BLI at sacrifice.

**SUPPLEMENTARY INFORMATION**

**Video 1: Dye Transfer from MDA231-BrM2 Cells and Astrocytes.**

MDA231-BrM2 cells with Calcein Red-Orange dye. A single-cell suspension of labeled cancer cells was added to the monolayer cultured astrocytes. Bright field and red fluorescent images in the same region were captured every 20 minutes.

**a**

7 days    21 days



GFP
GFAP
ColIV

**b**



MDA231-BrM2

MDA231-BrM2
+ Astrocytes

1000    5000

*P=0.01*

photon flux (10⁵)

−    +
Astrocytes

**c**

MDA231    H2030    ErbB2    Kras/p53

Par BrM2    Par BrM3    Par BrM1 BrM2    373N1 2691N1 393N1 482N1

Cx43
PCDH7
Tubulin

**d**

H2030-BrM3 MDA231-BrM2 Astrocyte Microglia Neuron HBMEC

Cx43
PCDH7
Tubulin

**e**

MDA231

Par BrM2 LM2 BoM

Cx43
PCDH7
Tubulin

**f**

Triple negative breast cancer

Brain met free survival

*p = 0.025*

*PCDH7/Cx43*high
*PCDH7/Cx43*low

0    50    100    150
Months

| Sites | P value |
|-------|---------|
| Brain | 0.025 |
| Lung | 0.159 |
| Bone | 0.163 |

**g**

Lung adenocarcinoma

Metastasis free survival

MSK set2

*p = 0.01*

*PCDH7/Cx43*high
*PCDH7/Cx43*low

0    10    20    30    40    50
Months

**a**

Cx43   PCDH7

CLuc   NLuc

*

**b**

| | 1 | 2 | 3 | 4 | 5 | 6 |
|---|---|---|---|---|---|---|
| Cx43-Nluc | - | - | - | + | - | - |
| Cx43-CLuc | - | + | - | + | + | + |
| PCDH7-NLuc | - | - | + | - | Low | High |

**c**

MDA231    H2030
1  5  6  4    1  5  6  4

PCDH7
Cx43
tubulin

**d**

MDA231    H2030

**e**

MDA231   H2030
Astro:  −  +    −  +

110   140   50   80

Astro:  −   +        −   +
MDA231   H2030
BrM2     BrM3

Normalized signal

**f**

Astrocyte

PCDH7
Cx43
Split Luc

*

Cancer cell

Cancer cells
± Astrocytes → Stress → Cleaved caspase 3

**H2030 + sFasL**

GFP — 20%

+ Astrocyte

GFP — 11%

GFP (vertical axis) → Cleaved Casp3

**H2030-BrM3 + Taxol**

GFP — 31%

+ Astrocyte

GFP — 13%

GFP (vertical axis) → Cleaved Casp3

**MDA231-BrM2 + Carboplatin**

GFP — 32%

+ Astrocyte

GFP — 19%

GFP (vertical axis) → Cleaved Casp3

**a**

MDA231

H2030

ErbB2

Kras/p53

*Cx43* mRNA

373N1
2691N1
393N1
482N1

**b**

MDA231

H2030

ErbB2

Kras/p53

*PCDH7* mRNA

373N1
2691N1
393N1
482N1

**c**

*Cx43* mRNA

H2030-BrM3
MDA231-BrM2
Astrocyte
Neuron
HBMEC

*PCDH7* mRNA

H2030-BrM3
MDA231-BrM2
Astrocyte
Neuron
HBMEC

**d**

GSE3141

*p = 0.002*

Metastasis free survival

*PCDH7/Cx43*high
*PCDH7/Cx43*low

Months

GSE8894

*P = 1.65e-05*

Metastasis free survival

Months

**a**



**b**

**a**

MDA231-BrM2 — Cx43, PCDH7
H2030-BrM3 — Cx43, PCDH7
Kras/p53-393N1 — Cx43, PCDH7

**b**

H2030-BrM3 — Cx43, PCDH7, Tubulin
Kras/p53-393N1 — Cx43, PCDH7, Tubulin

**c**

Kras/p53-393N1

$P<0.001$

% of dye+ cancer cells

**d**

Astrocyte — Cx43, PCDH7

**a**

H2030

| | 1 | 2 | 3 | 4 | 5 |
|---|---|---|---|---|---|
| Cx43-Cluc | - | + | + | + | + |
| Cx43-Nluc | - | + | - | - | - |
| ECad-Nluc | - | - | Low | High | - |
| NCad-Nluc | - | - | - | - | + |

**b**

H2030

1   3   4

ECad

Tubulin

1   5

NCad

Tubulin

**c**

H2030

**d**

*Cx43*   *PCDH7*

mRNA

Astrocyte   Fibroblast   Astrocyte   Fibroblast

**e**

Cancer cell
(Cx43-Cluc
PCDH7-Nluc) ± Fibroblast ➡ BLI

*15min*

MDA231   H2030
Fibroblast: -   +   -   +

150   400

Normalized signal

Fibro: +
MDA231   H2030

**a**



**b**

**a**

MDA231-BrM2
(GFP)

7d → GFP+ cell
counts in brain

GFP+ cells/brain

45
30
15
0

*P>0.5*

■ Control
■ *Cx43* sh1
■ *PCDH7* sh1

**b**

MDA231-BrM2

Brain
Microvascular
Endothelial Cells

Astrocytes

18 h

Control    *shCx43*    *shPCDH7*

■ Control
■ *Cx43* sh1
■ *PCDH7* sh1

Normalized signal

1.6
1.2
0.8
0.4
0

*P>0.5*

**a**

MDA231-BrM2
(GFP)

14d → GFP/Ki67
Staining

Control | *shCx43* | *shPCDH7*

DAPI
GFP
Ki67

**b**

■ Control  ■ *Cx43* sh1  ■ *PCDH7* sh1

% of total lesions

P<0.05 P<0.05 P<0.01

<10    10-20    >20 cells

**c**

% of Ki67+ cancer cells

P<0.001

■ Control
■ *Cx43* sh1
■ *PCDH7* sh1

**d**

MDA231-BrM2
(GFP+)

14d

*i.v.* injection
Dextran (70 KD)

Vessel/Cancer cell

Control | *Cx43* sh1 | *PCDH7* sh1

GFP
Dextran

**e**

HBMEC

Matrigel

O.N.

MDA231
BrM2

6h

Vascular Co-op

Control | *Cx43* sh1 | *PCDH7* sh1 | *L1CAM* sh1

**a**



**b**

**a**



**b**

**a**

Tet inducible promoter



RFP  shRNA

■ Control
■ *Cx43* sh1
■ *Cx43* sh2
■ *PCDH7* sh1
■ *PCDH7* sh2

*Cx43*

mRNA

Dox: -  24h  48h  72h

*PCDH7*

Dox: -  24h  48h  72h

**b**



| | - | | | Dox (24h) | | | Dox (48h) | | | Dox (72h) | | |
|---|---|---|---|---|---|---|---|---|---|---|---|---|
| *shCx43*: | Ctrl | 1 | 2 | Ctrl | 1 | 2 | Ctrl | 1 | 2 | Ctrl | 1 | 2 |

Cx43 [

Tubulin

| | - | | | Dox (24h) | | | Dox (48h) | | | Dox (72h) | | |
|---|---|---|---|---|---|---|---|---|---|---|---|---|
| *shPCDH7*: | Ctrl | 1 | 2 | Ctrl | 1 | 2 | Ctrl | 1 | 2 | Ctrl | 1 | 2 |

PCDH7 [

Tubulin

**c**

MDA231-BrM2

*14 days*

*ex vivo* brain BLI



Normalized Photon Flux ($10^5$)

| *Number of Lesions* | 2 | 2 | 3 | 1 | 1 | 1 | 1 | 1 | 1 | 1 |
|---|---|---|---|---|---|---|---|---|---|---|

**d**

MDA231-BrM2 + Astrocyte  *14 day*  **Dox**  *21 day*  BLI
Carboplatin (i.p./5 days)



Normalized photon flux

*P<0.0001*
*P<0.0001*

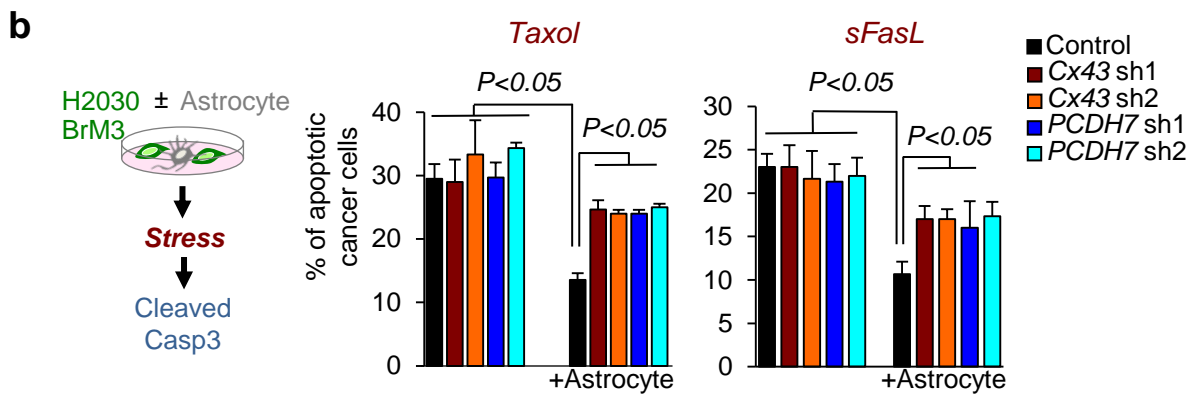| Ctrl | sh1 | sh2 | sh1 | sh2 |
|---|---|---|---|---|
| | *Cx43* | | *PCDH7* | |

**Extended Data Table 1.** Cancer cell lines used in this study.

| Cell line | Species | Tumor type | Brain mets | Ref. |
|---|---|---|---|---|
| MDA231-BrM2<br>MDA231-LM2<br>MDA231-BoM | Human | Breast adenocarcinoma (*ER-, PR-, HER2-*) | High<br>Low<br>Low | *Bos, 2009*<br>*Minn, 2005*<br>*Kang, 2003* |
| H2030-BrM3 | Human | Lung adenocarcinoma (*KRAS$^{G12C}$*) | High | *Nguyen, 2009* |
| ErbB2-BrM2 | Mouse | Breast (*ErbB2 hyperactive*) | High | *Valiente, 2014* |
| Kras/p53-393N1<br>Kras/p53-482N1<br>Kras/p53-373N1<br>Kras/p53-2691N1 | Mouse | Lung (*Kras$^{G12D}$;p53$^{-/-}$*) | High<br>High<br>Low<br>Low | *Valiente, 2014*<br>*Winslow, 2011* |